STOCHASTIC METHODS AND THEIR APPLICATIONS IN STATISTICAL ELECTROMAGNETIC MODELING

A Dissertation

Presented to

the Faculty of the Department of Electrical and Computer Engineering

University of Houston

In Partial Fulfillment

of the Requirements for the Degree

Doctor of Philosophy

in Electrical Engineering

by

Cong Gao

December 2012

STOCHASTIC METHODS AND THEIR APPLICATIONS IN STATISTICAL ELECTROMAGNETIC MODELING

Cong Gao

Approved:

Chairman of the Committee
Ji Chen, Associate Professor
Electrical and Computer Engineering

Committee Members:

David Jackson, Professor
Electrical and Computer Engineering

Donald Wilton, Professor Emeritus
Electrical and Computer Engineering

George Zouridakis, Professor
Engineering Technology

Driss Benhaddou, Associate Professor
Engineering Technology

Suresh K. Khator, Associate Dean
Cullen College of Engineering

Badrinath Roysam, Professor and Chairman
Electrical and Computer Engineering

Acknowledgements

First of all, I would like to thank my advisor, Dr. Ji Chen, for his creative ideas and academic suggestions on my research topic. During my Ph.D research, he always tried to encourage my independent thinking and problem-solving skills. This will remain with me as a positive impact on my new career and my whole life.

I would like to thank the faculty members of my dissertation committee: Dr. David Jackson, Dr. Donald Wilton, Dr. George Zouridakis, and Dr. Driss Benhaddou for their time and constructive suggestions to my dissertation.

I would also like to thank Dr. Jianxiang Shen, who provided me with a lot of discussions and guidance regarding the area of stochastic computational modeling. I also want to thank other members of our EM group, who have been helpful to my research: Dr. Yanmin Yu, Dr. Minshen Wang, Mr. Yan Liu, etc.

I also want to thank all the ECE staff members, especially Mytrang Beccam and Zaniffa Jan. They have been of great help during my studies at the University of Houston.

And last, but not least, I want to express my thanks to my parents. No matter what happens, they always have confidence in me. Their continuous courage and support help me overcome difficulties and move forward.

STOCHASTIC METHODS AND THEIR APPLICATIONS IN STATISTICAL ELECTROMAGNETIC MODELING

An Abstract

of a

Dissertation

Presented to

the Faculty of the Department of Electrical and Computer Engineering

University of Houston

In Partial Fulfillment

of the Requirements for the Degree

Doctor of Philosophy

in Electrical Engineering

by

Cong Gao

December 2012

Abstract

The stochastic computation of electromagnetic (EM) problems is a relatively new topic, yet very important in understanding the true physics due to uncertainties associated with them. To deal with these uncertainties, the traditional Monte Carlo (MC) method can be applied. However, it requires a very large number of simulations to reach convergence, which makes it very computationally expensive. This dissertation discusses alternative stochastic methods which are more efficient than the MC method as well as their applications in EM modeling. It consists of three major parts.

The first part presents the use of the generalized polynomial chaos (gPC) method for stochastic computation. In the gPC method, the stochastic solutions we are interested in are approximated by polynomial expansion in terms of input random variables, truncated at a finite order. Based on the distribution of random inputs, there is an optimal choice for a polynomial basis to achieve the fastest convergence. By taking the inner product of the testing basis, we seek to solve the Maxwell equations in a weak form.

The second part focuses on applying the Stochastic Collocation (SC) method for stochastic computation. In the SC method, the stochastic solution is constructed via polynomial interpolation. One only needs a small number of repeated simulations to get accurate statistics, which makes it computationally favorable. The selection of collocation points is of greatest importance in the SC method, especially in the multi-dimensional problems, since the total simulation cost is proportional to the number of collocation points. A sparse grid (SG) technique can be used for generating collocation points much easier than the tensor product rule in the multi-dimensional problems.

The third part emphasizes analyzing uncertainty problems with correlations. Most

of the stochastic methods are based on the assumption that the probability space can be characterized by a set of independent random variables (RV). However, this requirement may not be met in some cases. For example, the random process is a function of spatial coordinates or RVs that are correlated in the probability space. To deal with spatial correlation, the Karhunen-Loeve expansion technique can be applied. And for correlated Gaussian RVs, a linear mapping technique can transform them into uncorrelated RVs.

Table of Contents

List of Figures

List of Tables

Chapter 1 Introduction

1.1 Background

Numerical simulations have become an important tool to investigate and understand the physics of a complex system, since experimental studies can be very expensive, time consuming, and difficult to implement. Despite the continuous progress made in the accuracy of computational techniques, most numerical simulations assume that the entire physical problem can be described by a deterministic mathematical model. However, this is not always the case for representing the complex system. What has been less addressed in traditional simulations is the impact of uncertainties in input data such as material properties, geometry and boundary conditions, etc. All these uncertainties could possibly influence the output quantities we are interested in. To better predict the behaviors of the physical system, the uncertainty factors need to be taken into account in the numerical modeling. That is why there has been a growing interest in the area of uncertainty quantification (UQ). The goal of UQ is to investigate how the uncertainties would propagate through the system and their impacts to the output we are interested in. This is especially useful for the analysis of complex systems where mathematical models can serve only as simplified and reduced representation of the true physics.

Over the past few decades, the computational electromagnetics (CEM) techniques [1] have developed very quickly. Various methods, both in time domain and frequency domain, were developed to numerically solve the Maxwell Equations. Among them, the finite difference time domain (FDTD) method proves to be a very good way to analyze

complex electromagnetic problems [2]. While great efforts have been made to achieve more accuracy, less attention is paid to the uncertainties associated within practical problems. For example, in a manufacturing process, even with the same requirement, there will be variations between different products. Because of these uncertainties, the system response would be different. Uncertainty analysis has been conducted extensively in the field of computational fluid dynamics [30]-[33].

Recently, there has also been some progress [3][6] made in the area of stochastic EM modeling. In this dissertation, we will investigate several different UQ methods and combine them with the FDTD method for statistical modeling in EM simulations.

1.2 Overview of popular UQ method

The importance of understanding uncertainty has been realized for a long time, in the areas such as civil engineering, system control, hydrology [7][8][52], etc. Many methods have been proposed to address this issue. Because of the nature of "uncertain" in these problems, the most dominant approach is to treat uncertainties as random variables or random processes input to the systems and to remodel the original deterministic systems as stochastic systems [9][10].

1.2.1 Monte Carlo method and sampling based methods

One of the most commonly used sampling methods is the Monte Carlo (MC) method [11]. In the MC method, independent random inputs are generated based on their specified probability distribution. Then all the input samples would go through the system, and a corresponding output could be expected for each input. For each realization, the input data is fixed, and the problem becomes deterministic. After all the realizations

have been performed, statistical information can be extracted such as mean and variance, etc. Although the MC method is straightforward, its convergence rate is quite slow. For example, the mean value typically converges proportionally to $1/\sqrt{N}$, where N is the number of realizations. The need for a large number of realizations for accurate results makes it computationally expensive, especially for systems that are already computationally intensive in their deterministic settings as in computational fluid dynamics (CDF) and computational electromagnetics (CEM). Though derivative methods such as the Latin Hypercube sampling method [12] and Quasi-Monte Carlo method [13] have been proposed alternatively, additional requirements for implementing make their application limited.

However, the statistics of the MC method prove to be very accurate once convergence has been reached. And the MC method is independent of the dimensionality in the random space. So the MC method is often used as the control group to quantify the accuracy of other more efficient stochastic methods.

1.2.2 Perturbation methods

One popular non-sampling method is the perturbation method, where random fields are expanded as the Taylor series around their mean and truncated at a certain order. Typically applied perturbation methods are truncated at the first or second order because the resulting system of equations becomes very complicated beyond the second order. This approach has been used extensively in various engineering fields [14][15].

An implicit limitation of perturbation methods is that the magnitude of uncertainties, both for the inputs and outputs, cannot be too large (typically required deviation less than 10% away from the mean value); otherwise the methods do not

perform well due to the truncation error of the Taylor series.

1.2.3 Generalized polynomial chaos method

The generalized polynomials chaos (gPC) method for stochastic computation was first proposed by Xiu and Karniadakis based on Wiener-Askey polynomials, which are a class of hypergeometric orthogonal polynomials [16]. In the gPC method, stochastic solutions are expressed as orthogonal polynomials with input random parameters, and different types of distribution have a corresponding optimal choice of orthogonal polynomials in order to achieve better convergence. The basic idea is to form a spectral representation of the stochastic solution in the random space. The convergence of the stochastic solution depends on the smoothness of the random parameters.

1.3 Outline of the dissertation

This dissertation is aimed at introducing stochastic methods into EM simulation and developing approaches for efficient stochastic computation. Traditional techniques such as Monte Carlo method can be very time consuming and computationally expensive when dealing with complex systems. This dissertation introduces polynomial expansion based method to solve the Maxwell equations in statistical modeling efficiently. Most of the stochastic methods that are being used nowadays haven't considered the potential correlated associated within. This dissertation innovatively presents effective techniques to deal with correlation present both in spatial coordinate and probability space. This is also the biggest contribution of this dissertation. The dissertation is organized as follows:

Chapter 1 briefly introduces the background of uncertainty quantification in the numerical modeling and its importance in the area of EM simulations. Several popular

UQ methods are reviewed.

Chapter 2 recalls some basic mathematics concepts and definitions, which help to understand the techniques used in the following chapters for uncertainty analysis. These concepts and definitions include probability theory, orthogonal polynomials, and numerical integral technique such as Gaussian quadrature rule.

Chapter 3 describes how to formulate a stochastic system governed by a partial differential equation (PDE), including parameterization of input data and solving the stochastic PDE. As a demonstration, a simple first order differential equation is used to compare the results computed by the MC method, perturbation method, the 1-D gPC method, and the collocation method.

Chapter 4 presents the generalized polynomial chaos (gPC) method and how to implement it into the finite difference time domain (FDTD) method to solve the Maxwell equations in a stochastic Galerkin scheme. Wave propagation problems are investigated using the gPC-FDTD method.

Chapter 5 discusses solving Maxwell equations in a stochastic collocation scheme via polynomial interpolation. The sparse grid (SG) method is applied to handle multi-dimensional problems. Applications in high speed circuits demonstrate the computational efficiency of the sparse grid based collocation method. We also introduce the idea of stochastic analysis into the antenna array design problem, to provide a design margin in order to ensure the original design specification due to uncertainties.

Chapter 6 provides stochastic analysis of random medium with correlations, both in spatial domain and random space domain. Since traditional uncertainty analysis requires the random inputs to be independent, this chapter talks about de-correlation techniques to

transform the stochastic process or correlated random variables into independent random variables. Chapter 7 draws conclusions of this dissertation and suggests potential future works.

Chapter 2 Mathematic Fundamentals

This chapter only reviews some basic concepts and definitions about probability theory, orthogonal polynomials, and Gaussian quadrature rule. There are many text books [16][17] regarding these aspects and one can find more details there.

2.1 Probability Theory

2.1.1 Random variables

The outcome of an experiment, an event, or a realization is random. For example, if we flip a coin, the possible outcomes will be either heads or tails. Mathematically, we want to assign a value for every possible outcome. We can assign "1" to represent the heads and "0" to represent the tails. Thus, a random variable, $X \in \{0,1\}$, is established.

Formally, random variables are defined as a function of all the possible outcomes on the sample space. Random variables typically can be classified into two categories: discrete random variables and continuous random variables.

Discrete random variables are variables only having discrete values. The sample space for a discrete random variable can be discrete or continuous. For example, the outcome of rolling a dice can take only integer values from 1 to 6. Continuous random variables are variables which can have continuous values within an interval range. For example, the lifetime of a light bulb is a continuous random variable, which have any positive value.

2.1.2 Probability and Distribution

Probability is a term used to measure the likelihood of occurrence of a certain event.

The classic definition of probability of an event is defined as the ratio of the number of cases favorable to it to the number of all cases possible, when a large number of experiments are conducted. For example, when flipping a coin a large number of times, we can expect 50% of the time the results would be heads and the other 50% would be tails.

The probability of a certain event should be no less than 0 and no greater than 1. “0” means that the event will never happen, and “1” means that the event will always happen.

For continuous random variables, they are often characterized by their distribution functions since we cannot specify a probability that the random variable is exactly equal to.

Consider a continuous random variable X . Its distribution function is defined as the probability that a random variable X has a value less than or equal to x,

$$F_X(x) = P(X \le x), \tag{2.1}$$

and the probability that X lies between x_1 and x_2 is given by

$$\mathrm{P}\{x_1 \le X \le x_2\} = F_X(x_2) - F_X(x_1). \tag{2.2}$$

The derivative of the distribution function is called the probability density function

$$f_X(x) = \frac{dF_X(x)}{dx}. \tag{2.3}$$

2.1.3 Statistical characteristics

The Nth moments of a random variable X is defined as

$$\mu_X^N = \int_{-\infty}^{\infty} x^N f_X(x)\, dx. \tag{2.4}$$

The most important moment of a random variable is the first moment, which is also called the mean or expectation of the random variable. It represents the average value of the random variable over the probability space,

$$E[X] = \int_{-\infty}^{\infty} x\, f_X(x)\, dx . \tag{2.5}$$

The Nth central moment of random variable X is defined as

$$m_X^N = \int_{-\infty}^{\infty} (x - E[X])^N\, f_X(x)\, dx . \tag{2.6}$$

The most important central moment of a random variable is the second moment, which is also called the variation of the random variable, which denotes how the random variable is distributed around its mean value,

$$\sigma_X^2 = \int_{-\infty}^{\infty} (x - E[x])^2\, f_X(x)\, dy . \tag{2.7}$$

And the square root of variance is defined as the standard deviation of the random variable. Mean and variance are what we used most to characterize a random variable.

2.1.4 Jointly random variables

When the stochastic system has more than one random input, which is often the case, these random variables are related by their joint distribution function

$$F_{X_1, X_2 \cdots X_N}(x_1, x_2 \cdots x_N) = P(X_1 \le x_1, X_2 \le x_2, \cdots, X_N \le x_N) , \tag{2.8}$$

and their joint probability density function

$$f_{X_1, X_2 \cdots X_N}(x_1, x_2, \cdots, x_N) = \frac{\partial^N F_{X_1, X_2 \cdots X_N}(x_1, x_2, \cdots, x_N)}{\partial x_1 \partial x_2 \cdots \partial x_N} , \tag{2.9}$$

where $X_1, X_2, \cdots, X_N$ are N random variables. They are independent if and only if

$$f_{X_1, X_2 \cdots X_N}(x_1, x_2, \cdots, x_N) = f_{X_1}(x_1)\, f_{X_2}(x_2) \cdots f_{X_N}(x_N) . \tag{2.10}$$

2.2 Orthogonal Polynomials

2.2.1 General property

An nth order polynomial of variable x generally has the form [18] of

$$P_n(x) = a_n x^n + a_{n-1} x^{n-1} + \cdots + a_1 x + a_0 \qquad , a_n \neq 0 . \tag{2.11}$$

A set of polynomials $\{P_n(x)\}_{n=1}^{\infty}$ is orthogonal if the below relationship holds true

$$\int_D P_n(x) P_m(x) d\alpha(x) = \left\| P_n(x) \right\|^2 \delta_{ij} , \tag{2.12}$$

where $\alpha(x)$ is a positive measure of the polynomials and D is the support of this measure. δ_{ij} is the Kronecker delta function that

$$\delta_{ij} = \begin{cases} 1 & (i = j) \\ 0 & (i \neq j) \end{cases} . \tag{2.13}$$

$\left\| P_n(x) \right\|^2$ is a constant named the norm of the nth order polynomial, defined as

$$\left\| P_n(x) \right\|^2 = \int_D P_n^2(x) d\alpha(x) . \tag{2.14}$$

More specifically, if $\left\| P_n(x) \right\|^2 = 1$, $\{P_n(x)\}_{n=1}^{\infty}$ is called orthonormal.

Usually, there will be a corresponding weight function $\omega(x)$ associated with the measure $\alpha(x)$; then (2.12) becomes

$$\int_D P_n(x) P_m(x) \omega(x) dx = \left\| P_n(x) \right\|^2 \delta_{ij} , \tag{2.15}$$

or

$$\left\langle P_n(x), P_m(x) \right\rangle = \left\| P_n(x) \right\|^2 \delta_{ij} . \tag{2.16}$$

$\langle\ \rangle$ is the operator for the inner product.

2.2.2 Categories of orthogonal polynomials

Different types of polynomials have different weighting functions. The family of orthogonal polynomials from the Askey-scheme is summarized in [19] and listed in Tables 2-1 and 2-2 for discrete and continuous random variables, respectively. According to the distribution of the random variables, a corresponding polynomial basis can be chosen for optimal convergence, since its weight function is the same as the probability density function of the random variable.

Table 2-1 Discrete random variables and corresponding polynomials

Distribution of random variables	Polynomials type	Probability space
Poisson	Charlier	$0,1,2,\cdots,\infty$
Binomial	Krawtchouk	$0,1,2,\cdots,N$
Negative Binomial	Meixner	$0,1,2,\cdots,\infty$
Hypergeometric	Hahn	$0,1,2,\cdots,N$

Table 2-2 Discrete random variables and corresponding polynomials

Distribution of random variables	Polynomials type	Probability space
Gaussian	Charlier	$0,1,2,\cdots,\infty$
Uniform	Krawtchouk	$0,1,2,\cdots,N$
Beta	Meixner	$0,1,2,\cdots,\infty$
Gamma	Hahn	$0,1,2,\cdots,N$

Among them, the two most important polynomial bases are the Hermite polynomials and Legendre polynomials, as they correspond to Gaussian distribution and uniform distribution, which are most widely used for modeling real world uncertainty's probability distribution.

2.3 Gaussian Quadrature

In numerical computation, evaluation of the integral of a function can be very often, as in the form of (2.17),

$$I = \int_a^b g(x)dx, \tag{2.17}$$

where $g(x)$ is called the integrand, a is the lower limit of integration, and b is the upper limit of integration.

Gaussian quadrature [20] is a numerical integration technique to approximate the integral in (2.17) as

$$I = \int_a^b g(x)dx = \int_a^b f(x)W(x)dx \approx \sum_{i=1}^{N} \omega_i f(x), \tag{2.18}$$

given that the integrand $g(x)$ can be expressed as (2.19) in the integration interval

$$g(x) = f(x)W(x), \tag{2.19}$$

where $f(x)$ is the approximate polynomial and $W(x)$ is a non-negative weighting function. The formula is exact for polynomials $f(x)$ of an order up to $2N-1$.

For the *N*th order polynomial $f_N(x)$, consider its general form as

$$f_N(x) = a_N x^N + a_{N-1}x^{N-1} + \cdots + a_1 x + a_0 \quad , a_N \neq 0; \tag{2.20}$$

then the *N* points for quadrature rule $x_i (i = 1, 2, \cdots N)$ are the roots of $f_N(x)$.

To find the roots of the polynomial $f_N(x)$, factorization can be used for some special polynomials. But in most of the cases, they have to be found numerically. Various iterative roots finding algorithms such as the Newton method and the Secant method can be applied.

The formula for computing the weights is given by

$$\omega_i = \frac{a_N \int_a^b W(x)[f_{N-1}(x)]^2}{a_{N-1} \cdot f_N^{'}(x_i) f_{N-1}(x_i)}, i = 1, 2, \cdots N . \tag{2.21}$$

If one can express $f_N(x)$ using Lagrange polynomial interpolation

$$f_N(x) = \sum_{i=1}^{N} f(x_i) \prod_{1 \le i, j \le N}^{i \ne j} \frac{x - x_j}{x_i - x_j}, \tag{2.22}$$

then the weights can be further computed by

$$\omega_i = \int_a^b W(x) \prod_{1 \le i, j \le N}^{i \ne j} \frac{x - x_j}{x_i - x_j} dx . \tag{2.23}$$

Table 2-3 lists the three most commonly used weighting functions and corresponding polynomials in the Gauss quadrature rule.

Table 2-3 Polynomials and weight functions for Gauss quadrature rule

Polynomial type	Weighting function	Intervals
Chebyshev	$\sqrt{1-x^2}$	$[-1,1]$
Legendre	1	$[-1,1]$
Hermite	e^{-x^2}	$(-\infty, +\infty)$

2.4 Techniques for de-correlation

In most stochastic problems, the random inputs can be characterized by a set of independent variables. Clearly, this indicates there is no correlation effect considered. While in some special cases, we have to include the correlation for better modeling the real mechanism.

Generally, there are two types of correlation. One is the correlation spatial coordinates where the randomness should be modeled by a stochastic process. The other one is the correlation in the probability space where different random variables are

correlated and not independent with each other. For those two kinds of problems, there are corresponding techniques for de-correlation. They are discussed in detail in Chapter 6.

Chapter 3 Formulation of Stochastic System

A physical system can often be characterized by a governing partial differential equation (PDE), which is deterministic. This chapter provides general steps on how to reformulate the original deterministic system into a stochastic system. The key step is to characterize the probability space associated with the random inputs by a set of mutually independent random variables. To illustrate the idea, a simple ordinary differential equation is used as an example. Also, the stochastic methods which are reviewed in Chapter 1 are compared to help better understand the pros and cons between them.

3.1 Reformulation from a deterministic system

Consider a system PDE defined in a spatial domain $D \subset R^d, d = 1,2,3$, and a time domain $[t_0, T]$

$$\begin{cases} L(u(x,t)) = f(x,t) & x \in D, t \in (t_0, T] \\ B(u(x,t)) = 0 & x \in \partial D, t \in (t_0, T], \\ u(x,t_0) = u_0 \end{cases} \tag{3.1}$$

where L is a differential operator, B is the boundary condition operator, u_0 is the initial condition, and $f(x,t)$ is the source term. To take into account the randomness associated within the system, we can rewrite (3.1) as a stochastic PDE

$$\begin{cases} L(u(x,t,\xi)) = f(x,t,\xi) & x \in D, t \in (t_0, T], \xi \in \Omega \\ B(u(x,t,\xi)) = 0 & x \in \partial D, t \in (t_0, T], \xi \in \Omega, \\ u(x,t_0,\xi) = u_0 & \xi \in \Omega \end{cases} \tag{3.2}$$

where $\xi \in \Omega$ denotes the random inputs of the system in a properly defined probability space (Ω, F, P). Various numerical methods can be used to solve the PDE. In the

computational electromagnetics (CEM) area, where the governing PDE are the Maxwell equations, finite difference time domain (FDTD) method [2][21][22], finite element method (FEM) [23][24], and method of moment (MOM) [25] are the most commonly used methods.

3.2 Parameterization of random inputs

To solve (3.2) numerically, we need to reduce the infinite-dimensional probability space to a finite-dimensional space. This can be accomplished by characterizing the probability space by a finite number of random variables. Such a procedure, termed the "finite-dimensional noise assumption" in [26], is often achieved via a certain type of decomposition which can approximate the target random process with desired accuracy. Assume that they can be parameterized by a set of independent random variables $\xi = (\xi_1, \xi_2, \cdots, \xi_d) \in R^d, d = 1, 2, 3$. Their joint probability density function is given by

$$\rho(\xi) = \prod_{i=1}^{d} \rho_i(\xi_i) \quad i = 1, 2, \cdots d . \tag{3.3}$$

By characterizing the probability space with d random variables, we have effectively reduced the infinite-dimensional probability space to a d-dimensional space. The set of random variables is required to be mutually independent for implementing the most available numerical techniques for uncertainty analysis.

One should notice that the probability distribution of the random variables is also prescribed. However, the ability to correctly characterize randomness of the input parameters relies heavily on the experimental data of these parameters. There are two major difficulties: 1) for some cases, it is impossible to acquire a huge amount of data to get a reliable prediction of the probability distribution of the input parameter; and 2) for

some parameters, experiments can provide little information regarding the variations. According to the central limit theorem [27], for a large number of independent random variables, their mean will approximate a Normal distribution. Thus, throughout the dissertation, we assume the random variables will have a Gaussian distribution, which is also a common assumption in most engineering analysis.

3.3 Demonstration of an ODE case

In Chapter 2, different UQ methods are reviewed. In this section, we use a first order differential equation to illustrate their ideas.

3.3.1 Analytical Solution

Now, consider an ordinary differential equation as in (3.4) and (3.5),

$$\frac{dy(t)}{dt} = -ky(t), \tag{3.4}$$

$$y|_{t=0} = y_0, \tag{3.5}$$

where k is a random variable having Normal distribution with a mean of $\bar{k} = 0$ and a variation of $\sigma_k^2 = 1$. It has a probability density function (PDF)

$$f(k) = \frac{1}{\sqrt{2\pi}} e^{-\frac{1}{2}k^2}. \tag{3.6}$$

The analytic solution of the (3.4) differential equation is given by

$$y(t) = y_0 e^{-kt}. \tag{3.7}$$

The mean and variance of $y(t)$ can be computed by (3.8) and (3.9), respectively,

$$\bar{y}(t) = \int y_0 e^{-kt} \frac{1}{\sqrt{2\pi}} e^{-\frac{1}{2}k^2} dk = y_0 e^{\frac{t^2}{2}}, \tag{3.8}$$

$$\sigma^2(t) = \int y_0(e^{-kt} - e^{\frac{t^2}{2}})^2 \frac{1}{\sqrt{2\pi}} e^{-\frac{1}{2}k^2} dk = y_0(e^{2t^2} - e^{t^2}) . \qquad (3.9)$$

3.3.2 Monte Carlo Method

The Monte Carlo method samples the PDF of *k* purely randomly, and the statistics can be obtained after repeating *N* times solving (3.4)

$$\text{Mean} = \frac{1}{N}\sum_{i=1}^{N} e^{-k_i t} , \qquad (3.10)$$

$$\text{Variance} = \frac{1}{N}\sum_{i=1}^{N} (e^{-k_i t} - \text{mean})^2 . \qquad (3.11)$$

Figures 3-1 to 3-6 plot the mean and variation of $y(t)$ computed by 100 times, 1000 times and 20000 times the Monte Carlo method and compare them with analytical solutions.

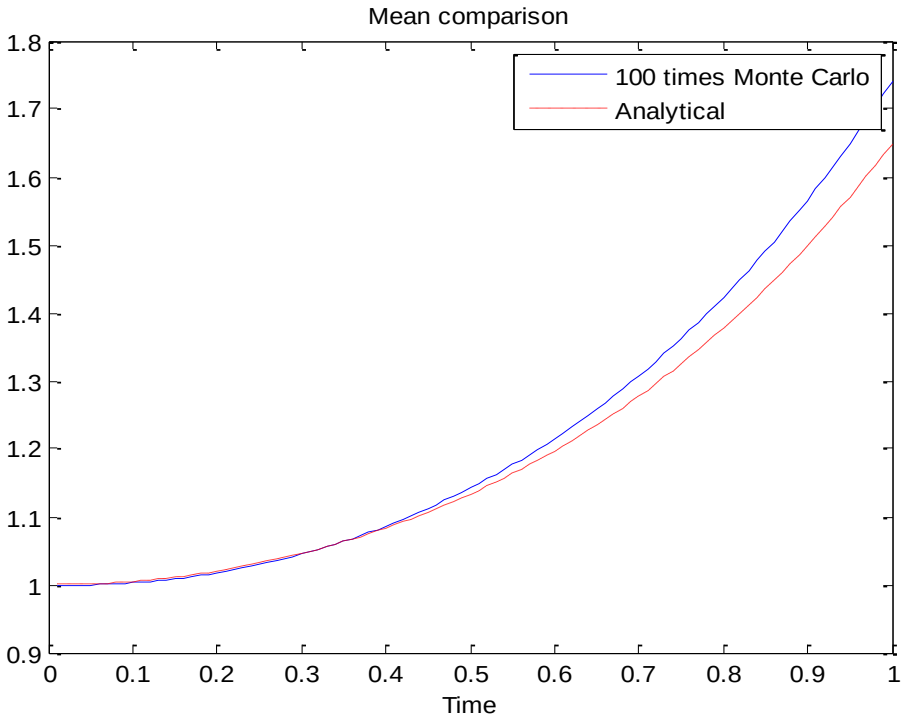

Figure 3-1 Mean comparison between analytical solution and 100 times Monte Carlo method.

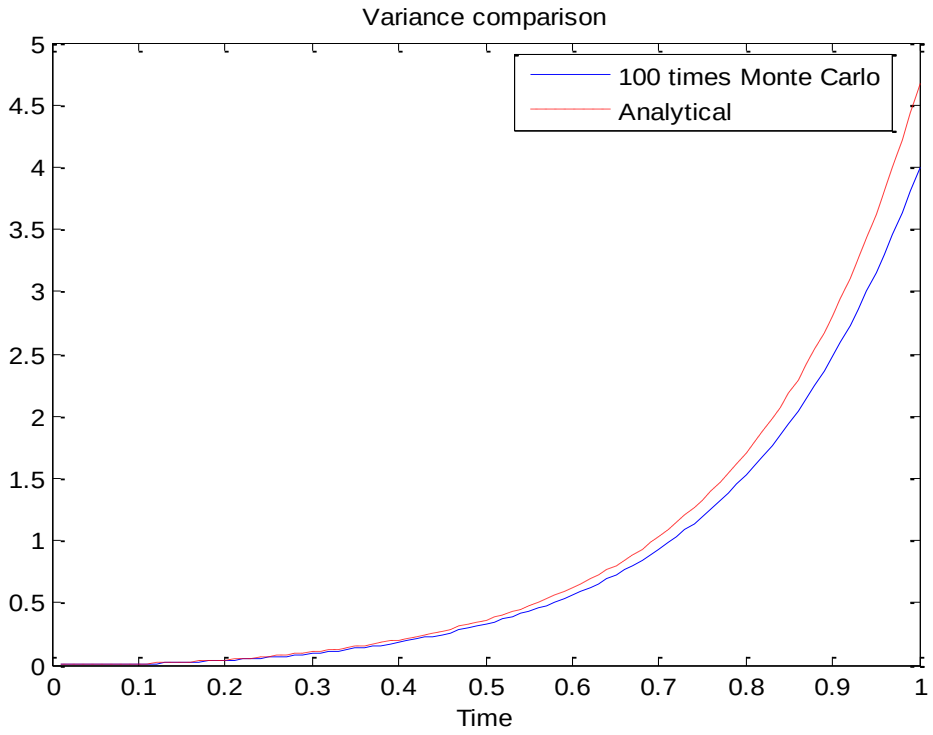

Figure 3-2 Variance comparison between analytical solution and 100 times Monte Carlo method.

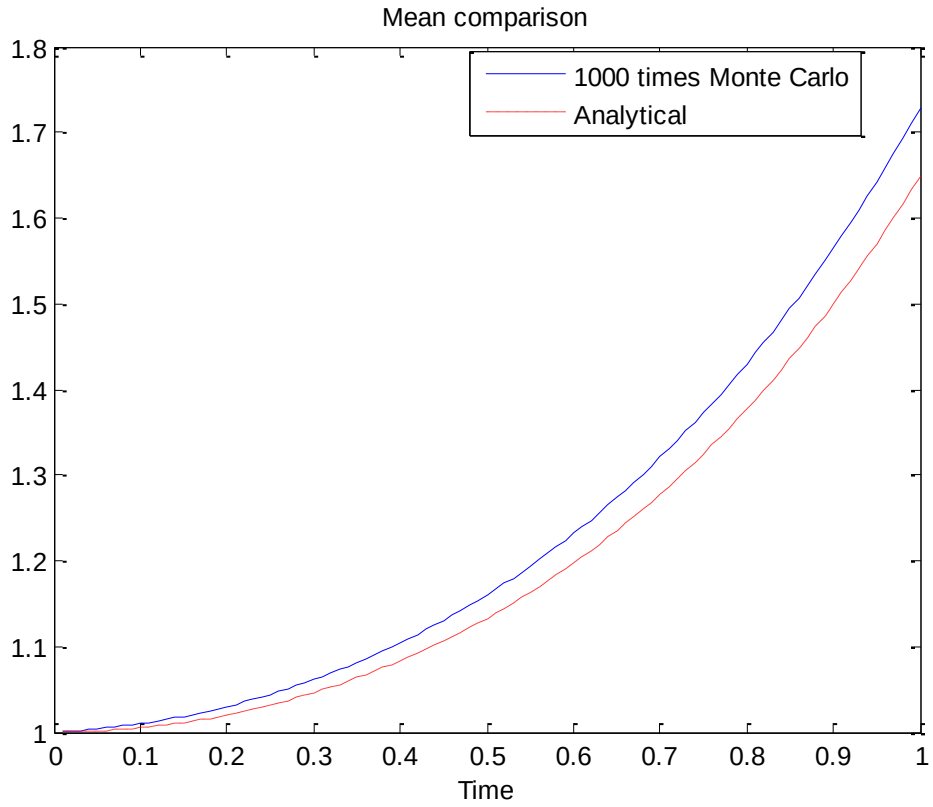

Figure 3-3 Mean comparison between analytical solution and 1000 times Monte Carlo method.

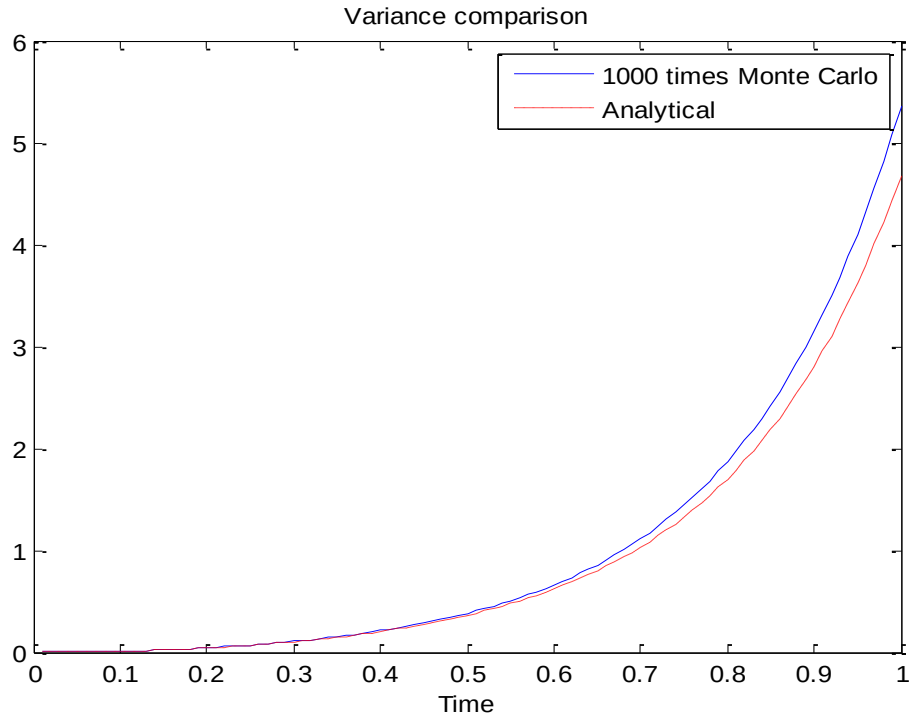

Figure 3-4 Variance comparison between analytical solution and 1000 times Monte Carlo method.

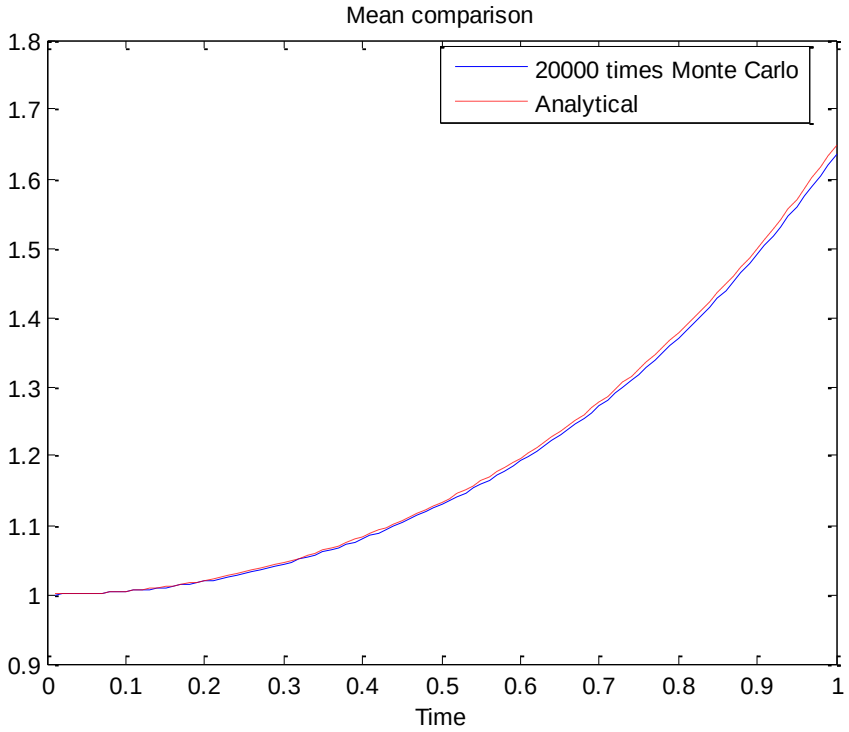

Figure 3-5 Mean comparison between analytical solution and 20000 times Monte Carlo method.

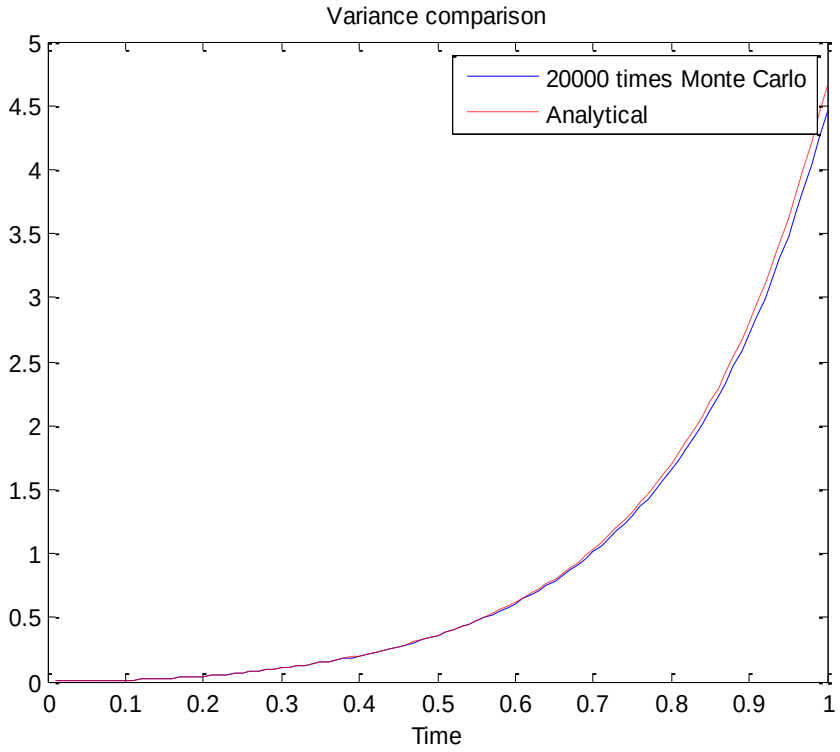

Figure 3-6 Variance comparison between analytical solution and 20000 times Monte Carlo method.

As mentioned in Chapter 1, the MC method has a relatively slow convergence rate.

3.3.3 Perturbation Method

The perturbation method is based on Taylor expansion. From the analytical solution,

$$y(k,t) = e^{-kt}, \tag{3.12}$$

the first three Taylor expansion coefficients around $\bar{k} = 0$ can be obtained:

$$y(\bar{k},t) = e^{-kt}\,|_{k=0} = 1, \tag{3.13}$$

$$y'(\bar{k},t) = (-te^{-kt})\,|_{k=0} = -t, \tag{3.14}$$

$$y''(\bar{k},t) = (t^2 e^{-kt})\,|_{k=0} = t^2. \tag{3.15}$$

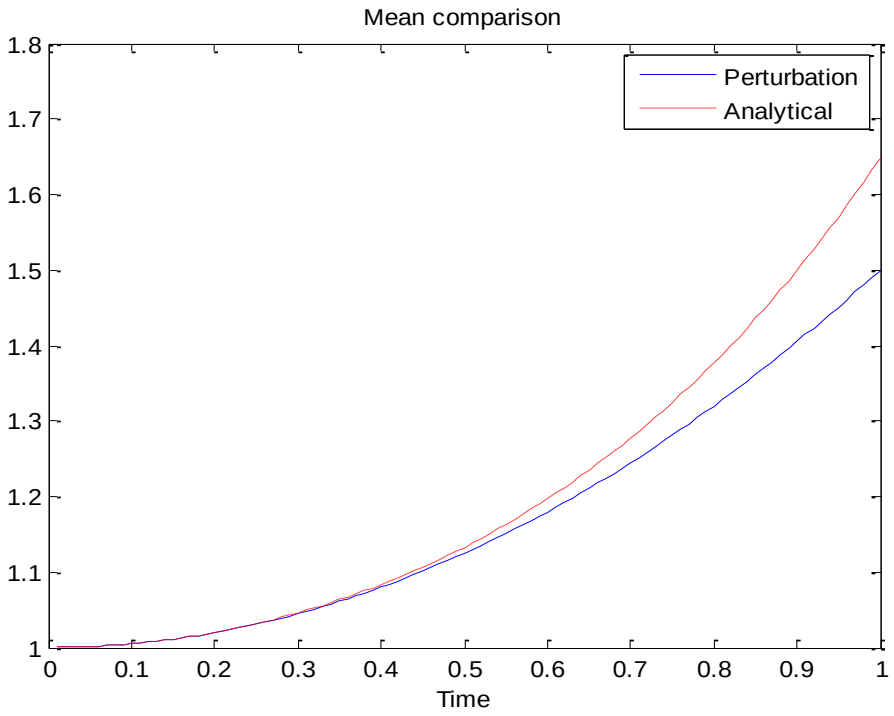

Figure 3-7 Mean comparison between analytical solution and second order perturbation method.

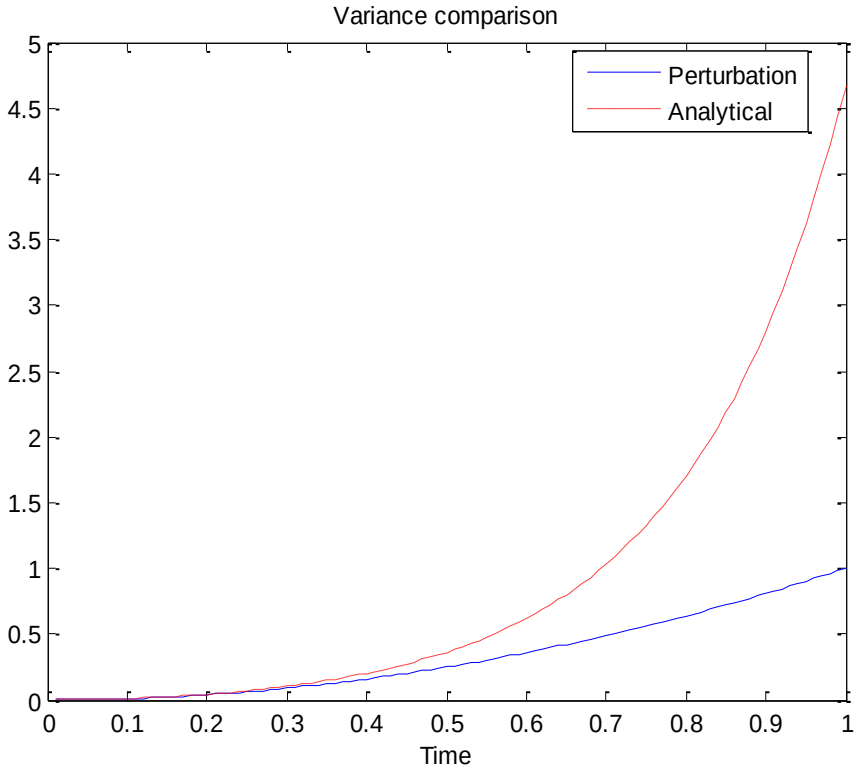

Figure 3-8 Variance comparison between analytical solution and second order perturbation method.

The output mean and variance can be approximated by

$$\overline{y(k,t)} \approx y(\bar{k},t) + y''(\bar{k},t)\left(\frac{\sigma_k^2}{2}\right) + \frac{t^2}{2}, \text{ and} \tag{3.16}$$

$$\sigma_{y(k,t)}^2 \approx \left|y'(\bar{k},t)\right|^2 \sigma_k^2 = t^2. \tag{3.17}$$

As we can see from Figures 3-7 and 3-8, the statistics using the second order perturbation method are pretty unfavorable compared to the analytical solution. This is mainly due to the large variation of the *k* parameter around its mean value.

3.3.4 General polynomial chaos method

According to the gPC method, we can expand the solution $y(t)$ and the random variable k using the polynomial basis $\{\Phi_i\}_{i=0}^{\infty}$, truncated at order of P.

$$y(t) = \sum_{i=0}^{P} y_i(t)\Phi_i(k), \text{ and} \tag{3.18}$$

$$k = \sum_{i=0}^{P} k_i \Phi_i(k), \tag{3.19}$$

where $y_i(t)|_{i=0,1,\cdots,P}$ are the coefficients for the stochastic solution $y(t)$, and $k_i|_{i=0,1,\cdots,P}$ are the coefficients for the random parameter *k*. Since *k* has normal distribution, so the corresponding polynomial basis is Hermite polynomials, of which the first five polynomials are shown in (3.20).

$$\begin{cases} \Phi_0(k) = 1 \\ \Phi_1(k) = k \\ \Phi_2(k) = k^2 - 1 \\ \Phi_3(k) = k^3 - 3k \\ \Phi_4(k) = k^4 - 6k^2 + 3 \end{cases}. \tag{3.20}$$

Plug (3.18) and (3.19) into (3.4),

$$\sum_{i=0}^{P}\frac{dy_i(t)}{dt}\Phi_i=-\sum_{i=0}^{P}k_i\Phi_i\sum_{j=0}^{P}y_j(t)\Phi_i=-\sum_{i=0}^{P}\sum_{j=0}^{P}k_iy_j(t)\Phi_i\Phi_j. \tag{3.21}$$

To solve the *Nth* coefficient $y_N(t)$, multiply the *Nth* order polynomial Φ_N, and take the inner product on both sides,

$$\left\langle\Phi_N^2\right\rangle\frac{dy_N(t)}{dt}=-\sum_{i=0}^{P}\sum_{j=0}^{P}k_iy_j(t)\left\langle\Phi_i\Phi_j\Phi_N\right\rangle. \tag{3.22}$$

Divide $\left\langle\Phi_N^2\right\rangle$ on both sides, and it yields

$$\frac{dy_N(t)}{dt}=-\frac{1}{\left\langle\Phi_N^2\right\rangle}\sum_{i=0}^{P}\sum_{j=0}^{P}k_iy_j(t)\left\langle\Phi_i\Phi_j\Phi_N\right\rangle. \tag{3.23}$$

For Hermite polynomials, inner products have an analytical solution as in (3.24) and (3.25),

$$\left\langle\Phi_N^2\right\rangle=N!\qquad N=0,1\ldots\ldots,\ P, \tag{3.24}$$

$$\left\langle\Phi_i\Phi_j\Phi_N\right\rangle=\frac{i!\,j!N!}{(s-i)!(s-j)!(s-N)!} \tag{3.25}$$
$0\le i,\ j,N\le s$ and $2s=i+j+k$ is an even number.

Let the highest order *P*=4, and the expansion coefficient of *k* is given in (3.26),

$$k_i=\frac{\left\langle k\Phi_i\right\rangle}{\left\langle\Phi_i^2\right\rangle}=\begin{cases}k_1=1\\k_0=k_2=k_3=k_4=0\end{cases}, \tag{3.26}$$

and the initial value for $y_i(t)|_{i=0,1,2,3,4}$ is obtained in (3.27)

$$\begin{aligned}&y|_{t=0}=\sum_{i=0}^{4}y_i|_{t=0}\Phi_i(k)=1\\&\Rightarrow\begin{cases}y_0|_{t=0}=1\\y_1|_{t=0}=y_2|_{t=0}=y_3|_{t=0}=y_4|_{t=0}=0.\end{cases}\end{aligned} \tag{3.27}$$

Thus the original ODE becomes a five-coupled initial value problem with explicit updating equations as in (3.28). For each updating equation in (3.28), the Euler method is

used to solve the expansion coefficient.

$$\begin{cases} \dfrac{dy_0(t)}{dt} = -\dfrac{1}{\left\langle \Phi_0^2 \right\rangle} \sum_{i=0}^{4}\sum_{j=0}^{4} k_i y_j(t) \left\langle \Phi_i \Phi_j \Phi_0 \right\rangle \\ \dfrac{dy_1(t)}{dt} = -\dfrac{1}{\left\langle \Phi_1^2 \right\rangle} \sum_{i=0}^{4}\sum_{j=0}^{4} k_i y_j(t) \left\langle \Phi_i \Phi_j \Phi_1 \right\rangle \\ \dfrac{dy_2(t)}{dt} = -\dfrac{1}{\left\langle \Phi_2^2 \right\rangle} \sum_{i=0}^{4}\sum_{j=0}^{4} k_i y_j(t) \left\langle \Phi_i \Phi_j \Phi_2 \right\rangle \\ \dfrac{dy_3(t)}{dt} = -\dfrac{1}{\left\langle \Phi_3^2 \right\rangle} \sum_{i=0}^{4}\sum_{j=0}^{4} k_i y_j(t) \left\langle \Phi_i \Phi_j \Phi_3 \right\rangle \\ \dfrac{dy_4(t)}{dt} = -\dfrac{1}{\left\langle \Phi_4^2 \right\rangle} \sum_{i=0}^{4}\sum_{j=0}^{4} k_i y_j(t) \left\langle \Phi_i \Phi_j \Phi_4 \right\rangle \end{cases}, \tag{3.28}$$

After all the coefficients have been solved, the mean value and variance can be computed by (3.29) and (3.30). It indicates that the mean value of the gPC method is equal to the zero-order expansion coefficient. and the square summation of all the high order expansion coefficients yields the variance of the stochastic solution,

$$E[y(t)] = y_1(t), \tag{3.29}$$

$$Var[y(t)] = \sum_{i=1}^{4} \left\langle \Phi_N^2 \right\rangle y_i^2(t). \tag{3.30}$$

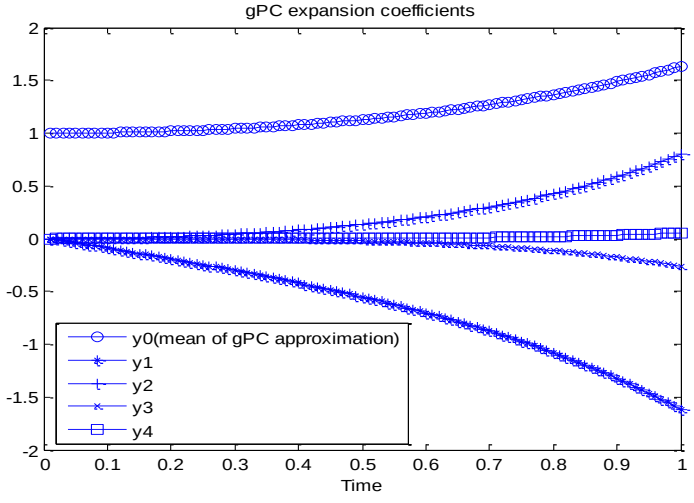

Figure 3-9 Solutions of the first five gPC expansion coefficients.

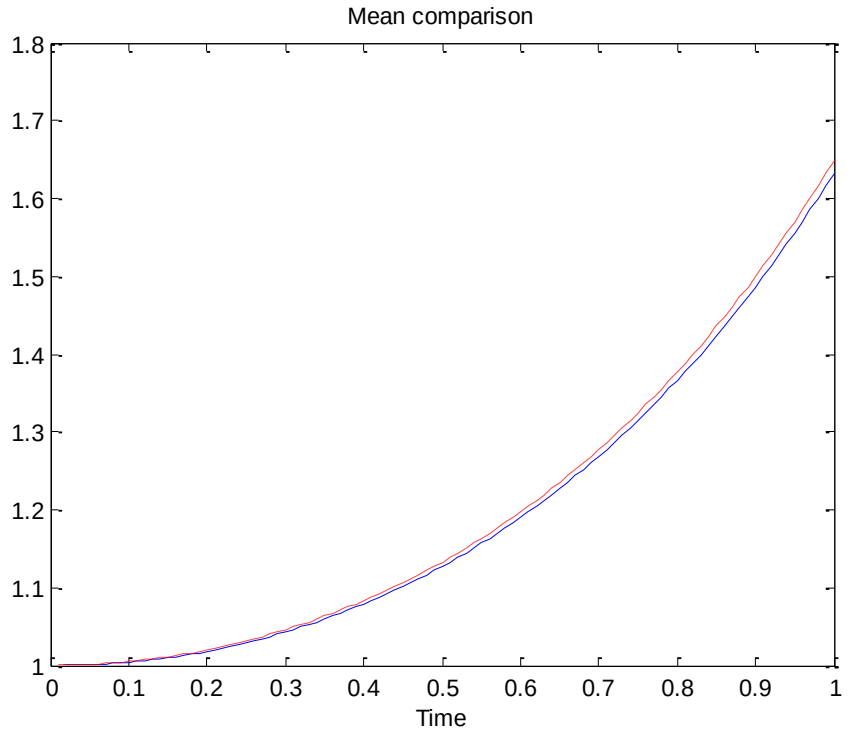

Figure 3-10 Mean comparison between analytical solution and generalized polynomial chaos method.

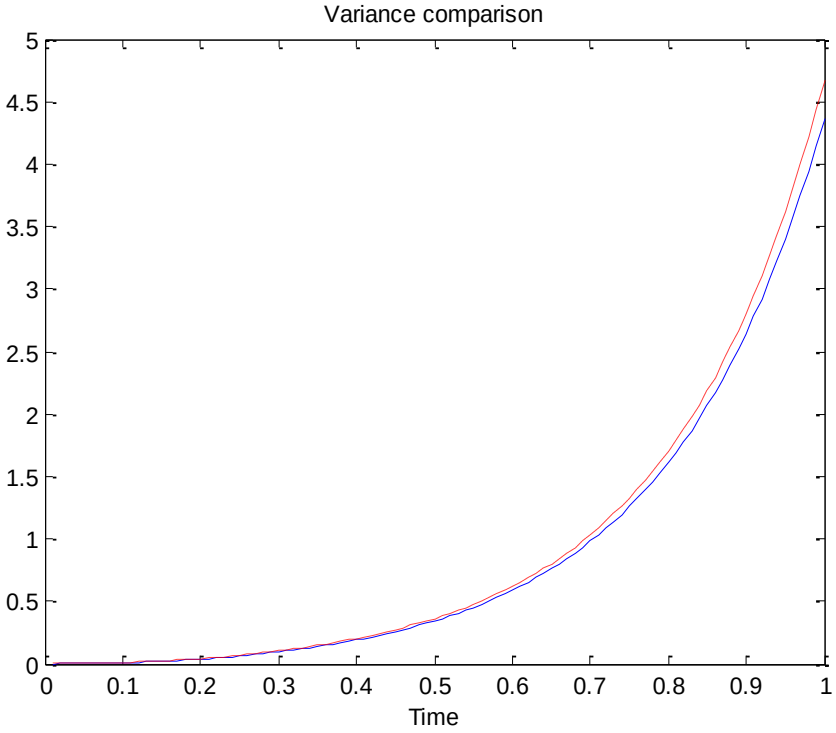

Figure 3-11 Variance comparison between analytical solution and generalized polynomial chaos method.

The results for the expansion coefficients are shown in Figure 3-9. And the mean and variance comparison are shown in Figures 3-10 and 3-11. As we can see, the mean and variance predicted by the gPC method are pretty close to the analytical solutions. Furthermore, the expansion coefficients are solved simultaneously, which reduces the total computation time compared to the MC method.

3.3.5 Stochastic collocation method

The idea of the stochastic collocation method is to sample the random input in a much more efficient way than the brute force of the MC method. In this 1-D problem, the well-known Gaussian quadrature rule can be applied. Table 3-1 shows the data of random input *k* and corresponding weights by the 7-point Gaussian quadrature rule.

Table 3-1 7-point Gaussian quadrature rule

index	inputs	weights
1	-2.6519613568352334e+000	9.7178124509951914e-004
2	-1.6735516287674714e+000	5.4515582819127030e-002
3	-8.1628788285896470e-001	4.2560725261012777e-001
4	0.0000000000000000e+000	8.1026461755680734e-001
5	8.1628788285896470e-001	4.2560725261012777e-001
6	1.6735516287674714e+000	5.4515582819127030e-002
7	2.6519613568352334e+000	9.7178124509951914e-004

Mean and variance can be computed by (3.31) and (3.32),

$$\text{Mean} = \frac{1}{\sqrt{\pi}} \sum_{i=1}^{7} \text{weight}(i) \times e^{-k_i t} , \tag{3.31}$$

$$\text{Variance} = \frac{1}{\sqrt{\pi}} \sum_{i=1}^{7} \text{weight}(i) \times (e^{-k_i t} - \text{Mean})^2 . \tag{3.32}$$

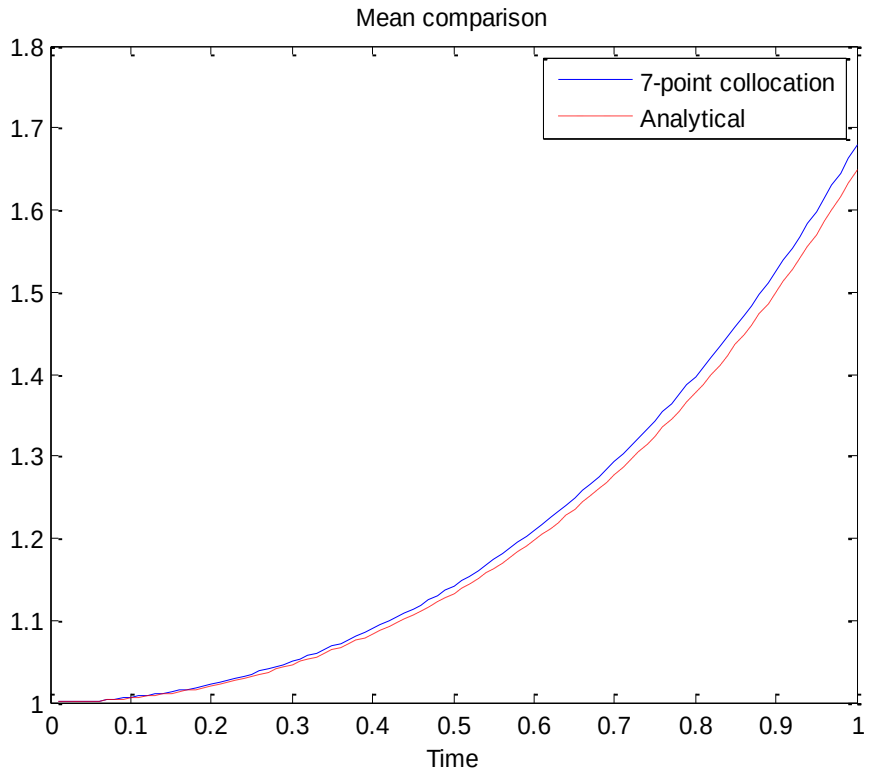

Figure 3-12 Mean comparison between analytical solution and 1-D collocation method.

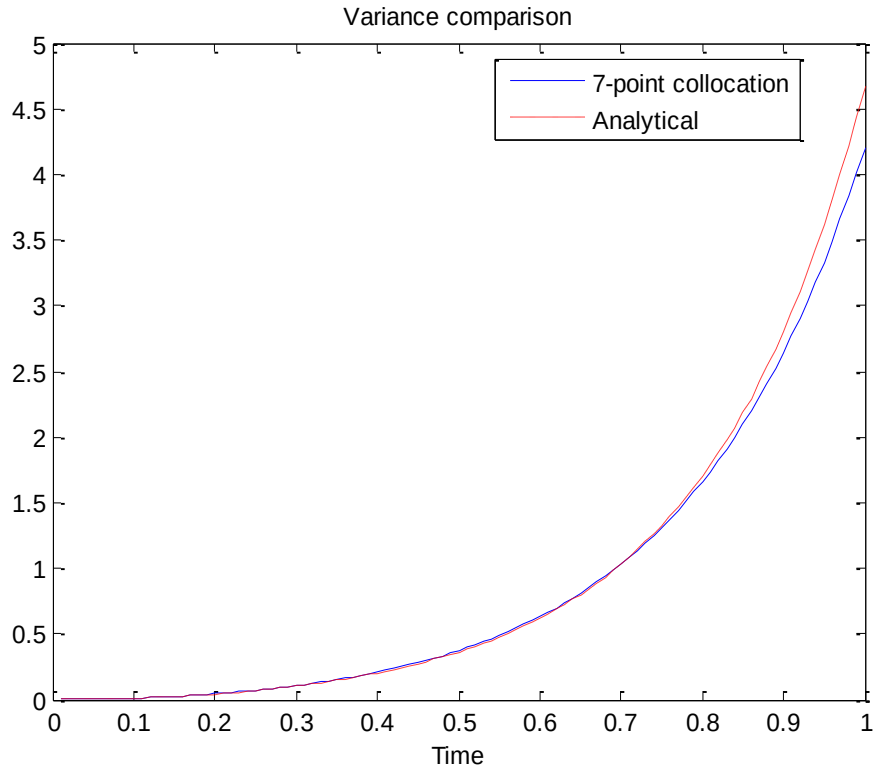

Figure 3-13 Variance comparison between analytical solution and 1-D collocation method.

The term "$\frac{1}{\sqrt{\pi}}$" in the front of (3.31) and (3.32) is a normalized factor for 1-D Gaussian random variables. Figures 3-12 and 3-13 show the comparison results. Good agreements are achieved with only a small number of simulations. This is a tremendous advantage compared to the MC method, which requires thousands of simulations.

3.3.5 Summary

From the above comparison results, it is easy to summarize the advantages of gPC method and stochastic collocation method. For the gPC method, it only requires one single simulation to solve the expansion coefficients; for the stochastic collocation method, only a small number of simulations are required to achieve certain accuracy. Both of these two methods are more efficient than the MC method. In Chapter 4, the stochastic Galerkin scheme based on the gPC method is discussed. In Chapter 5, the stochastic collocation scheme based on multi-dimensional sparse grid method is investigated.

Chapter 4 Stochastic Galerkin Scheme: An intrusive approach using the gPC method

4.1 General procedure

When applying the generalized polynomial chaos (gPC) method to practical problems with random inputs, the quantities to be solved are the expansion coefficients of the gPC expansion. A typical approach is to conduct a Galerkin projection to a finite-order gPC truncation, and the resulting set of equations for the expansion coefficients are deterministic and can be solved via conventional numerical techniques. This is the Stochastic Galerkin scheme [26][34][35][37] and has been proved to be effective. This section will have a detailed discussion about this with numerical examples.

Consider a system PDE defined in a spatial domain $D \subset R^d, d = 1,2,3$, and a time domain $[t_0, T]$

$$\begin{cases} L(u(x,t,\xi)) = f(x,t,\xi) & x \in D, t \in (t_0, T], \xi \in \Omega \\ B(u(x,t,\xi)) = 0 & x \in \partial D, t \in (t_0, T], \xi \in \Omega, \\ u(x,t_0,\xi) = u_0 & \xi \in \Omega \end{cases} \tag{4.1}$$

where L is a differential operator, B is the boundary condition operator, u_0 is the initial condition, and $\xi = (\xi_1, \xi_2, \cdots, \xi_d) \in R^d, d = 1,2,3$ are a set of mutually independent random variables characterizing the random inputs to the governing equation with a probability density function of $\rho(\xi)$.

Let $\{\Phi_k(\xi)\}_{i=0}^{\infty}$ be the gPC basis functions which are orthogonal to each other, so

that

$$E[\Phi_i(\xi)\Phi_i(\xi)] = \left\|\Phi_i(\xi)\right\|^2 \delta_{ij}. \tag{4.2}$$

$E[\cdot]$ is the expectation of a quantity of random ξ, which is defined as

$$E[f(\xi)] = \int f(\xi)\rho(\xi)d\xi, \tag{4.3}$$

and let $\Gamma_N^d(Z)$ be the space of all polynomials of $Z \in R^d$ of a degree up to *N*. Then the gPC projection of the stochastic solution can be approximated by

$$u(x,t,\xi) \approx u_N(x,t,\xi) = \sum_{i=o}^{N} u_i(x,t)\Phi_i(\xi), \tag{4.4}$$

$$u_i(x,t) = \frac{1}{\left\|\Phi_i(\xi)\right\|^2} E[u_N(x,t,\xi)\Phi_i(\xi)]. \tag{4.5}$$

Substitute (4.4) into (4.1),

$$\begin{cases} L(\sum_{i=o}^{N} u_i(x,t)\Phi_i(\xi)) = f(x,t,\xi) \\ B(\sum_{i=o}^{N} u_i(x,t)\Phi_i(\xi)) = 0 \\ \sum_{i=o}^{N} u_i(x,t_0)\Phi_i(\xi) = u_0 \end{cases}. \tag{4.6}$$

Then apply the orthogonality of the polynomial basis, and we seek to solve the weak form of Equation (4.7), which becomes

$$\begin{cases} E[L(u_k(x,t))\Phi_k(\xi)] = E[f(x,t,\xi),\Phi_k(\xi)] \\ E[B(u_k(x,t))] = 0 \\ u_k(x,t_0) = u_{0,k} \end{cases}, \tag{4.7}$$

where $u_{0,k}$ are the gPC projection coefficients for the initial conditions, given in (4.8)

$$u_{0,k} = \frac{E[u_0 \Phi_k(\xi)]}{\left\|\Phi_k(\xi)\right\|^2}. \tag{4.8}$$

We can see from (4.7) that the expectations on both sides make the dependence in ξ disappear. The result is then a system of deterministic equations (usually coupled). The size of the system is

$$\dim \Gamma_N^d = \frac{(N+d)!}{N!d!}. \tag{4.9}$$

After solving (4.7), we can get N+1 expansion coefficients. Following the mathematical definition, the statistics can be obtained by

$$E[u(x,t,\xi)] = \int \sum_{i=0}^{N} u_i(x,t)\Phi_i(\xi)\rho(\xi)d\xi = u_0(x,t), \text{ and} \tag{4.10}$$

$$Var[u(x,t,\xi] = E[(\sum_{i=0}^{N} u_i(x,t)\Phi_i(\xi) - E[u(x,t,\xi)])^2] = \sum_{i=1}^{N} [u_i(x,t)]^2. \tag{4.11}$$

4.2 Implementation gPC into FDTD

This section demonstrates how the gPC method can be implemented into the FDTD formulation of Maxwell equations. Two curl operators as in (4.12) will become six scalar functions in (4.13)

$$\begin{cases} \nabla \times \vec{E} = -\mu \dfrac{\partial \vec{E}}{\partial t} \\ \nabla \times \vec{H} = \sigma \vec{E} + \varepsilon \dfrac{\partial \vec{E}}{\partial t} \end{cases}, \tag{4.12}$$

$$\begin{cases} \dfrac{\partial H_x}{\partial t} = \dfrac{1}{\mu}\left(\dfrac{\partial E_y}{\partial z} - \dfrac{\partial E_z}{\partial y}\right) \\ \dfrac{\partial H_y}{\partial t} = \dfrac{1}{\mu}\left(\dfrac{\partial E_z}{\partial x} - \dfrac{\partial E_x}{\partial z}\right) \\ \dfrac{\partial H_z}{\partial t} = \dfrac{1}{\mu}\left(\dfrac{\partial E_x}{\partial y} - \dfrac{\partial E_y}{\partial x}\right) \\ \dfrac{\partial E_x}{\partial t} = \dfrac{1}{\varepsilon}\left(\dfrac{\partial H_z}{\partial y} - \dfrac{\partial H_y}{\partial z} - \sigma E_x\right) \\ \dfrac{\partial E_y}{\partial t} = \dfrac{1}{\varepsilon}\left(\dfrac{\partial H_x}{\partial z} - \dfrac{\partial H_z}{\partial x} - \sigma E_y\right) \\ \dfrac{\partial E_z}{\partial t} = \dfrac{1}{\varepsilon}\left(\dfrac{\partial H_y}{\partial x} - \dfrac{\partial H_x}{\partial y} - \sigma E_z\right) \end{cases} . \tag{4.13}$$

In FDTD modeling, we usually include electric flux density (*D*) and magnetic flux density (*B*) in the updating equations, since it is easier to formulate by introducing them. Their relationship to the electric intensity (*E*) and the magnetic intensity (*H*) is shown in (4.14)

$$\begin{cases} \vec{D} = \overline{\overline{\varepsilon}}\vec{E} \\ \vec{B} = \overline{\overline{\mu}}\vec{H} \end{cases} . \tag{4.14}$$

For the discretization in the FDTD method, Figure 4-1 shows how the electric and magnetic fields are placed alternatively in a Yee's FDTD grid [29]. As we can see, the electric fields are sampled at the center of every edge on each cell, and the magnetic field values are sampled at the center of each cell's faces. Following the notation as in [2], any function of both space and time is denoted as

$$f^n(i, j, k) = (i\Delta x, j\Delta y, k\Delta z, n\Delta t), \tag{4.15}$$

where Δx, Δy and Δz are the spatial steps in the x, y, z directions, respectively, and Δt is the time step. In order to achieve second-order accuracy, the central difference

approximation is applied

$$\frac{\partial f(x)}{\partial x} = \frac{f(x+\frac{\Delta x}{2}) - f(x-\frac{\Delta x}{2})}{\Delta x} + O([\Delta x]^2) . \tag{4.16}$$

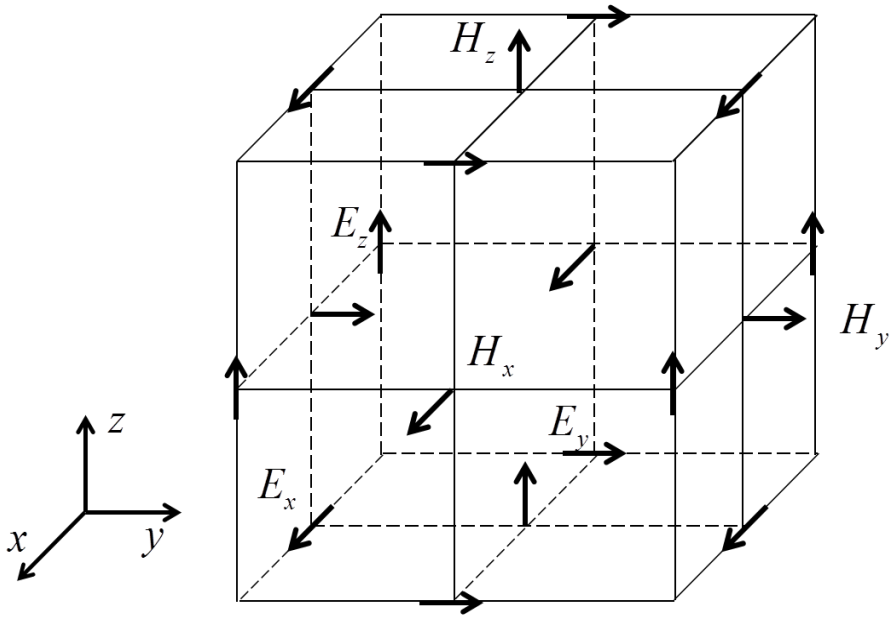

Figure 4-1 Yee's FDTD grid.

In the FDTD method, electric and magnetic fields are sampled alternatively both in space and time, and the central difference approximation in space and time are shown in (4.17) and (4.18), respectively

$$\frac{\partial f^n(i,j,k)}{\partial x} \approx \frac{f^n(i+\frac{1}{2},j,k) - f^n(i-\frac{1}{2},j,k)}{\Delta x} , \tag{4.17}$$

$$\frac{\partial f^n(i,j,k)}{\partial t} \approx \frac{f^{n+\frac{1}{2}}(i,j,k) - f^{n-\frac{1}{2}}(i,j,k)}{\Delta t} . \tag{4.18}$$

Then (4.13) can be written in the discrete forms as from (4.19) to (4.36).

$$D_x^{n+1}(i+\frac{1}{2},j,k)=C_{1x}\cdot D_x^n(i+\frac{1}{2},j,k)+C_{2x}\cdot(\frac{H_z^{n+\frac{1}{2}}(i+\frac{1}{2},j+\frac{1}{2},k)-H_z^{n+\frac{1}{2}}(i+\frac{1}{2},j-\frac{1}{2},k)}{\Delta y}-C_{2x}\cdot(\frac{H_y^{n+\frac{1}{2}}(i+\frac{1}{2},j,k+\frac{1}{2})-H_y^{n+\frac{1}{2}}(i+\frac{1}{2},j,k-\frac{1}{2})}{\Delta z}) \quad (4.19)$$

$$E_x^{n+1}(i+\frac{1}{2},j,k)=C_{3x}\cdot E_x^n(i+\frac{1}{2},j,k)+C_{4x}\cdot(C_{5x}\cdot D_x^{n+1}(i+\frac{1}{2},j,k)-C_{6x}\cdot D_x^n(i+\frac{1}{2},j,k)) \quad (4.20)$$

$$B_x^{n+\frac{1}{2}}(i,j+\frac{1}{2},k+\frac{1}{2})=D_{1x}\cdot B_x^{n-\frac{1}{2}}(i,j+\frac{1}{2},k+\frac{1}{2})-D_{2x}\cdot(\frac{E_z^n(i,j+1,k+\frac{1}{2})-E_z^n(i,j,k+\frac{1}{2})}{\Delta y})+D_{2x}(\frac{E_y^n(i,j+\frac{1}{2},k+1)-E_y^n(i,j+\frac{1}{2},k)}{\Delta z}) \quad (4.21)$$

$$H_x^{n+\frac{1}{2}}(i,j+\frac{1}{2},k+\frac{1}{2})=H_x^{n-\frac{1}{2}}(i,j+\frac{1}{2},k+\frac{1}{2})+D_{4x}\cdot(D_{5x}\cdot B_x^{n+\frac{1}{2}}(i,j+\frac{1}{2},k+\frac{1}{2})-D_{6x}\cdot B_x^{n-\frac{1}{2}}(i,j+\frac{1}{2},k+\frac{1}{2})) \quad (4.22)$$

where

$$C_{1x}=\frac{2\varepsilon-\sigma_y\Delta t}{2\varepsilon+\sigma_y\Delta t},C_{2x}=\frac{2\varepsilon\Delta t}{2\varepsilon+\sigma_y\Delta t}$$

$$C_{3x}=\frac{2\varepsilon-\sigma_z\Delta t}{2\varepsilon+\sigma_z\Delta t},C_{4x}=\frac{1}{2\varepsilon+\sigma_z\Delta t} \quad (4.23)$$

$$C_{5x}=2\varepsilon+\sigma_x\Delta t,C_{6x}=2\varepsilon-\sigma_x\Delta t$$

and

$$D_{1x} = \frac{2\varepsilon - \sigma_y \Delta t}{2\varepsilon + \sigma_y \Delta t}, D_{2x} = \frac{2\varepsilon \Delta t}{2\varepsilon + \sigma_y \Delta t}$$

$$D_{3x} = \frac{2\varepsilon - \sigma_z \Delta t}{2\varepsilon + \sigma_z \Delta t}, D_{4x} = \frac{1}{(2\varepsilon + \sigma_z \Delta t)\mu} \quad , \tag{4.24}$$

$$D_{5x} = 2\varepsilon + \sigma_x \Delta t, D_{6x} = 2\varepsilon - \sigma_x \Delta t$$

$$\begin{aligned} D_y^{n+1}(i, j+\frac{1}{2}, k) &= C_{1y} \cdot D_y^n(i, j+\frac{1}{2}, k) \\ &+ C_{2y} \cdot (\frac{H_x^{n+\frac{1}{2}}(i, j+\frac{1}{2}, k+\frac{1}{2}) - H_x^{n+\frac{1}{2}}(i, j+\frac{1}{2}, k-\frac{1}{2})}{\Delta z} \\ &- C_{2y} \cdot (\frac{H_z^{n+\frac{1}{2}}(i+\frac{1}{2}, j+\frac{1}{2}, k) - H_z^{n+\frac{1}{2}}(i-\frac{1}{2}, j+\frac{1}{2}, k)}{\Delta x}) \end{aligned} \quad , \tag{4.25}$$

$$\begin{aligned} E_y^{n+1}(i, j+\frac{1}{2}, k) &= C_{3y} \cdot E_y^n(i, j+\frac{1}{2}, k) \\ &+ C_{4y} \cdot (C_{5y} \cdot D_y^{n+1}(i, j+\frac{1}{2}, k) - C_{6y} \cdot D_y^n(i, j+\frac{1}{2}, k)) \end{aligned} \quad , \tag{4.26}$$

$$\begin{aligned} B_y^{n+\frac{1}{2}}(i+\frac{1}{2}, j, k+\frac{1}{2}) &= D_{1y} \cdot B_y^{n-\frac{1}{2}}(i+\frac{1}{2}, j, k+\frac{1}{2}) \\ &- D_{2y} \cdot (\frac{E_x^n(i+\frac{1}{2}, j, k+1) - E_x^n(i+\frac{1}{2}, j, k)}{\Delta z}) \\ &+ D_{2y} (\frac{E_z^n(i+1, j, k+\frac{1}{2}) - E_z^n(i, j, k+\frac{1}{2})}{\Delta x}) \end{aligned} \quad , \tag{4.27}$$

$$\begin{aligned} H_y^{n+\frac{1}{2}}(i+\frac{1}{2}, j, k+\frac{1}{2}) &= H_y^{n-\frac{1}{2}}(i+\frac{1}{2}, j, k+\frac{1}{2}) \\ &+ D_{4y} \cdot (D_{5y} \cdot B_y^{n+\frac{1}{2}}(i+\frac{1}{2}, j, k+\frac{1}{2}) - D_{6y} \cdot B_y^{n-\frac{1}{2}}(i+\frac{1}{2}, j, k+\frac{1}{2})) \end{aligned} \quad , \tag{4.28}$$

where

$$C_{1y} = \frac{2\varepsilon - \sigma_z \Delta t}{2\varepsilon + \sigma_z \Delta t}, C_{2y} = \frac{2\varepsilon \Delta t}{2\varepsilon + \sigma_z \Delta t}$$

$$C_{3y} = \frac{2\varepsilon - \sigma_x \Delta t}{2\varepsilon + \sigma_x \Delta t}, C_{4y} = \frac{1}{2\varepsilon + \sigma_x \Delta t} \quad , \tag{4.29}$$

$$C_{5y} = 2\varepsilon + \sigma_y \Delta t, C_{6y} = 2\varepsilon - \sigma_y \Delta t$$

and

$$D_{1y} = \frac{2\varepsilon - \sigma_z \Delta t}{2\varepsilon + \sigma_z \Delta t}, D_{2y} = \frac{2\varepsilon \Delta t}{2\varepsilon + \sigma_z \Delta t}$$

$$D_{3y} = \frac{2\varepsilon - \sigma_x \Delta t}{2\varepsilon + \sigma_x \Delta t}, D_{4y} = \frac{1}{(2\varepsilon + \sigma_x \Delta t)\mu}, \tag{4.30}$$

$$D_{5y} = 2\varepsilon + \sigma_y \Delta t, D_{6y} = 2\varepsilon - \sigma_y \Delta t$$

$$\begin{aligned} D_z^{n+1}(i, j, k+\frac{1}{2}) &= C_{1z} \cdot D_z^n(i, j, k+\frac{1}{2}) \\ &+ C_{2z} \cdot (\frac{H_y^{n+\frac{1}{2}}(i+\frac{1}{2}, j, k+\frac{1}{2}) - H_y^{n+\frac{1}{2}}(i-\frac{1}{2}, j, k+\frac{1}{2})}{\Delta x} \\ &- C_{2z} \cdot (\frac{H_x^{n+\frac{1}{2}}(i, j+\frac{1}{2}, k+\frac{1}{2}) - H_x^{n+\frac{1}{2}}(i, j-\frac{1}{2}, k+\frac{1}{2})}{\Delta y}) \end{aligned} \quad , \tag{4.31}$$

$$\begin{aligned} E_z^{n+1}(i, j, k+\frac{1}{2}) &= C_{3z} \cdot E_z^n(i, j, k+\frac{1}{2}) \\ &+ C_{4z} \cdot (C_{5z} \cdot D_z^{n+1}(i, j, k+\frac{1}{2}) - C_{6z} \cdot D_z^n(i, j, k+\frac{1}{2})) \end{aligned} \quad , \tag{4.32}$$

$$\begin{aligned} B_z^{n+\frac{1}{2}}(i+\frac{1}{2}, jk+\frac{1}{2},) &= D_{1z} \cdot B_z^{n-\frac{1}{2}}(i+\frac{1}{2}, j+\frac{1}{2}, k) \\ &- D_{2z} \cdot (\frac{E_y^n(i+1, j+\frac{1}{2}, k) - E_y^n(i, j+\frac{1}{2}, k)}{\Delta x}) \\ &+ D_{2z} (\frac{E_x^n(i+\frac{1}{2}, j+1, k+\frac{1}{2}) - E_x^n(i+\frac{1}{2}, j, k)}{\Delta y}) \end{aligned} \quad , \tag{4.33}$$

$$H_z^{n+\frac{1}{2}}(i+\frac{1}{2}, j+\frac{1}{2}, k) = H_z^{n-\frac{1}{2}}(i+\frac{1}{2}, j+\frac{1}{2}, k) + D_{4z} \cdot (D_{5z} \cdot B_z^{n+\frac{1}{2}}(i+\frac{1}{2}, j+\frac{1}{2}, k) - D_{6z} \cdot B_z^{n-\frac{1}{2}}(i+\frac{1}{2}, j+\frac{1}{2}, k)) \quad , (4.34)$$

where

$$C_{1z} = \frac{2\varepsilon - \sigma_x \Delta t}{2\varepsilon + \sigma_x \Delta t}, C_{2z} = \frac{2\varepsilon \Delta t}{2\varepsilon + \sigma_x \Delta t}$$

$$C_{3z} = \frac{2\varepsilon - \sigma_y \Delta t}{2\varepsilon + \sigma_y \Delta t}, C_{4z} = \frac{1}{2\varepsilon + \sigma_y \Delta t}, \quad (4.35)$$

$$C_{5z} = 2\varepsilon + \sigma_z \Delta t, C_{6z} = 2\varepsilon - \sigma_z \Delta t$$

and

$$D_{1z} = \frac{2\varepsilon - \sigma_x \Delta t}{2\varepsilon + \sigma_x \Delta t}, D_{2z} = \frac{2\varepsilon \Delta t}{2\varepsilon + \sigma_x \Delta t}$$

$$D_{3z} = \frac{2\varepsilon - \sigma_y \Delta t}{2\varepsilon + \sigma_y \Delta t}, D_{4z} = \frac{1}{(2\varepsilon + \sigma_y \Delta t)\mu}. \quad (4.36)$$

$$D_{5z} = 2\varepsilon + \sigma_z \Delta t, D_{6z} = 2\varepsilon - \sigma_z \Delta t$$

In the following derivation, only the x components of *E*, *H*, *D*, *B* are listed; y and z components can be formulated in the same manner. In this chapter, we consider the relative permittivity of the medium as a random variable. We can expand the permittivity, electric and magnetic intensity, and electric and magnetic flux density using the same polynomial basis Φ_i, truncated at the order of P, as shown in (4.37).

$$\begin{aligned} \varepsilon_r &= \sum_{m=0}^{P} \varepsilon_i \Phi_i, \\ E_L &= \sum_{m=0}^{P} e_{Li} \Phi_i, D_L = \sum_{m=0}^{P} d_{Li} \Phi_i \qquad L = x, y, z. \\ H_L &= \sum_{m=0}^{P} h_{Li} \Phi_i, B_L = \sum_{m=0}^{P} b_{Li} \Phi_i \end{aligned} \quad (4.37)$$

Substituting (4.31) into (4.13) - (4.16) yields

$$\sum_{m=0}^{P} d_x^{n+1}(i+\frac{1}{2},j,k)\ \Phi_m = C_{1x}\cdot\sum_{m=0}^{P} d_x^{n}(i+\frac{1}{2},j,k)\ \Phi_m + C_{2x}\cdot\left(\frac{\sum_{m=0}^{P} h_z^{n+\frac{1}{2}}(i+\frac{1}{2},j+\frac{1}{2},k)\Phi_m - \sum_{m=0}^{P} h_z^{n+\frac{1}{2}}(i+\frac{1}{2},j-\frac{1}{2},k)\Phi_m}{\Delta y}\right), \quad (4.38)$$
$$- C_{2x}\cdot\left(\frac{\sum_{m=0}^{P} h_y^{n+\frac{1}{2}}(i+\frac{1}{2},j,k+\frac{1}{2})\Phi_m - \sum_{m=0}^{P} h_y^{n+\frac{1}{2}}(i+\frac{1}{2},j,k-\frac{1}{2})\Phi_m}{\Delta z}\right)$$

$$\sum_{m=0}^{P} e_x^{n+1}(i+\frac{1}{2},j,k)\ \Phi_m = C_{3x}\cdot\sum_{m=0}^{P} e_x^{n}(i+\frac{1}{2},j,k)\ \Phi_m + C_{4x}\cdot C_{5x}\cdot\sum_{m=0}^{P} d_x^{n+1}(i+\frac{1}{2},j,k)\ \Phi_m, \quad (4.39)$$
$$- C_{4x}\cdot C_{6x}\cdot\sum_{m=0}^{P} d_x^{n}(i+\frac{1}{2},j,k)\ \Phi_m$$

$$\sum_{m=0}^{P} b_x^{n+\frac{1}{2}}(i,j+\frac{1}{2},k+\frac{1}{2})\Phi_m = D_{1x}\cdot\sum_{m=0}^{P} b_x^{n-\frac{1}{2}}(i,j+\frac{1}{2},k+\frac{1}{2})\Phi_m - D_{2x}\cdot\left(\frac{\sum_{m=0}^{P} e_z^{n}(i,j+1,k+\frac{1}{2})\Phi_m - \sum_{m=0}^{P} e_z^{n}(i,j,k+\frac{1}{2})\Phi_m}{\Delta y}\right), \quad (4.40)$$
$$+ D_{2x}\cdot\left(\frac{\sum_{m=0}^{P} e_y^{n}(i,j+\frac{1}{2},k+1)\Phi_m - \sum_{m=0}^{P} e_y^{n}(i,j+\frac{1}{2},k)\Phi_m}{\Delta z}\right)$$

$$\sum_{m=0}^{P} h_x^{n+\frac{1}{2}}(i,j+\frac{1}{2},k+\frac{1}{2})\Phi_m = D_{3x}\cdot\sum_{m=0}^{P} h_x^{n+\frac{1}{2}}(i,j+\frac{1}{2},k+\frac{1}{2})\Phi_m + D_{4x}\cdot D_{5x}\cdot\sum_{m=0}^{P} b_x^{n+\frac{1}{2}}(i,j+\frac{1}{2},k+\frac{1}{2})\Phi_m, \quad (4.41)$$
$$- D_{4x}\cdot D_{6x}\cdot\sum_{m=0}^{P} b_x^{n-\frac{1}{2}}(i,j+\frac{1}{2},k+\frac{1}{2})\Phi_m$$

After the gPC projection, the new updating equations are (4.42) - (3.45), where $m = 0,1,\cdots,P$

$$d_{xm}^{n+1} = C_{1x} \cdot d_{xm}^{n} + C_{2x} \cdot \left(\frac{h_{zm}^{n+\frac{1}{2}} - h_{zm}^{n+\frac{1}{2}}}{\Delta y} - \frac{h_{ym}^{n+\frac{1}{2}} - h_{ym}^{n+\frac{1}{2}}}{\Delta z}\right), \tag{4.42}$$

$$e_{xm}^{n+1} = C_{3x} \cdot e_{xm}^{n} + C_{4x} \cdot \sum_{i=0}^{P} \frac{1}{\left\langle \Phi_m^2 \right\rangle} \cdot \left\langle \frac{\Phi_i}{\mu^{\varepsilon} + \sigma^{\varepsilon} \Phi_1}, \Phi_m \right\rangle (C_{5x} \cdot d_{xm}^{n+1} - C_{6x} \cdot d_{xm}^{n}), \tag{4.43}$$

$$b_{xm}^{n+\frac{1}{2}} = D_{1x} \cdot b_{xm}^{n-\frac{1}{2}} - D_{2x} \cdot \left(\frac{e_{zm}^{n} - e_{zm}^{n}}{\Delta y} - \frac{e_{yk}^{n} - e_{ym}^{n}}{\Delta z}\right), \tag{4.44}$$

$$h_{xm}^{n+\frac{1}{2}} = D_{3x} \cdot h_{xm}^{n-\frac{1}{2}} + D_{4x} \cdot (D_{5x} \cdot b_{xm}^{n+\frac{1}{2}} - D_{6x} \cdot b_{xm}^{n-\frac{1}{2}}). \tag{4.45}$$

All $\langle \square \rangle$ terms denote the inner product which can be done by numerical integration as preprocess. As we can see, different expansion coefficients are coupled with each other in the FDTD updating equations. A similar but more general formulation for 1-D FDTD updating with the gPC method is described in [38].

4.3 Numerical Example

4.3.1 Example I: 1D wave propagation in homogeneous medium

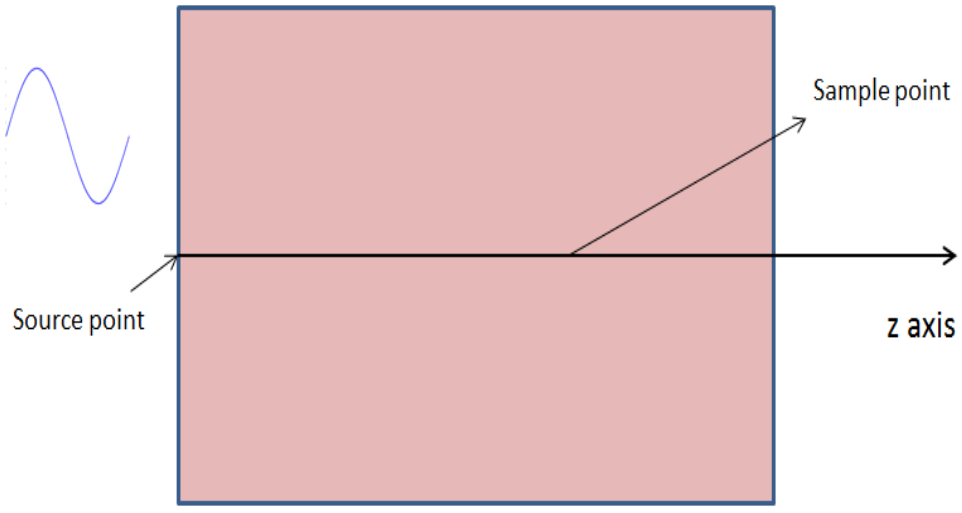

Figure 4-2 1-D wave propagation problem.

The first example is the follow up from the previous derivation as shown in Figure 4-2. A sinusoid wave is travelling along the z axis in a homogeneous medium and the permittivity of the media is set to be a Gaussian variable with a mean of 6.5 and standard deviation of 0.5. The amplitude of the sin wave is unit, and the frequency is 10 MHz. The highest expansion order of the gPC method is 4.

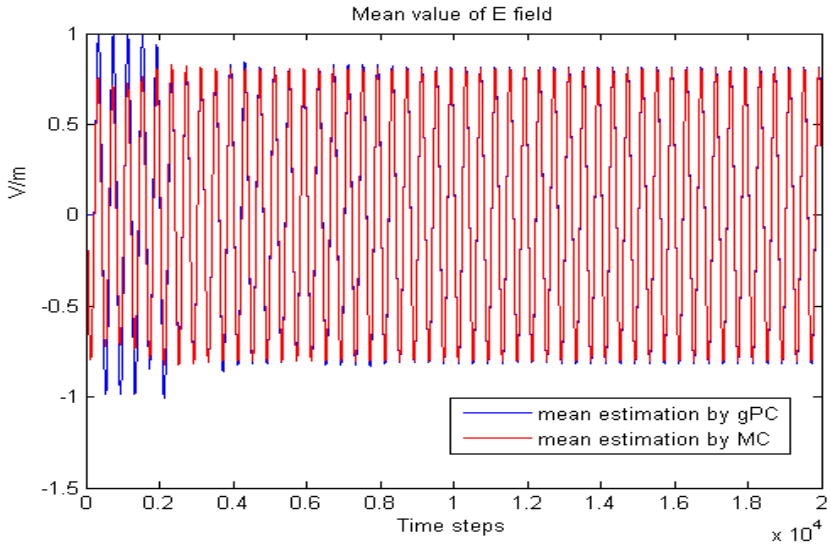

Figure 4-3 Mean value of sampled electric field.

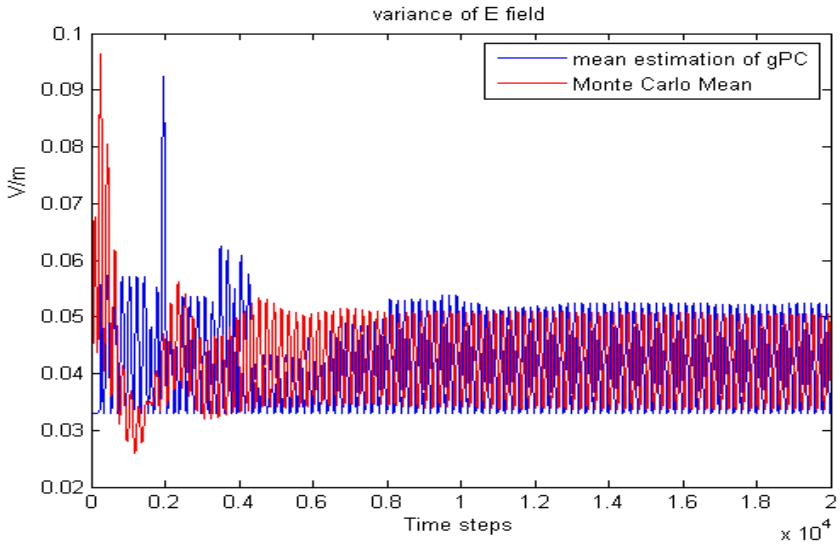

Figure 4-4 Variance of sampled electric field.

Figures 4-3 and 4-4 show the comparison of mean and variance of the sampled electric field predicted by the gPC method and the 1000 times MC method. The percentage errors are calculated based on the peak-to-peak value of the electric field, using the results of the MC method as references.

Table 4-1 shows the percentage error of the gPC method with respect to the number of realizations of the MC method. The percentage errors for both mean and variance become smaller with a larger number of MC simulations. After the MC method reaches its convergence (over 1000 times), the gPC method gives good estimation of the mean and variance of the electric field.

Table 4-1 gPC error estimation with respect to number of MC simulations

Number of realization of MC	Mean percentage error	Variance percentage error
100	2.0%	20.6%
500	1.14%	11.0%
1000	0.23%	3.8%
2000	0.14%	2.5%

4.3.2 Example II: 3D wave propagation in inhomogeneous medium

The second example is a 3-D wave propagation problem as shown in Figure 4-5, and the top view in Figure 4-6. A z-direction polarized sinusoid wave is placed in the middle of an inhomogeneous media. The inhomogeneous media consists of four parts. Each of them has a random permittivity which is set to be a Gaussian variable with mean of μ and standard deviation of σ. The amplitude of the sin wave is unit and the frequency is 1 GHz. The highest expansion order of the gPC method is 3. Outside is

the PML region [39]-[41].

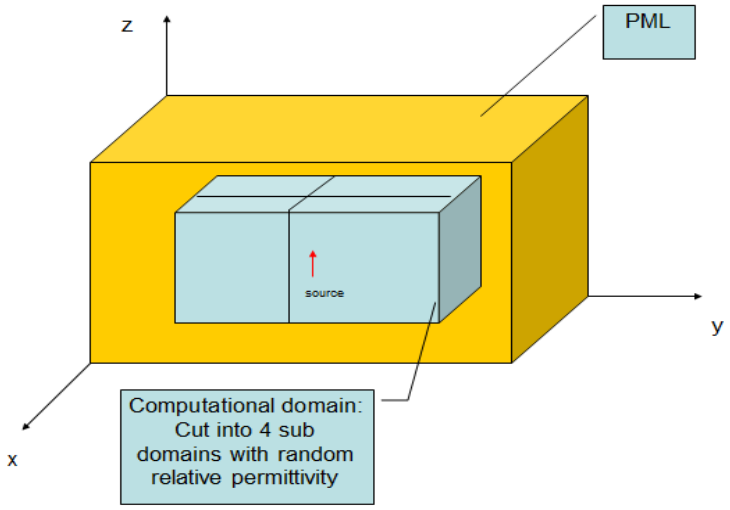

Figure 4-5 3-D wave propagation problem.

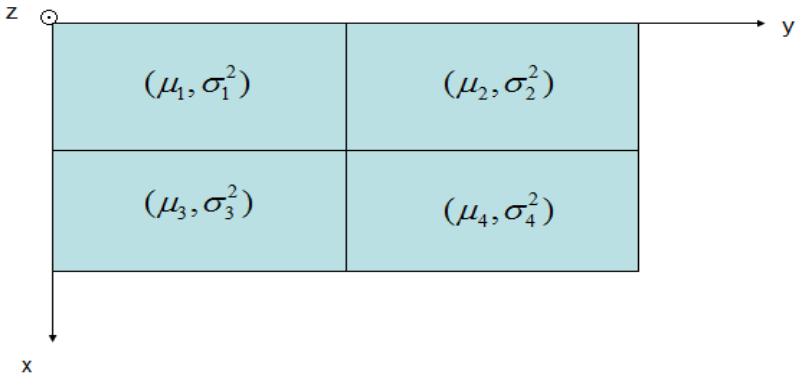

Figure 4-6 Top view for computational domain.

If we set $\mu_1 = \mu_2 = \mu_3 = \mu_4 = \mu$ and $\sigma_1 = \sigma_2 = \sigma_3 = \sigma_4 = 0$, then all the higher order coefficients will vanish, only the zero order term exists. As shown in Figure 4-7, the value of the zero order coefficient for the Ez component creates exactly the same results as when we set the media to be homogeneous with a permittivity of μ, symmetric to the middle point. If the permittivity values are taken as in (4.46),

$$\begin{cases} \mu_1 = 6.0 \\ \sigma_1 = 0.5 \end{cases} \begin{cases} \mu_2 = 5.5 \\ \sigma_2 = 0.25 \end{cases} \begin{cases} \mu_3 = 6.5 \\ \sigma_3 = 0.75 \end{cases} \begin{cases} \mu_4 = 7.0 \\ \sigma_4 = 0.5 \end{cases}, \tag{4.46}$$

then the mean value plot is like Figure 4-8. Different permittivity makes the wave front not symmetric to the center.

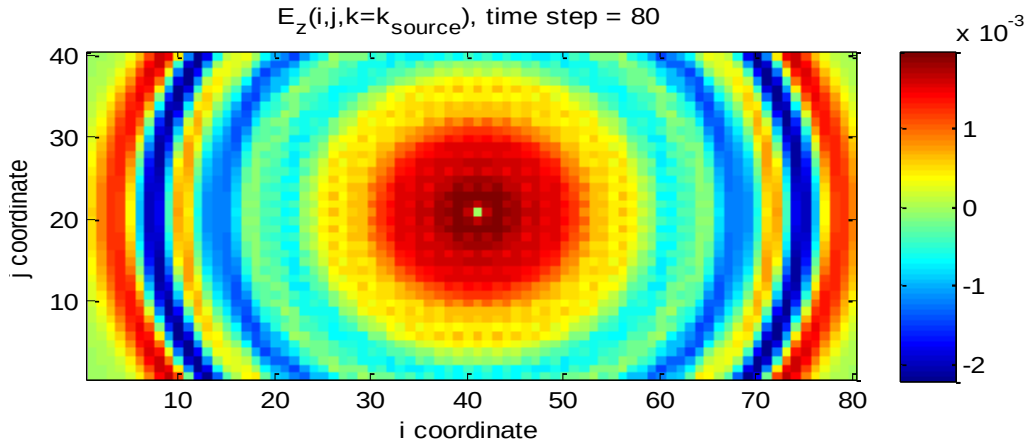

Figure 4-7 z component of the electric field for homogeneous case.

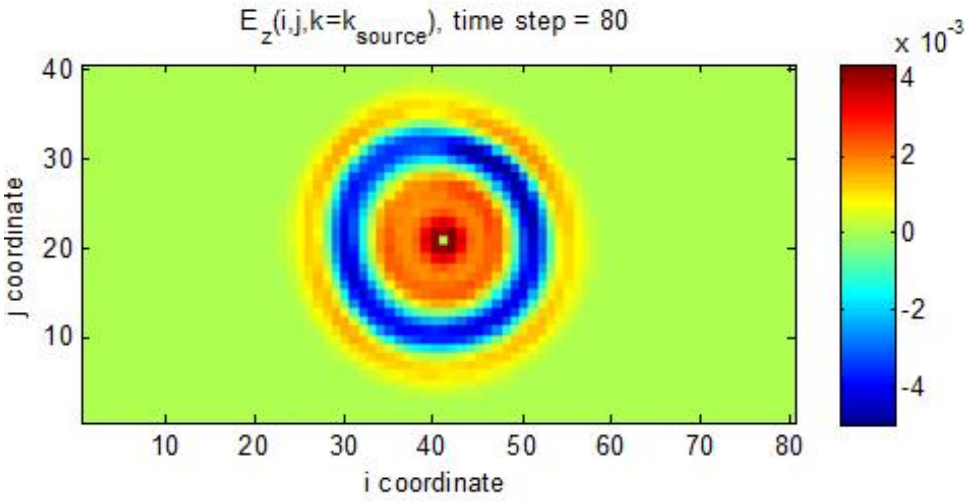

Figure 4-8 z component of the electric field for inhomogeneous case.

While it is not easy to visualize the shape of the variations, we can always pick up any point we are interested in inside the media, record the value of the higher order coefficients during the time marching loop of FDTD. Then post processing can be done after the simulation to get the time domain statistics.

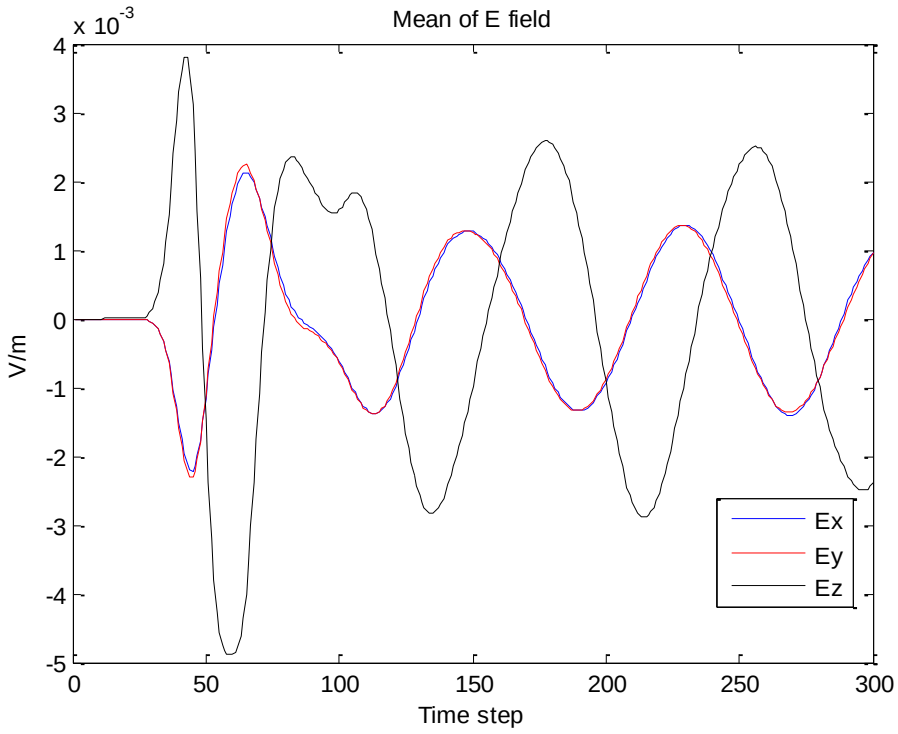

Figure 4-9 Mean value of electric field at point (is+4, js+4, ks+4).

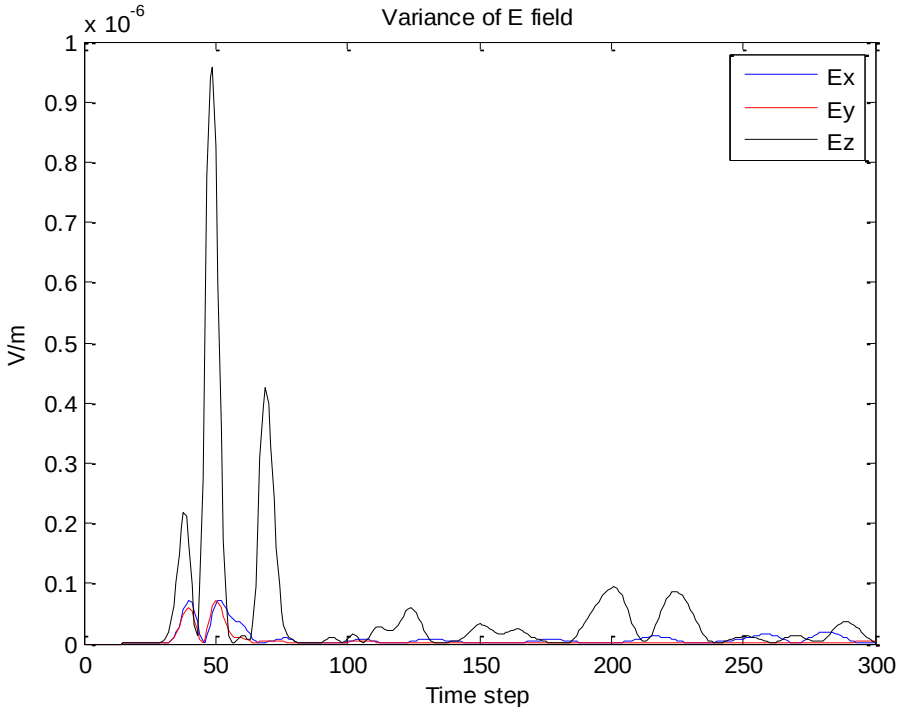

Figure 4-10 Variance of electric field at point (is+4, js+4, ks+4).

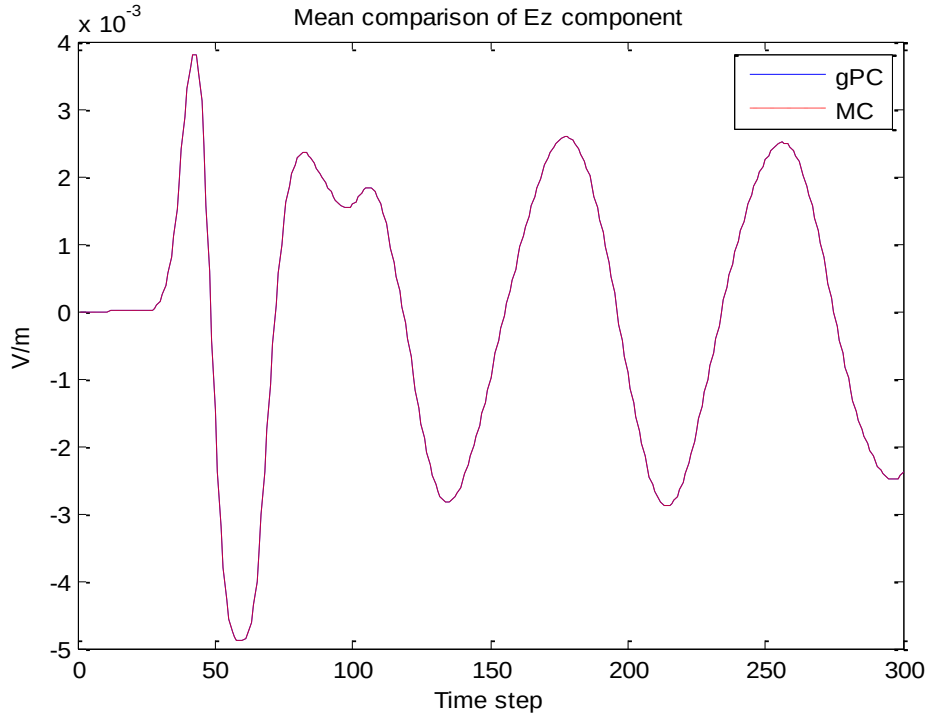

Figure 4-11 Mean value comparison of Ez component at point (is+4, js+4, ks+4) between gPC method and Monte Carlo method.

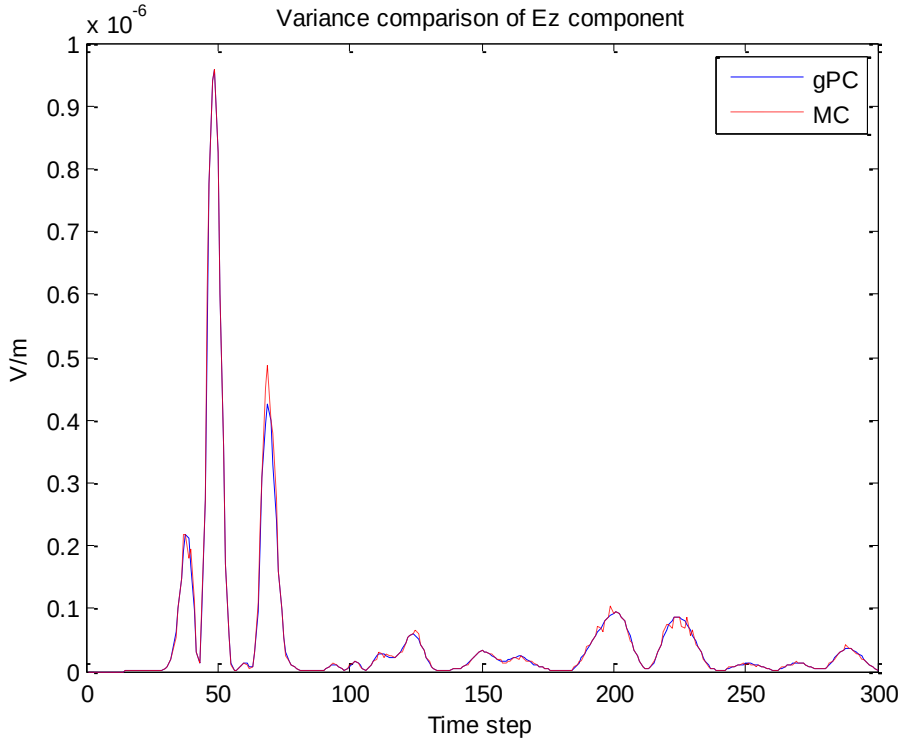

Figure 4-12 Variance comparison of Ez component at point (is+4, js+4, ks+4) between gPC method and Monte Carlo method.

If we denote the coordinates of the middle point in the media to be (is, js, ks), Figures 4-9 and 4-10 show the mean value and variation of E field recorded at the point of (is+4,js+4, ks+4). To validate the results, 500 times MC simulations are performed. To see the figures more clearly, only the Ez component is shown. As shown in Figures 4-11 and 4-12, both the mean value and variations have good agreement. And mean value tends to be more accurate than variation.

4.4 Summary

This chapter discussed the generalized polynomial chaos (gPC) method and how to implement it into the FDTD method for analysis wave propagation problems in a random medium. As we can see from the derivation, the gPC-FDTD formulation requires a modification from the original Maxwell equations. Compared to the Monte Carlo (MC) method, it only needs one simulation instead of a large number of repeated simulations. This is the biggest advantage over the MC method.

However, the gPC method also has its disadvantages. From the derivation in Section 4.2, we know that all the field components should be stored during the FDTD updating loop. This requires P times more memory than an ordinary simulation, if the highest order of expansion is P. In the previous work in [36], it is noted that sometimes the gPC method cannot converge if the expansion order is greater than 3. This could result in a larger truncation error than desired. Also, for multi-dimensional problems, the polynomials can be very complicated, thus it is very difficult to modify the ordinary FDTD code. So when dealing with a large complex system which requires a lot of memory or multi-variant problems, the gPC method will have its limitations.

Chapter 5 Stochastic Collocation Scheme: A non-intrusive approach

5.1 Introduction

As mentioned above, one major difficulty with the stochastic Galerkin approach is modification of the Maxwell equations. Can we find an alternative way that is efficient but at the same time, not change the deterministic system formulation? Very recently, there has been a surge of interest in the stochastic collocation approach that was proposed in the work of [6] [42]-[48]. By taking advantage of the existing theory on multivariate polynomial interpolations, the stochastic collocation method achieves fast convergence when the solutions possess sufficient smoothness in random space, similar to the stochastic Galerkin scheme. Traditional work of the stochastic collocation method uses tensor products of one-dimensional quadrature points as "sampling points" for multidimensional problems, which restricts its applicability to a smaller number of random variables as the number of sampling points grows exponentially otherwise. A sparse grid (SG) method is then proposed that can significantly reduce the number of sampling points required in higher random dimensions. In this way the stochastic collocation method combines the advantages of both the MC method and the stochastic Galerkin method. The implementation of the stochastic collocation method is similar to that of the MC method, i.e., only repetitive realizations of a deterministic solver is required; and by choosing a proper set of sampling points such as the sparse grid, it can achieve high accuracy and fast convergence as in the stochastic Galerkin method. In this

chapter, we are using the sparse grid based stochastic collocation method to analyze different channel structures in high speed circuits.

5.2 General procedure

Again, we use a stochastic PDE to explain the main idea,

$$\begin{cases} L(u(x,t,\xi)) = f(x,t,\xi) & x \in D, t \in (t_0, T], \xi \in \Omega \\ B(u(x,t,\xi)) = 0 & x \in \partial D, t \in (t_0, T], \xi \in \Omega, \\ u(x,t_0,\xi) = u_0 & \xi \in \Omega \end{cases} \tag{5.1}$$

where L is a differential operator, B is the boundary condition operator, and u_0 is the initial condition.

Let $\Theta_N = \{\xi^{(i)}\}_{i=1}^N \subset I_\xi$ be a set of prescribed nodes in the random space, where $N \geq 1$ is the number of the nodes, $u^{(i)} = u(x,t,\xi^{(i)}), i = 1, \cdots N$ is the solution of the governing equation (5.1), and I_ξ is the support of random variable ξ. The basic idea of the stochastic collocation method is to find an approximate solution $v(x,t,\xi)$ so that the difference between it and the real solution $\|v(x,t,\xi) - u(x,t,\xi)\|$ is sufficiently small in a strong norm defined on I_ξ,

$$\|v(x,t,\xi) - u(x,t,\xi)\| \to 0 \quad \text{when } N \to \infty. \tag{5.2}$$

These nodes $\Theta_N = \{\xi^{(i)}\}_{i=1}^N \subset I_\xi$ are called collocation points,

$$\begin{cases} L(u(x,t,\xi^{(i)})) = f(x,t,\xi^{(i)}) \\ B(u(x,t,\xi^{(i)})) = 0 \\ u(x,t_0,\xi^{(i)}) = u_0 \end{cases}. \tag{5.3}$$

It is observed that for each realization, (5.3) is a deterministic problem since the random input parameter $\xi^{(i)}$ is a fixed value. Therefore, there is no need to change the

existing numerical method to solve (5.3). The results of (5.3) are denoted as $\{u^{(i)}\}_{i=1}^{N}$. The remaining question becomes how to construct the approximate solution and how to extract the statistical information in the post processing.

Interpolation is a natural approach to the stochastic collocation problem. The most commonly used interpolation technique is Lagrange interpolation [51]. That is, let

$$u(x,t,\xi) \approx v(x,t,\xi) = \sum_{i=1}^{N} u(x,t,\xi^{(i)}) L_i(\xi^{(i)}), \tag{5.4}$$

where

$$L_j(\xi^{(i)}) = \delta_{ij}, 1 \le i, j \le N, \tag{5.5}$$

are the Lagrange interpolating polynomials.

Then the mean and variance can be obtained by

$$\begin{aligned} E(u) &= \int_D u(x,t,\xi) \cdot f(\xi) d\xi \\ &= \int_D \{\sum_{i=1}^{N} u(x,t,\xi^{(i)}) L_i(\xi^{(i)})\} \cdot f(\xi) d\xi \\ &= \sum_{i=1}^{N} u(x,t,\xi^{(i)}) \{\int_D L_i(\xi^{(i)}) \cdot f(\xi) d\xi\} \\ &= \sum_{i=1}^{N} u(x,t,\xi^{(i)}) \omega_i \end{aligned}, \tag{5.6}$$

$$\begin{aligned} Var(u) &= \int_D \{u(x,t,\xi) - E(u)\}^2 \cdot f(\xi) d\xi \\ &= \sum_{i=1}^{N} u^2(\mathbf{X},t,\xi_i) \omega_i - [E(u)]^2 \end{aligned}, \tag{5.7}$$

$$\omega_i = \int_D L_i(\xi^{(i)}) \cdot f(\xi) d\xi. \tag{5.8}$$

where $\{\omega_i\}_{1 \le i \le N}$ are the integration weights based on the Gaussian quadrature rule as in (5.8), D is the domain where the random variables are defined, and $f(\xi)$ is the joint probability density function (PDF) of the random variables $\xi = [\xi_1, \xi_2, \cdots \xi_N]$.

5.3 Collocation points

In the collocation method, the overall simulation time is *N*, with *N* being the total number of collocation points. Thus, it is essential to choose proper nodes (minimum number to achieve a certain degree of accuracy), especially for multi-dimensional problems.

In one-dimensional problems, how to choose the collocation points are well studied, such as the Gaussian quadrature rule as discussed in Chapter 2. The choice of collocation points in the multi-dimensional problems remains challenging work.

5.3.1 Tensor product rule

One direct way to construct collocation points in multi-dimension space is to use the tensor product rule [49][50] as in (5.9)

$$\Theta_d = \Theta_1^{n_1} \times \Theta_1^{n_2} \times \cdots \times \Theta_1^{n_d}, \tag{5.9}$$

where n_i is the number of nodes in the *i*th dimension, *d* is the total problem dimension, and Θ_d is the collocation node set. Then the total number of nodes is

$$N = \prod_i^d n_i . \tag{5.10}$$

By using the tensor product construction, all the properties of underlying a one-dimensional interpolating scheme can be well controlled. However, with a large dimension when $d \gg 1$, the total number of points grows extremely fast. This is well known as the curse of dimensionality, which makes the overall numerical simulation very time consuming.

5.3.2 Sparse grid method

One alternative approach is the sparse grid method, which can be used to significantly reduce the number of points in multi-dimensional problems. The sparse grid method was first proposed by Smolyak [49]. It has been proved useful in solving stochastic partial differential equations using the stochastic collocation scheme [6].

Following the notation in [50], the construction of the sparse grid interpolation takes the form of

$$Q_N = \sum_{N-d+1 \le |i| \le N} (-1)^{N-|i|} \cdot \binom{d-1}{N-|i|} \cdot (Q_{i_1} \otimes \cdots \otimes Q_{i_d}), \tag{5.11}$$

where d is the dimension of the problem, N is an integer larger than d, denoting the construction level of interpolation. The total number of spare grid nodes can be expressed as

$$\Theta_M = \sum_{N-d+1 \le |i| \le N} (\Theta_1^{i_1} \times \cdots \times \Theta_1^{i_d}). \tag{5.12}$$

Clearly, the spare grid nodes are a subset of the full tensor product nodes set.

One popular choice of constructing a sparse grid is the Clenshaw-Curtis nodes [53] , which is defined as

$$Z_i^{(j)} = -\cos\frac{\pi(j-1)}{m_i^k - 1},\ j = 1, 2, \cdots, m_i^k. \tag{5.13}$$

Figure 5-1 shows the point choice of the sparse grid method versus the tensor product rule in 20D. In an example of a 2-D case, the total number of points is 145 based on the sparse grid compared to 1089 based on the tensor product rule. A significant reduction of collocation nodes is obtained using sparse grid method. For more details on a sparse grid method, one can find them in [54]-[56].

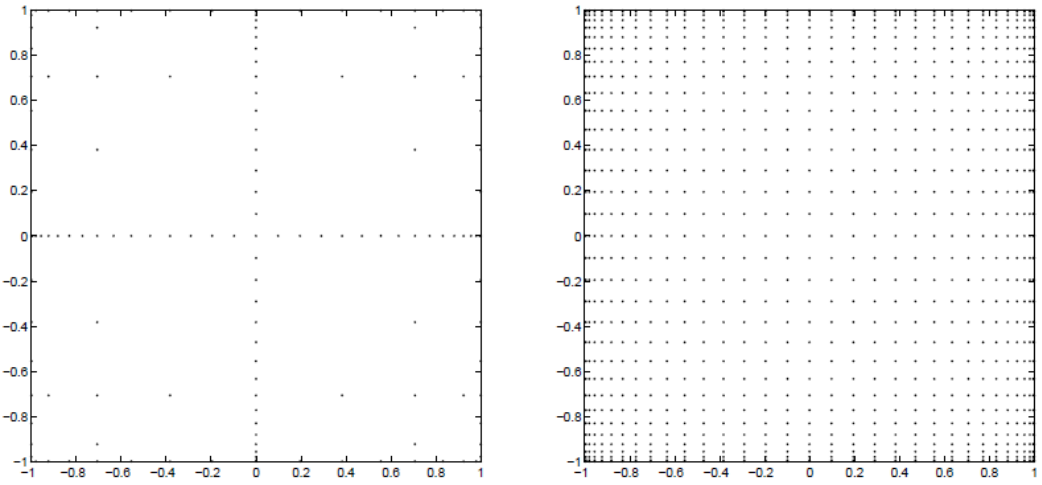

Figure 5-1 Comparison of choice of collocation points by sparse grid method and tensor product rule in two-dimensional space.

5.4 Application in high speed circuits modeling

5.4.1 Example I: Microstrip line

The structure we studied is a microstrip line as shown in Figure 5-2. Microstrip lines [57] are commonly used in high speed circuits as interconnecting channels to transfer data between different circuit elements. It has a dielectric substrate, usually made of FR4. There are printed metal traces with a thickness of t, width of W, and length of L. On the bottom is the ground plane, proving a return pass for the current.

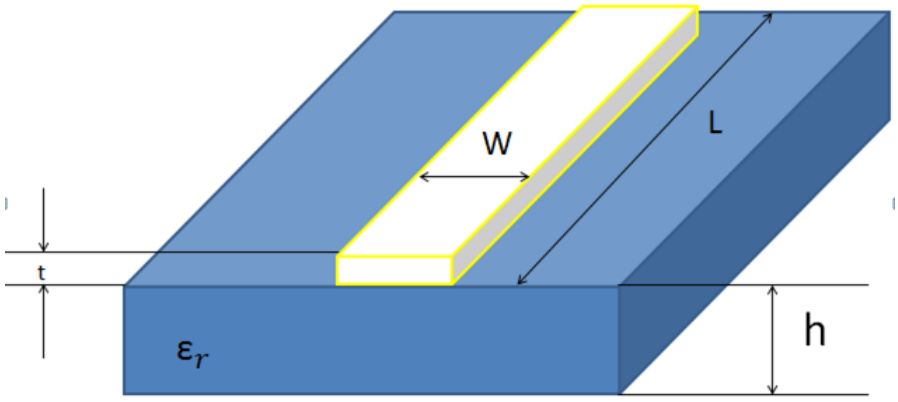

Figure 5-2 Microstrip line.

The quantity we are interested in is the eye diagram at the output end of the transmission line. Figure 5-3 shows a typical eye diagram. The eye diagram is often used in communication systems because it can provide us with visual information for evaluating the channel performance, such as signal-to-noise ratio and jitter [58]. Analyzing the eye diagram is a major work in the area of signal integrity.

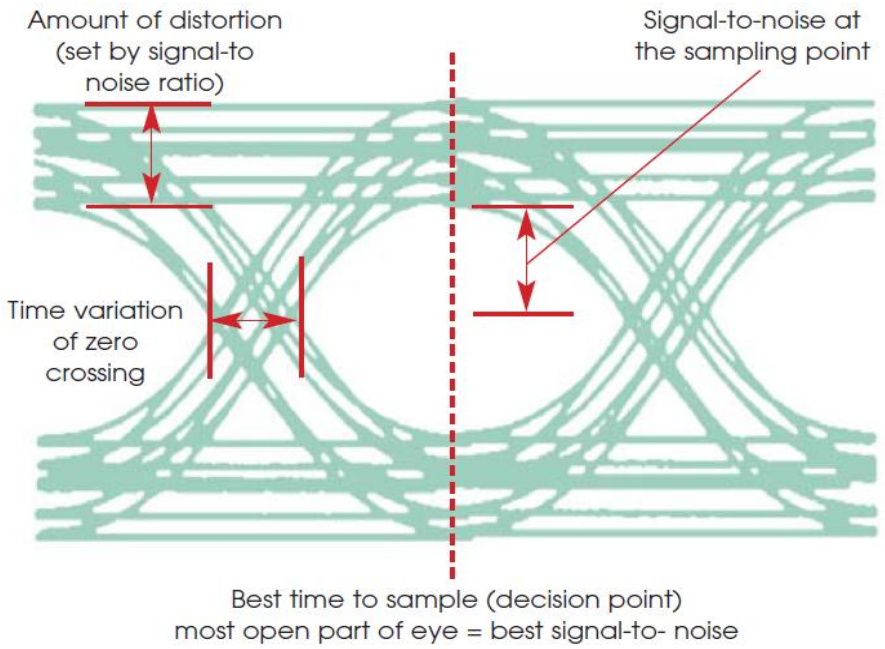

Figure 5-3 Typical eye diagram.

There are two types of uncertainties within this problem. The first one is the geometry uncertainty. We assume that the permittivity of the substrate ε_r, the substrate height *h* and the trace width *W* are three Gaussian random variables with mean values of 4.3, 0.8 mm, and 1.6 mm, respectively; and each of them has a 10% standard deviation from its mean value. All these parameters can affect the impedance of the microstrip line. Signals propagating on the transmission line can get reflections once the impedance of the transmission line changes. This is used to model errors existing during the manufacturing process.

The second type of uncertainty is the clock variation since CPU clocks tend to have different arrival times. This is also called jitter in signal integrity terms [59], as shown in Figure 5-4. The jitter of the signal is set to be a Gaussian variable with a 10 ps mean and a 1 ps standard deviation.

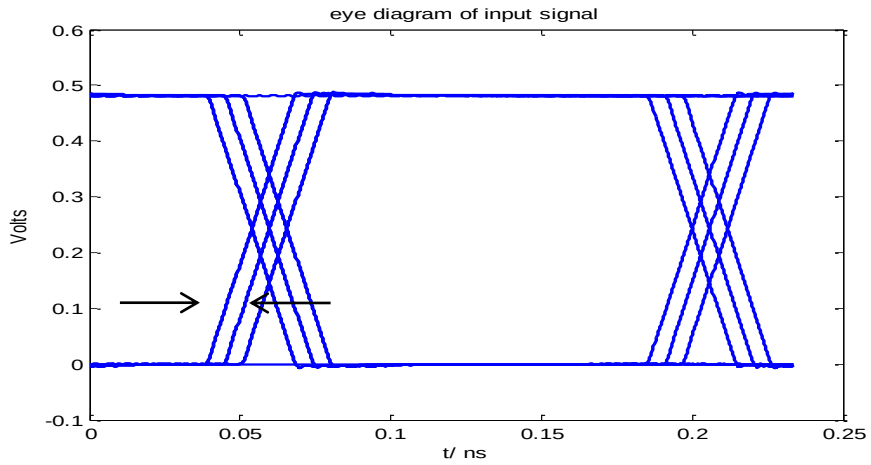

Figure 5-4 Eye diagram of the input signal with a jitter of 10 ps.

Since we have four parameters varying at the same time, we apply the 4-D sparse grid method to generate 57 input samples, each one with a corresponding weight in the sample space. The statistics for the output signal is shown in figure 5-5.

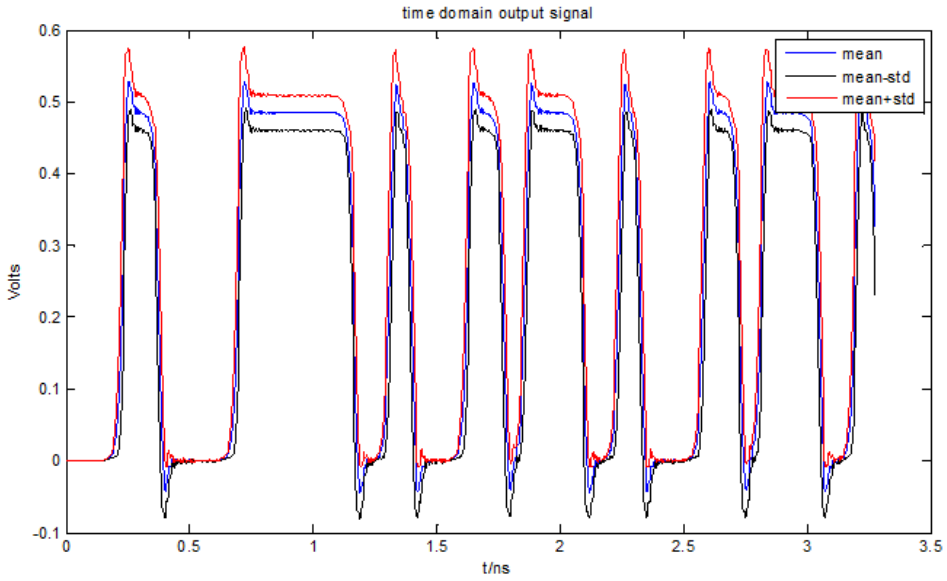

Figure 5-5 Mean and +/- standard deviation for the output time domain signal.

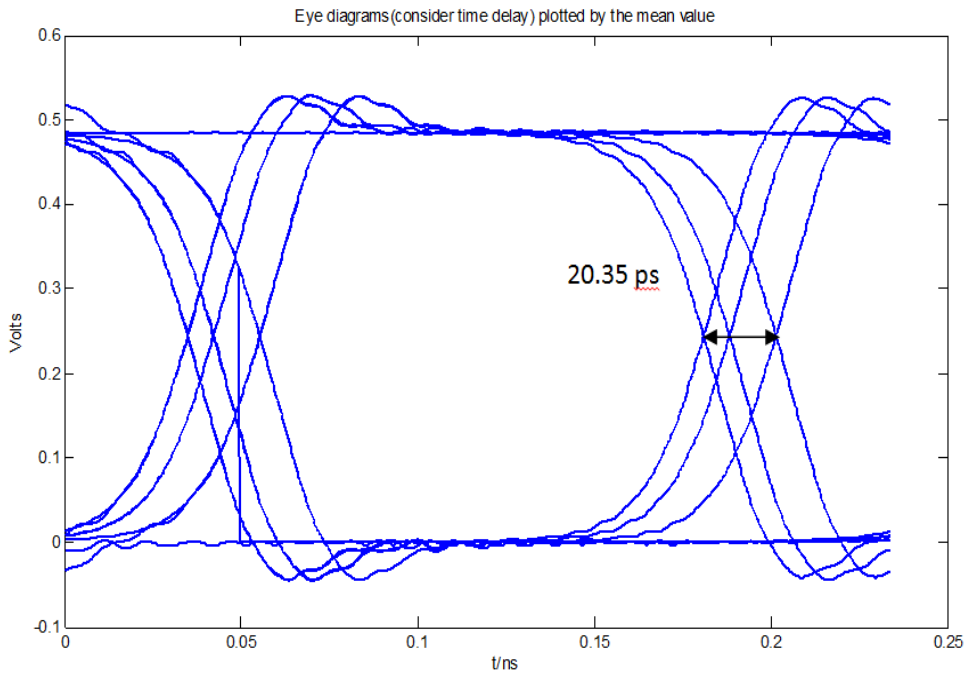

Figure 5-6 Eye diagram at the output end of the microstrip line plotted by mean value.

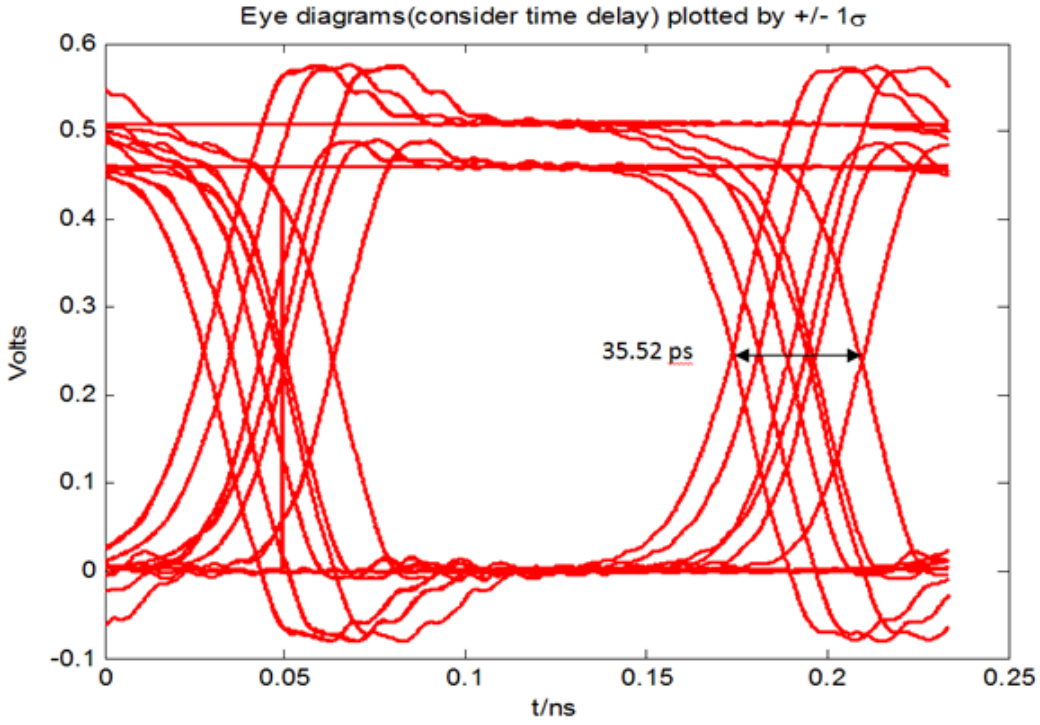

Figure 5-7 Eye diagram at the output end of the microstrip line by mean value +/- one standard deviation.

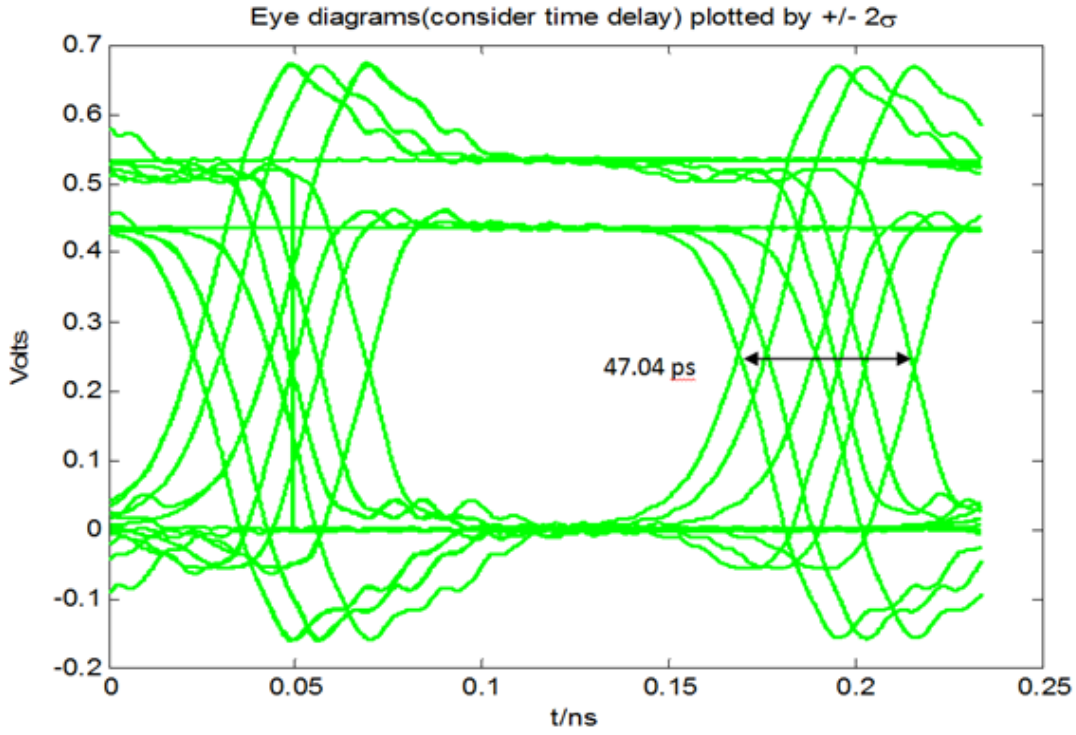

Figure 5-8 Eye diagram at the output end of the microstrip line by mean value +/- two standard deviation.

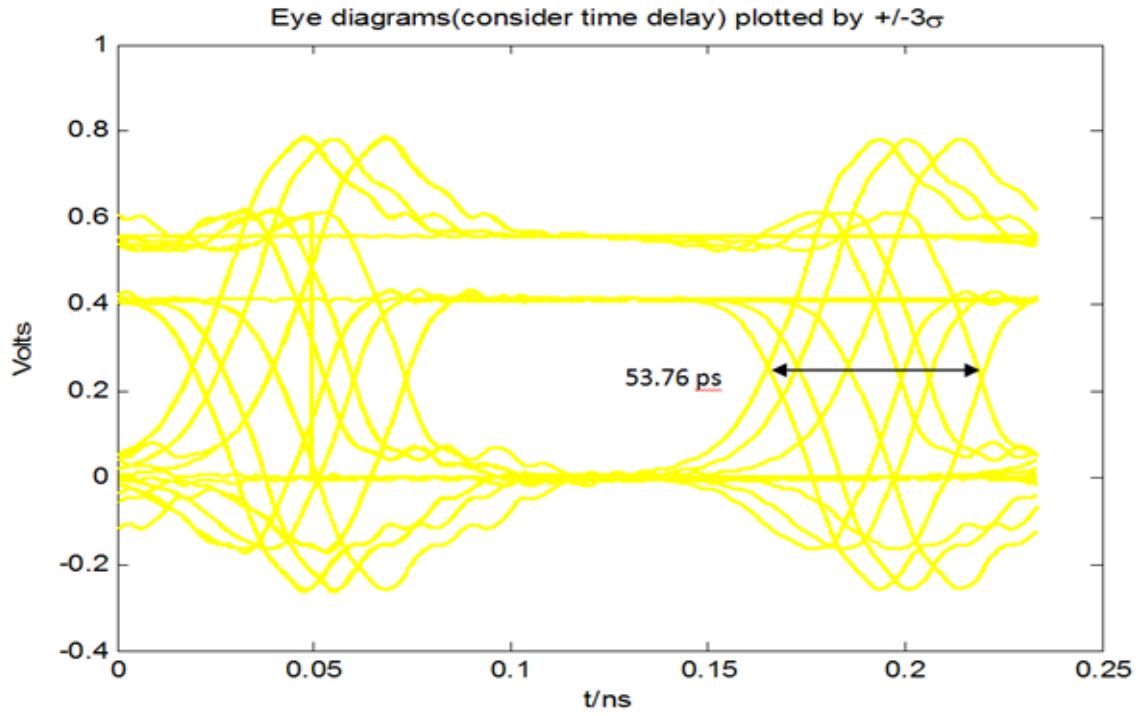

Figure 5-9 Eye diagram at the output end of the microstrip line by mean value +/- three standard deviation.

Figure 5-5 shows the statistics of the time domain output signal. Both mean value and standard deviation are calculated. Then we plot four different eye diagrams using the mean value, mean value +/- one standard deviation, mean value +/- twice the standard deviation, and mean value +/- three times the standard deviation, as shown from Figure 5-6 to Figure 5-9. If we denote the mean value as μ and standard deviation as σ, then μ represents the expectation value; and $\mu \pm \sigma$, $\mu \pm 2\sigma$, $\mu \pm 3\sigma$ stand for three confidence intervals. A good estimation must give an accurate prediction for both mean values and variations.

Then 1000 times Monte Carlo simulations are performed to validate the accuracy of the sparse grid method. As show in Figures 5-10 and 5-11, both mean and standard deviation show good agreement with each other. That is to say, we are able to obtain the same accuracy with a speed-up factor of almost 20.

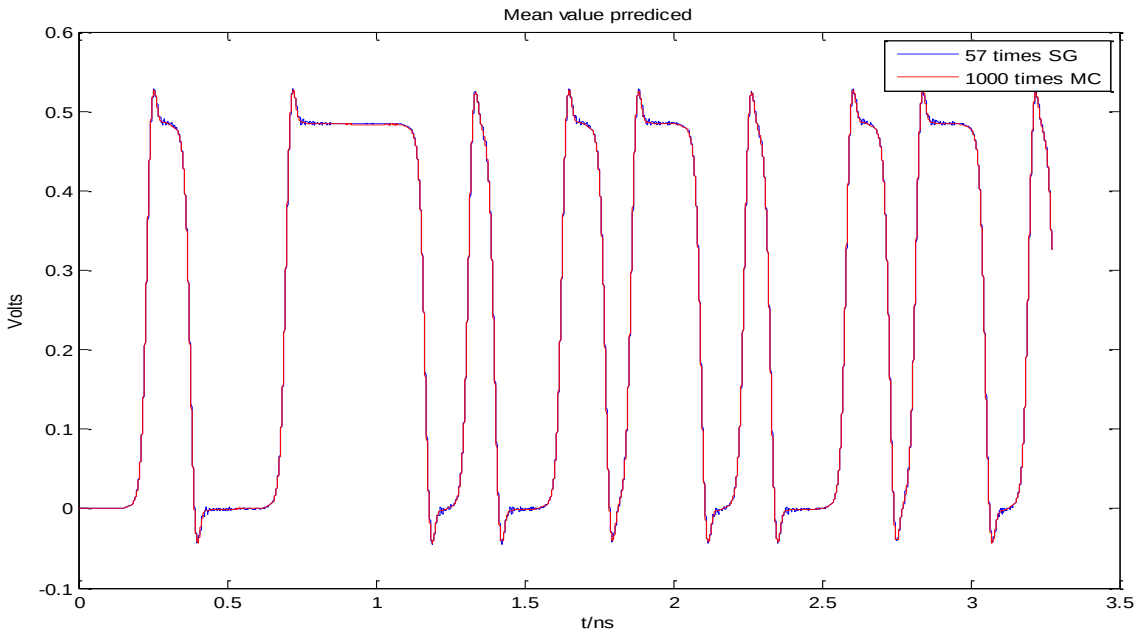

Figure 5-10 Comparison of mean value predicted by sparse grid method and Monte Carlo method.

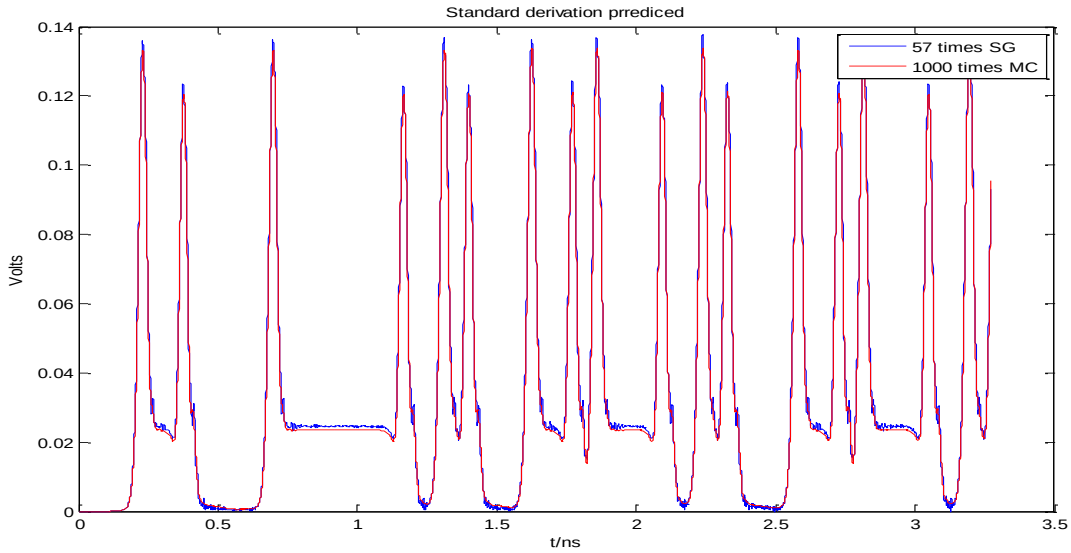

Figure 5-11 Comparison of standard deviation predicted by Sparse grid method and Monte Carlo method.

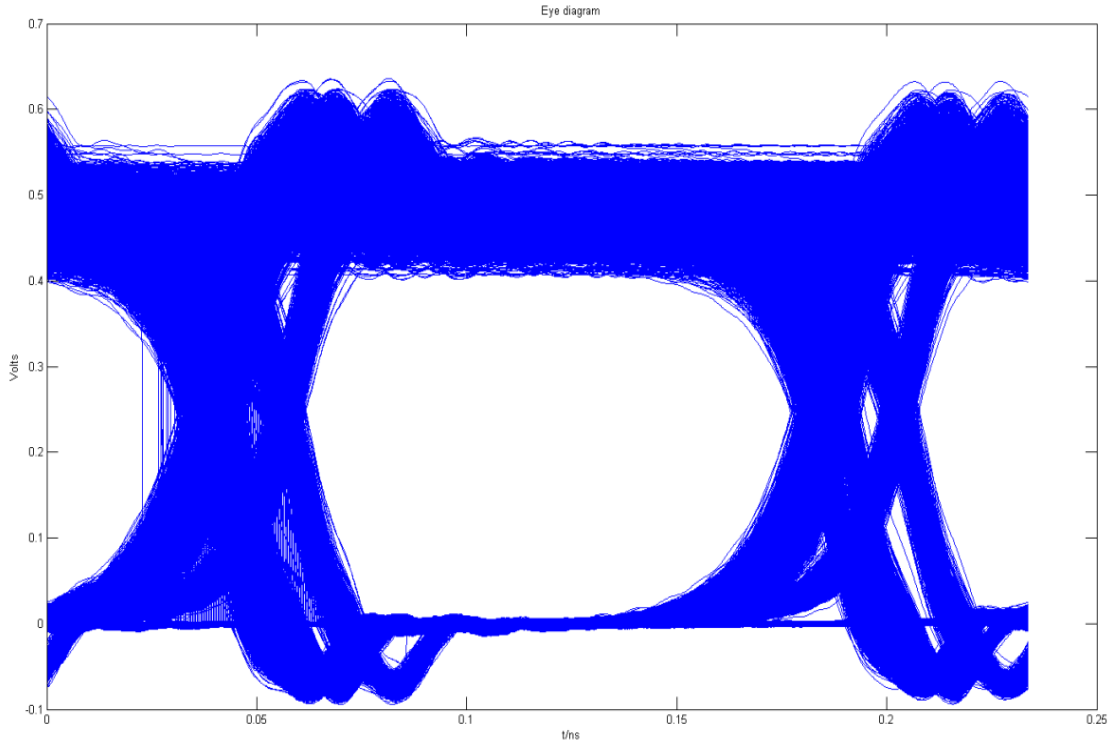

Figure 5-12 Eye diagram plotted by the results of 1000 times Monte Carlo simulations.

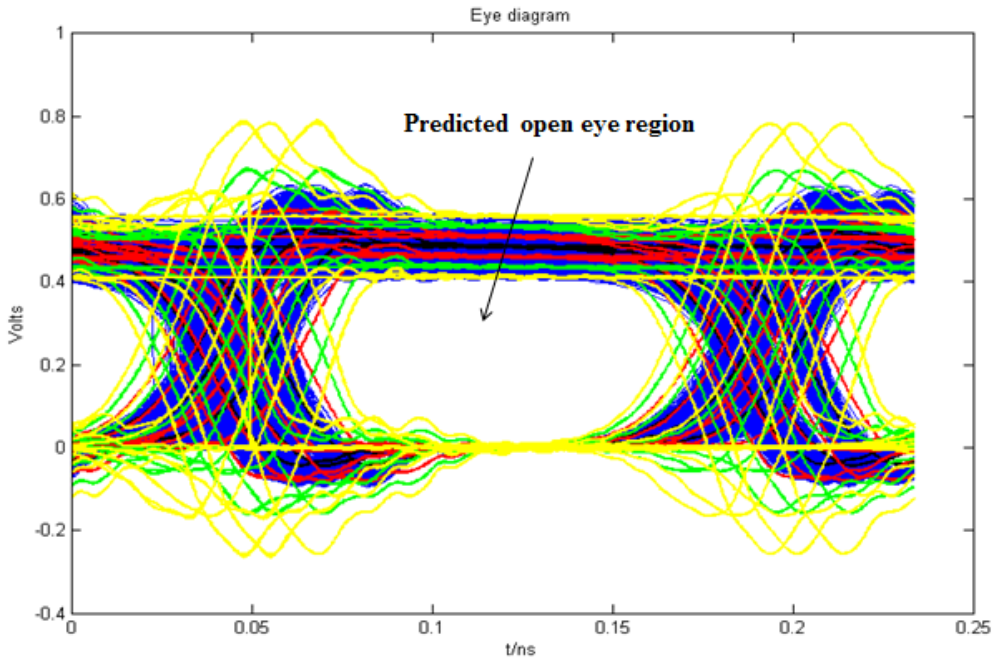

Figure 5-13 Statistical eye diagram.

Figure 5-12 shows the eye diagram plotted by the results of the 1000 MC simulations. Because the number of random MC simulations is relatively large, we can assume that, when given the parameters changing the channel, this eye diagram can represent all the possible outcomes of the output signals. Our idea is to use the statistics we computed by the sparse grid method to bound this eye diagram, to give a prediction of the eye lid, open eye region, etc., as shown in Figure 5-13.If we count the lines of random simulation results that fall into these three different confidence intervals, we can get corresponding probabilities. As shown in Table 5-1, they are 69.9%, 96.7%, and 99.9%, respectively.

Table 5-1 Probability comparison between sparse grid statistics and Normal distribution

Confidence Interval	$\pm\sigma$	$\pm 2\sigma$	$\pm 3\sigma$
Count lines within	699	967	999
Percentage	69.9%	96.7%	99.9%
Normal Distribution	68.2%	96.8%	99.8%

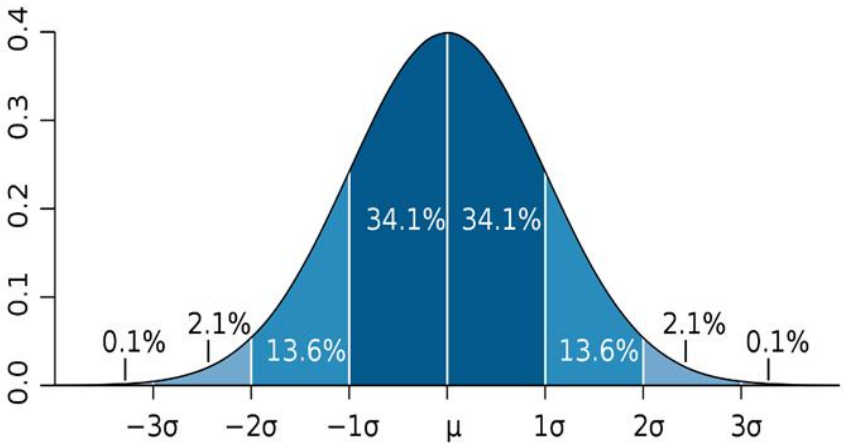

Figure 5-14 Probability density function of a Guassian distribution.

Figure 5-14 shows a probability density function of a normal Gaussian distribution. If we compare the probability within these confidence intervals, we can see that they have a good agreement.

5.4.2 Example II: Two Layer structure with via through

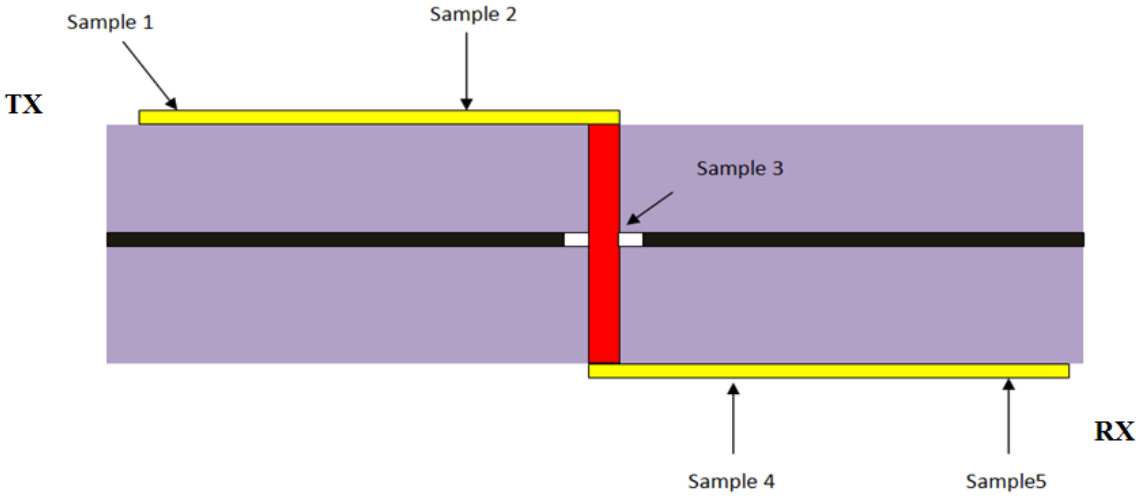

Figure 5-15 Two layer structure with through via.

Next we consider a two-layer structure with via, as shown in Figure 5-15. The signal is transmitted from the top layer to the bottom layer through a via. What are

considered random variables are the dielectric permittivity, via height, via radius, and input signal jitter. Their mean values are 4.3, 0.4 mm, 1.7 mm, and 10 ps, respectively. and 10% standard deviation from their mean values. The sparse grid method is applied to select collocation points (57 points for 4D). The results are plotted from Figure 5-16 to Figure 5-19.

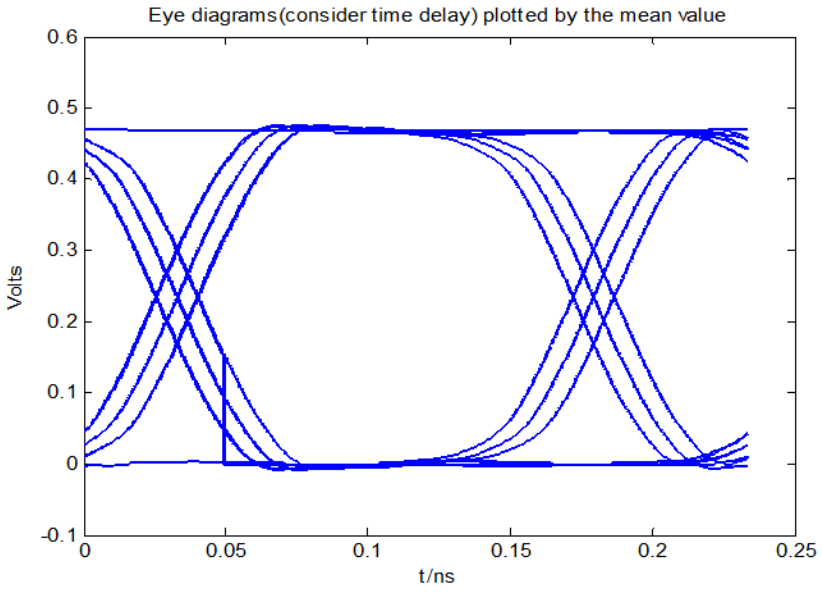

Figure 5-16 Eye diagram at sample point 5 by mean value.

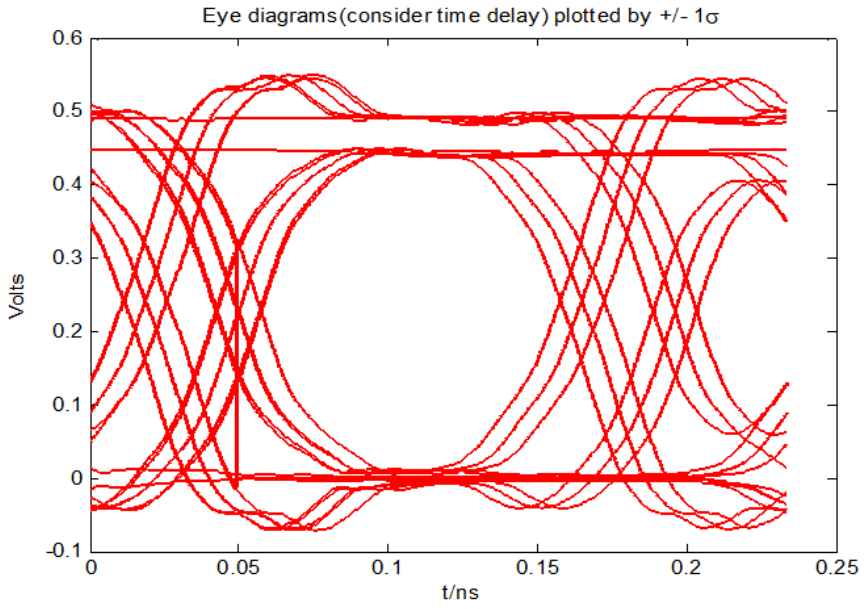

Figure 5-17 Eye diagram at sample point 5 by mean value +/- one standard deviation.

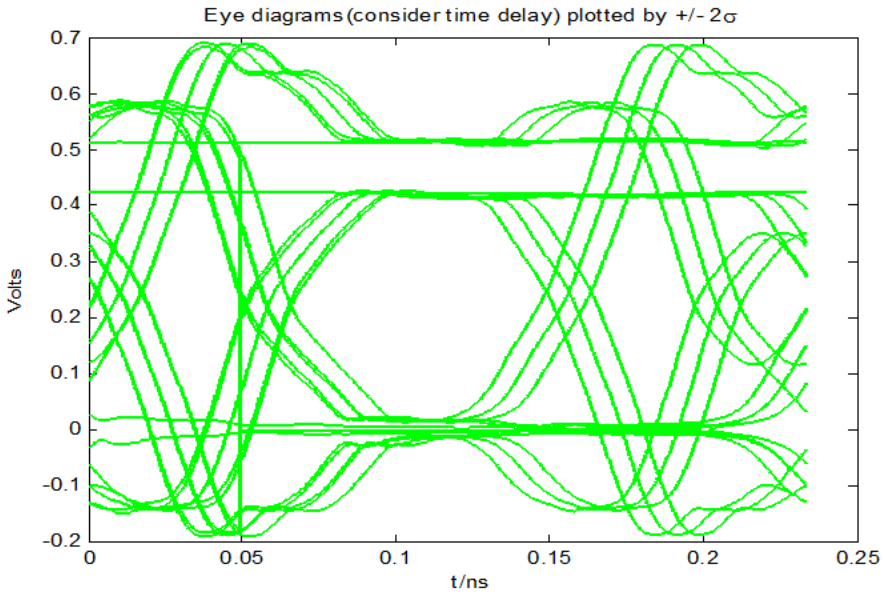

Figure 5-18 Eye diagram at sample point 5 by mean value +/- two standard deviation.

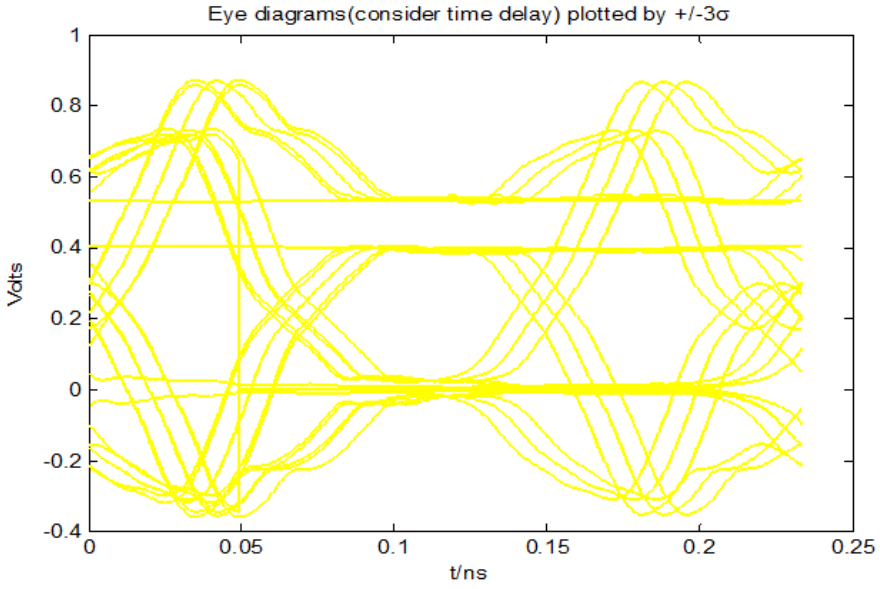

Figure 5-19 Eye diagram at sample point 5 by mean value +/- three standard deviation.

Validation is also performed using the 1000 Monte Carlo method. The comparison results are shown in Figures 5-20 and 5-21. Both the mean value and standard deviation of the output signal have good agreement. Again, we can achieve satisfactory accuracy and give good a estimation of the output signals.

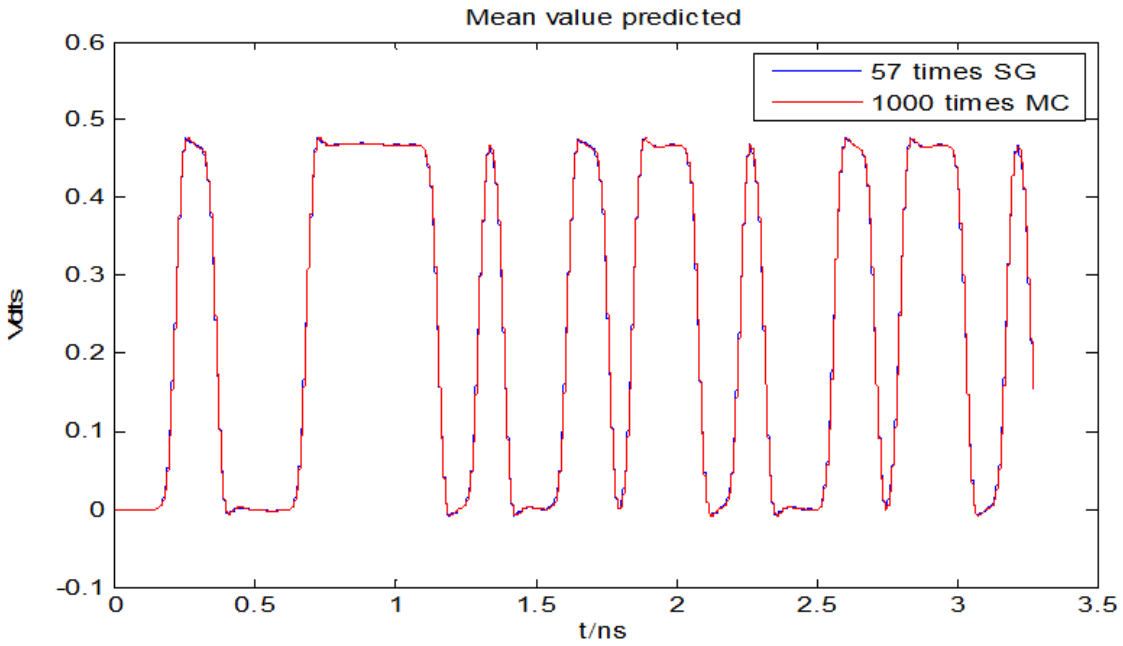

Figure 5-20 Mean comparison between sparse grid method and Monte Carlo method.

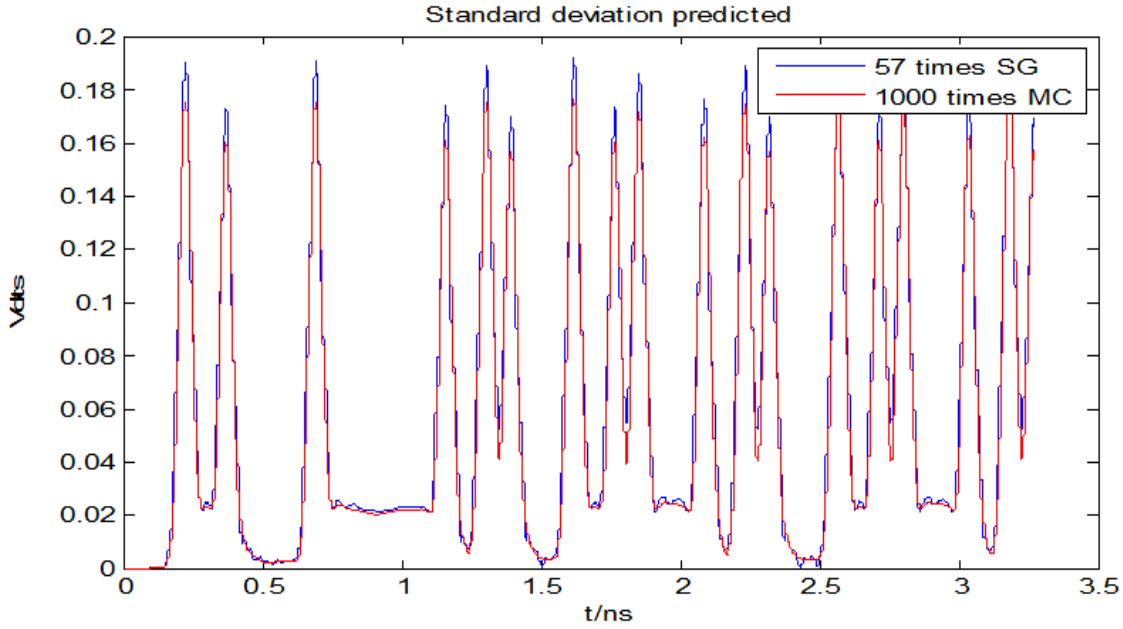

Figure 5-21 Standard deviation comparison between sparse grid method and Monte Carlo method.

Similarly, Figure 5-22 shows the statistical eye diagram. As shown in Table 5-2, a good agreement with the Normal distribution is observed.

Table 5-2 Probability comparison between sparse grid statistics and normal distribution.

Confidence Interval	$\pm\sigma$	$\pm 2\sigma$	$\pm 3\sigma$
Count lines within	694	967	997
Percentage	69.4%	96.7%	99.7%
Normal Distribution	68.2%	96.8%	99.8%

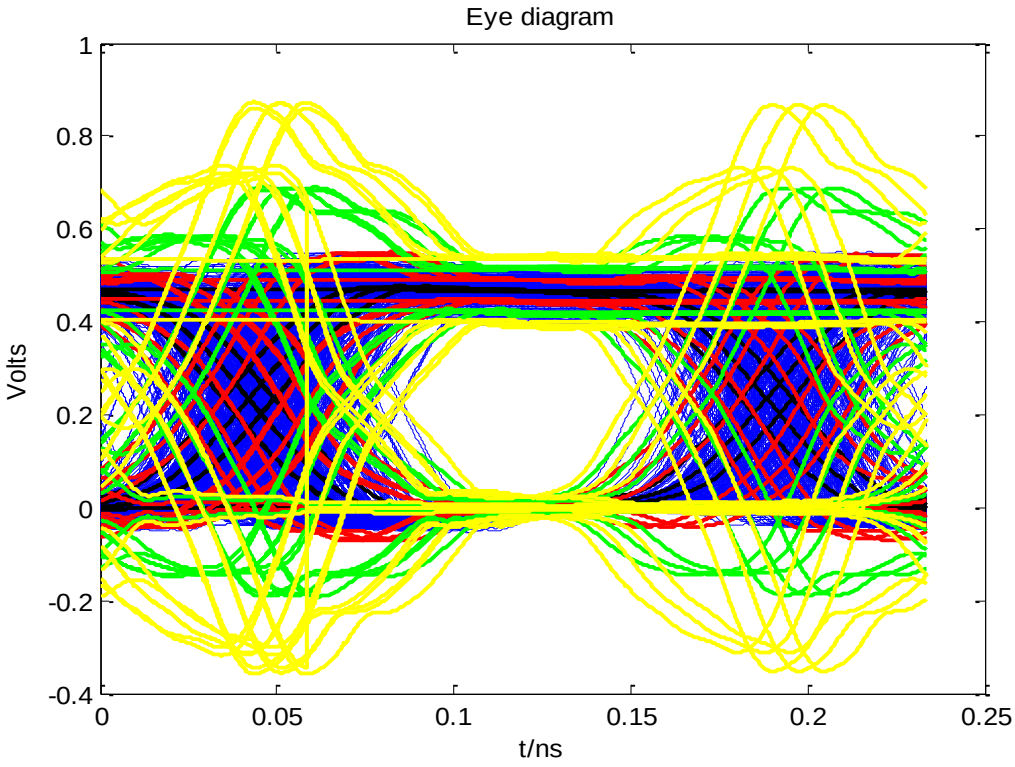

Figure 5-22 Statistical eye diagram.

Using the sparse grid method in the collocation scheme, we can give an accurate prediction of signal behaviors after propagating through a channel with existing uncertainties. This can serve as a guide for measurement when given the manufacturing error of products.

5.4.3 Example III: Analysis of commercial connector

From the previous examples, we can see that the stochastic collocation method

gives a good estimation of the signal propagating through high-speed circuit components. However, practical products can be much more complex than just a single transmission line. Luckily, commercial software can be used to analyze these complex structures. A 10-pin connector is shown in Figure 5-23. It has two differential pairs for transmitting differential signals and six ground pins. The mesh view is shown in Figure 5-24 in XFDTD.

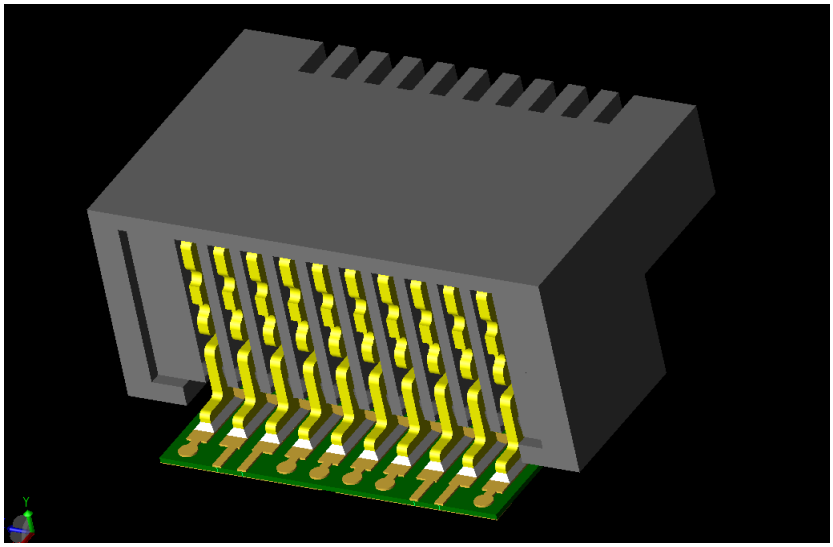

Figure 5-23 10-pin connector CAD model.

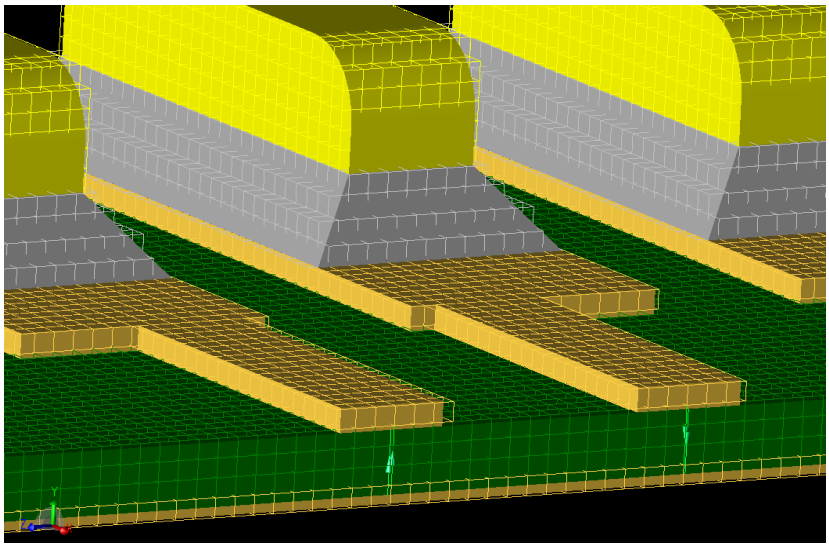

Figure 5-24 Mesh view of the differential pair in XFDTD.

As we can see in Figure 5-24, the two differential microstrip lines are fed with two voltage sources with the same amplitude but opposite polarization. Both of them have a source resistance as well. Differential signaling is widely used in the PCB design, since it can take advantage of the robustness of differential pairs to crosstalk and discontinuities in the return path. By changing the size of the FDTD grid, we can equivalently change the line width, substrate height, etc. Also, it is easier to reassign the material properties such as permittivity and conductivity if they are considered as random variables.

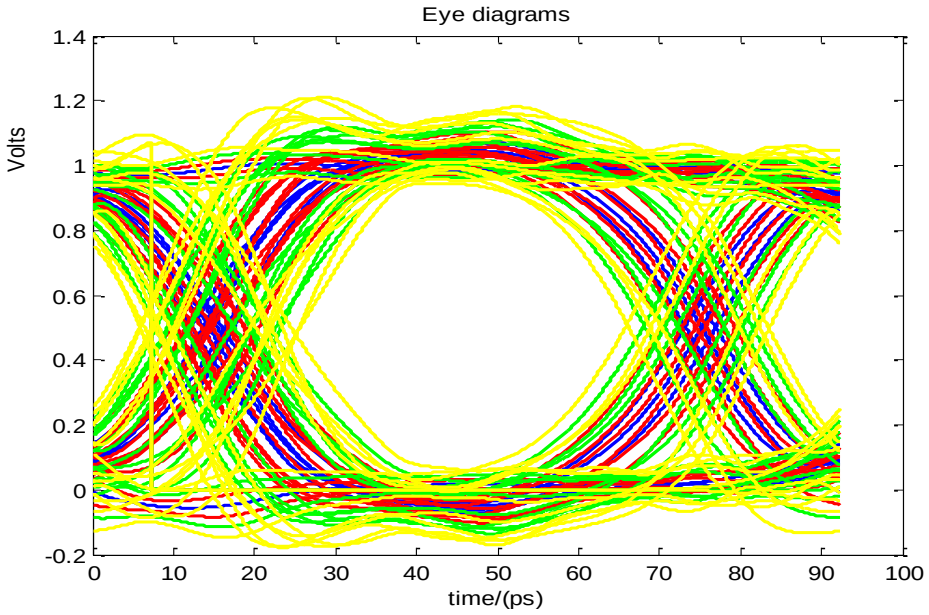

Figure 5-25 Statistical eye diagram after signal propagating through the connector.

Figure 5-25 shows the eye diagram at the output end of the connector. The blue lines, red lines, green lines, and yellow lines are mean values, +/- one standard deviation, +/- two standard deviation, and +/- three standard deviation, respectively. We can see that compared to the previous two cases, the variation of the output signal is obviously less. This is due to the differential pair structure [62] for signal transmitting. Table 5-3 lists the eye diagram statistics such as jitter and open eye region.

Table 5-3 Statistical data of eye diagrams for the connector model

Case	Mean	+/- 1 σ	+/- 2 σ	+/- 3 σ
Jitter (ps)	3.76	9.04	13.59	17.82
Eye width (ps)	56.40	50.58	45.39	40.78
Eye lid (V)	0.086	0.133	0.183	0.239
Eye height (V)	0.963	0.943	0.919	0.885

Figure 5-26s and 5-27 compare the mean and standard deviation for single variable cases and the 3-D sparse grid case. The mean values are more or less the same, because both in multi-variable and single-variable cases, the mean values are taken as the same. The multi-variable case has the largest variation because it has three parameters varying at the same time. For the single-variable case, we can see that the substrate height has the largest impact on the variance, then permittivity, and finally trace width.

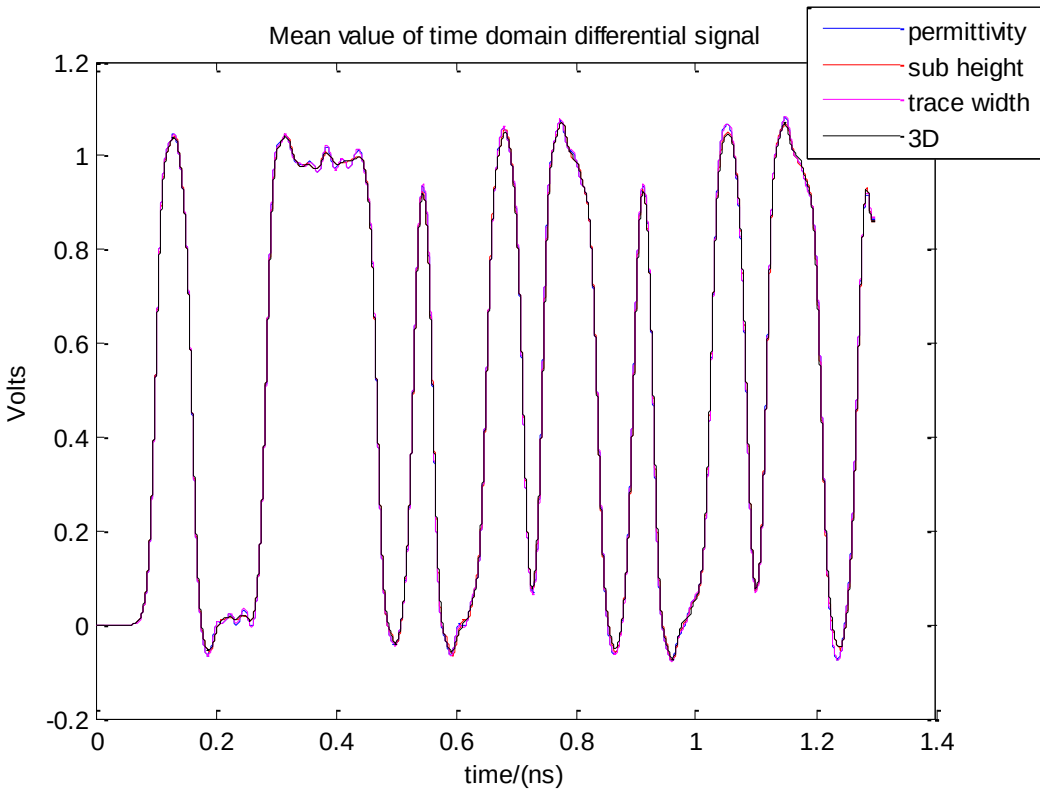

Figure 5-26 Mean value comparison of different uncertainties.

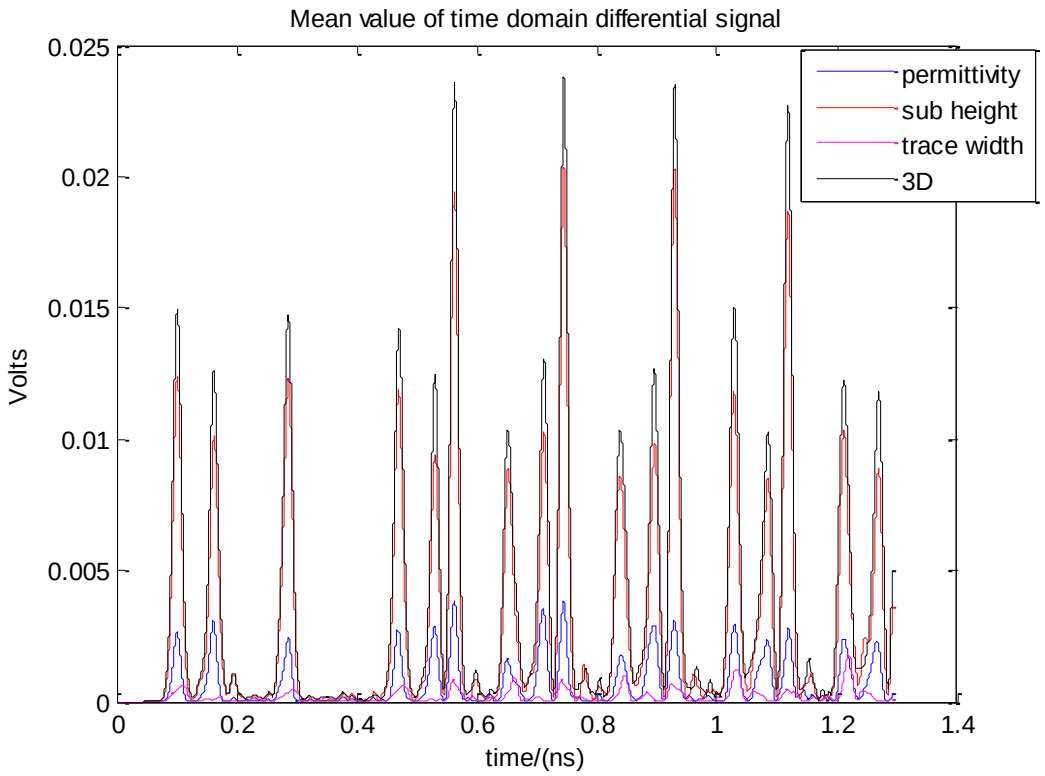

Figure 5-27 Standard deviation comparison of different uncertainties.

5.5 Application in antenna array design problem

The antenna is a device used to wirelessly transmit or receive radio waves. It is widely used today in such things as mobile communication, TV, satellite, etc. Usually, a single element antenna will have a relatively low gain. In many applications where there is a need to acquire a higher gain for longer distance communication, antenna array is often used to meet this requirement. In this section, we investigate the uncertainties of the antenna geometric and material parameters' impact on the gain and side lobe ratio of the antenna array. The design and simulation are done in HFSS.

5.5.1 Array element: microstrip antenna

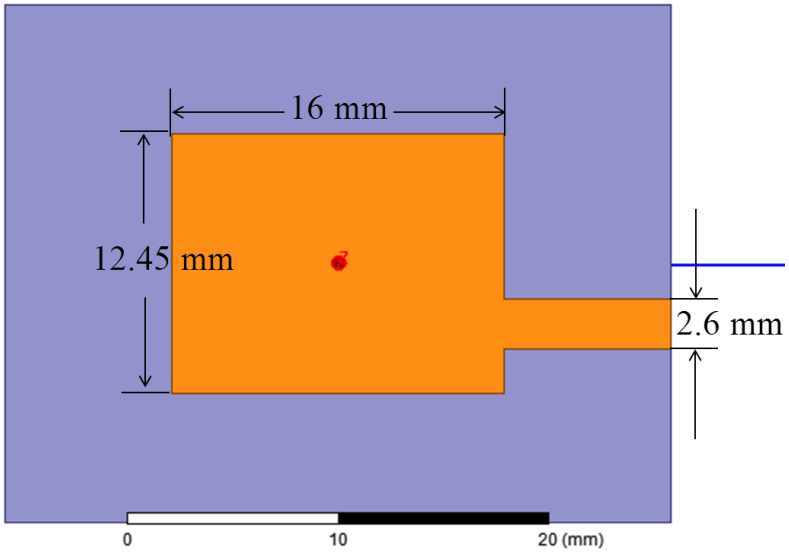

Figure 5-28 Top view of microstrip antenna

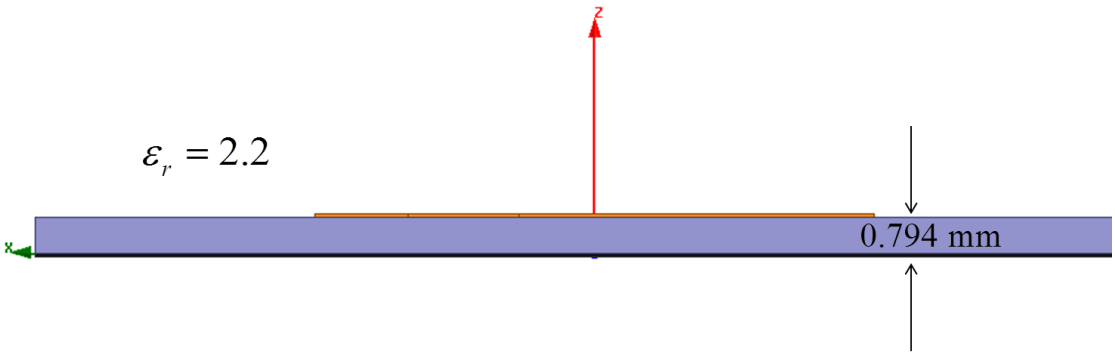

Figure 5-29 Side view of microstrip antenna

The element antenna we used is a microstrip antenna. Its top view and side view are shown in Figure 5-28 and Figure 5-29, respectively. The microstrip antenna has a length of 16 mm and width of 12.45 mm. The antenna is fed by a microstrip line from the right side. The substrate is made of Teflon which has a relative permittivity of 2.2 and has a height of 0.794 mm. The resonant frequency of the antenna is controlled by the patch width. 12.45 mm with the Teflon substrate material corresponds to a resonant frequency

of around 7.5 GHz.

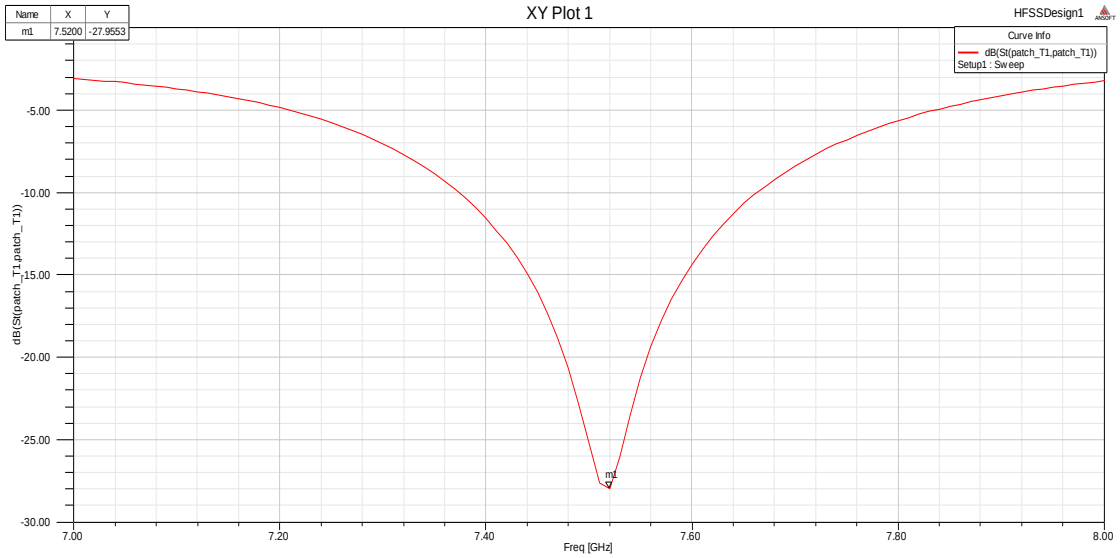

Figure 5-30 S11 plot of the microstrip antenna

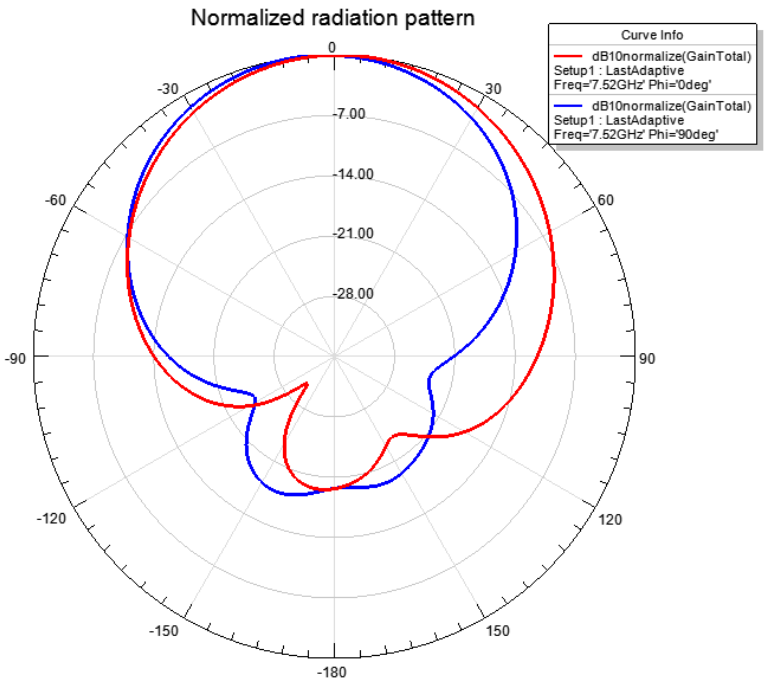

Figure 5-31 Normalized radiation pattern of the microstrip antenna

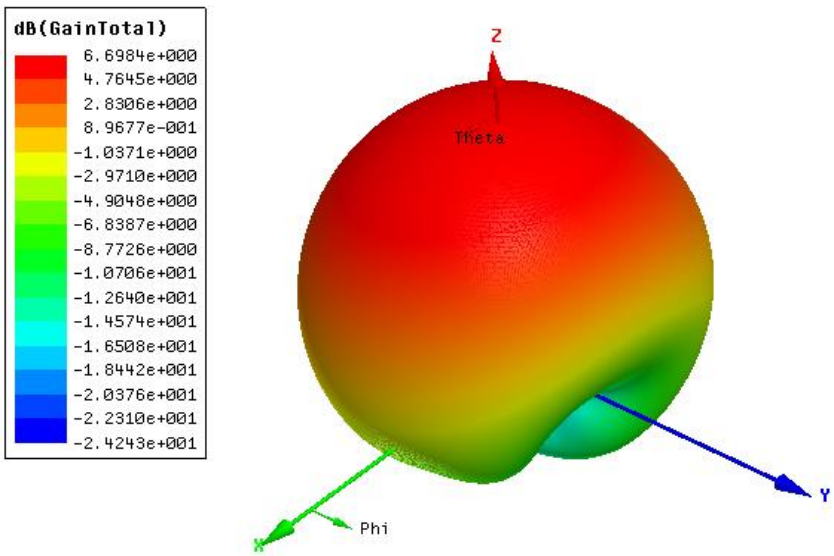

Figure 5-32 3-D polar plot of the radiation pattern

Figure 5-30 shows the S11 of the antenna from 7 GHz to 8 GHz. As we can see, the null of the S11 happens at the frequency of 7.52 GHz. The normalized radiation pattern is shown in Figure 5-31. The red curve shows the radiation pattern in the $\phi=0^0$ plane (E plane), and the blue curve shows the radiation pattern in the $\phi=90^0$ plane (H plane). The 3-D polar plot of the radiation pattern is shown in Figure 5-32 with a color bar for the antenna gain. As we can see, the maximum gain is at $\theta=0^0$, and the value is 6.7 dB, which is a typical moderate gain for microstrip antenna.

5.5.2 Antenna array synthesis

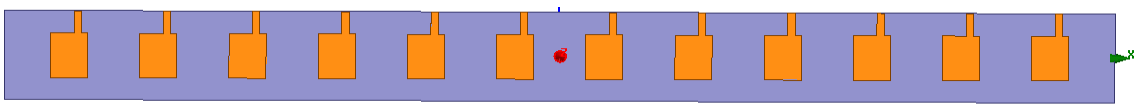

Figure 5-33 12-element linear array

The structure we simulate is a 12-element linear array, as shown in Figure 5-33. The spacing between the antenna patches is 20 mm, approximately half the wavelength at the operating frequency 7.52 GHz. Each patch is excited individually. The amplitude for each excitation is shown below. They are denoted as a_1 through a_6 and symmetric to the center.

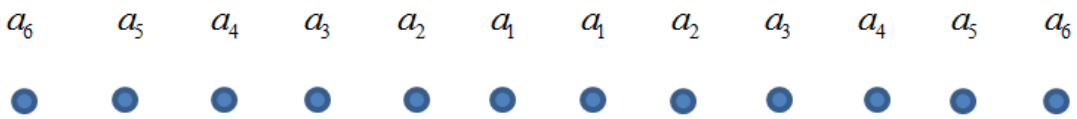

For the uniform spacing linear array, there are different types of excitation for different radiation properties. If each patch is excited with equal amplitude, the side lobe ratio is around -13.2 dB. Our goal is to achieve a lower side lobe ratio that is below -20 dB. A commonly used excitation technique to suppress the side lobe ratio is the Chebyshev array excitation [83]. The good thing about the Chebyshev design is that the side lobe ratio can be controlled. Denote the side lobe ratio as R_0, and the formulas to compute the excitation coefficients are given in (5.14) and (5.15),

$$z_0 = \frac{1}{2}[(R_0 + \sqrt{R_0^2 - 1})^{\frac{1}{11}} + (R_0 - \sqrt{R_0^2 - 1})^{\frac{1}{11}}], \tag{5.14}$$

$$a_n = \sum_{i=n}^{6} (-1)^{6-i} \cdot (z_0)^{2i-1} \frac{(i+4)! \times 11}{(i-n)!(i+n-1)!(6-i)!}. \tag{5.15}$$

Also, we apply a triangle shape of amplitude distribution for the excitation coefficients. The values for the excitation coefficients for the Chebyshev design with a -25 dB, -30 dB, -35 dB side lobe ratios and the triangle distribution are listed in Table 5-4. The coefficients for the Chebyshev design is normalized to the value of a_1. The normalized radiation patterns are shown in Figure 5-34.

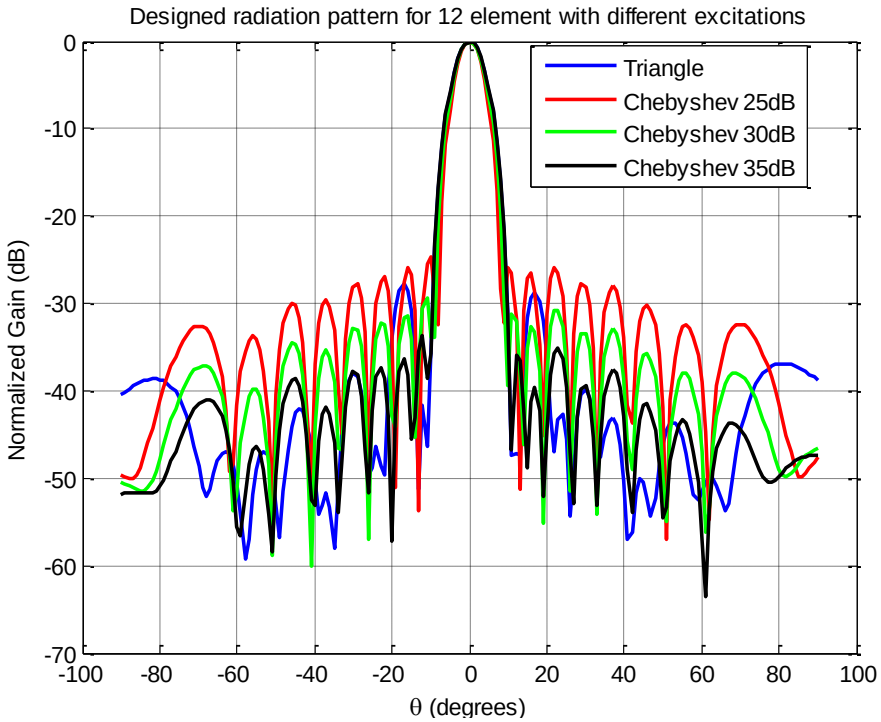

Figure 5-34 Normalized radiation pattern with Chebyshev and triangle excitations

Table 5-4 Excitation coefficients for Chebyshev and triangle distribution

Excitation	a_1	a_2	a_3	a_4	a_5	a_6
Triangle	1	2	3	4	5	6
Chebyshev 25dB	1.00	1.08	1.51	1.90	2.20	2.37
Chebyshev 30dB	1.00	1.43	2.17	2.89	3.47	3.79
Chebyshev 35dB	1.00	1.80	2.98	4.21	5.22	5.80

5.5.3 Stochastic analysis

The parameters that are considered as random variables are the substrate permittivity, substrate height, and patch width. We want to see how these uncertainties would affect the side lobe ratio and the maximum gain of the antenna array. The designed properties of the original antenna array are shown below in Table 5-5. Both the 3-D sparse grid collocation case and individual cases are studied. In each case, the

percentages of the standard deviations of the random inputs are 5%, 10%, and 20%.

Table 5-5 Maximum gain and side lobe ratio for antenna array with different excitations

Excitation	Maximum Gain	Side lobe ratio
Triangle	18.01 dB	-28.0 dB
Chebyshev 25dB	18.52 dB	-24.9 dB
Chebyshev 30dB	18.23 dB	-29.6 dB
Chebyshev 35dB	17.96 dB	-34.1 dB

In Figure 5-35 to Figure 5-46, normalized radiation patterns are shown with one, two, and standard deviation margins for the 10% permittivity variation case. In every figure, the side lobe ratio can be read due to the substrate permittivity's uncertainty. Similarly, these can be done for substrate height, patch width, and 3-D cases with 5%, 10%, and 20% variations.

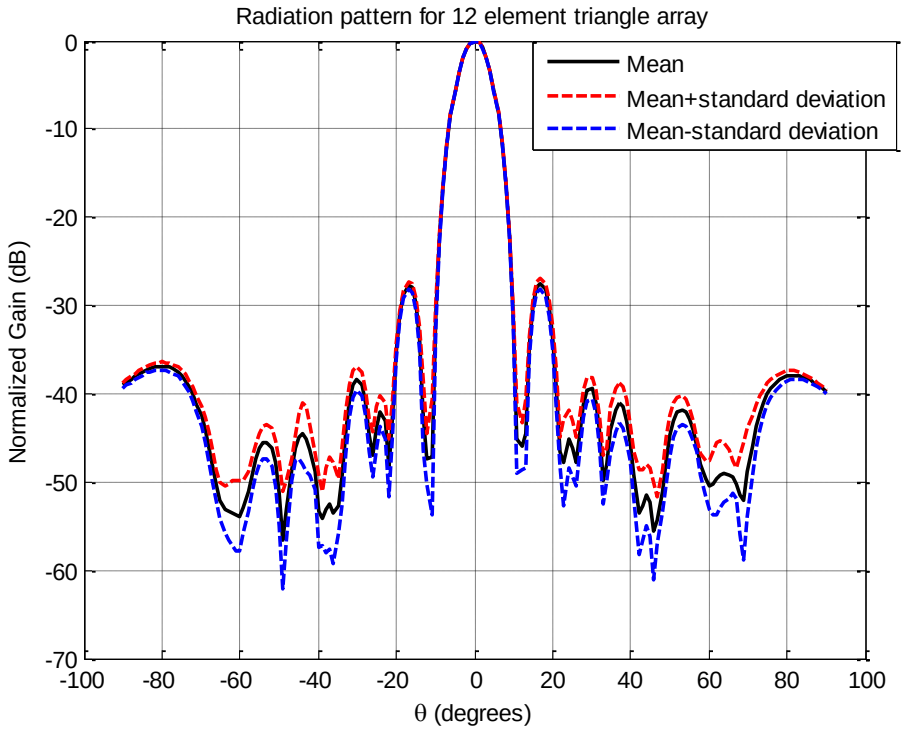

Figure 5-35 Statistical normalized radiation pattern with one standard deviation margin for triangle excitation with 10% permittivity variation.

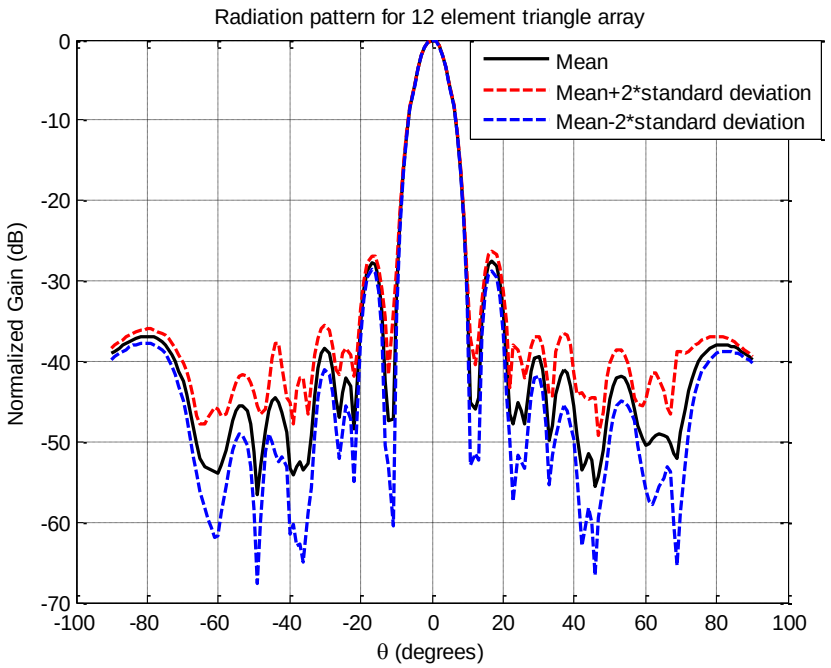

Figure 5-36 Statistical normalized radiation pattern with two standard deviation margin for triangle excitation with 10% permittivity variation.

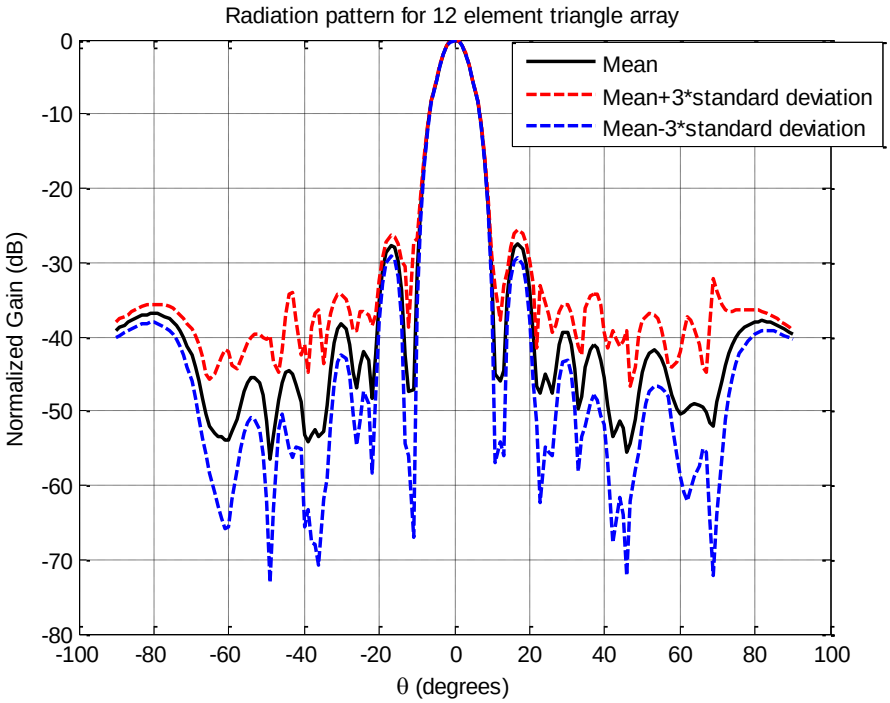

Figure 5-37 Statistical normalized radiation pattern with three standard deviation margin for triangle excitation with 10% permittivity variation.

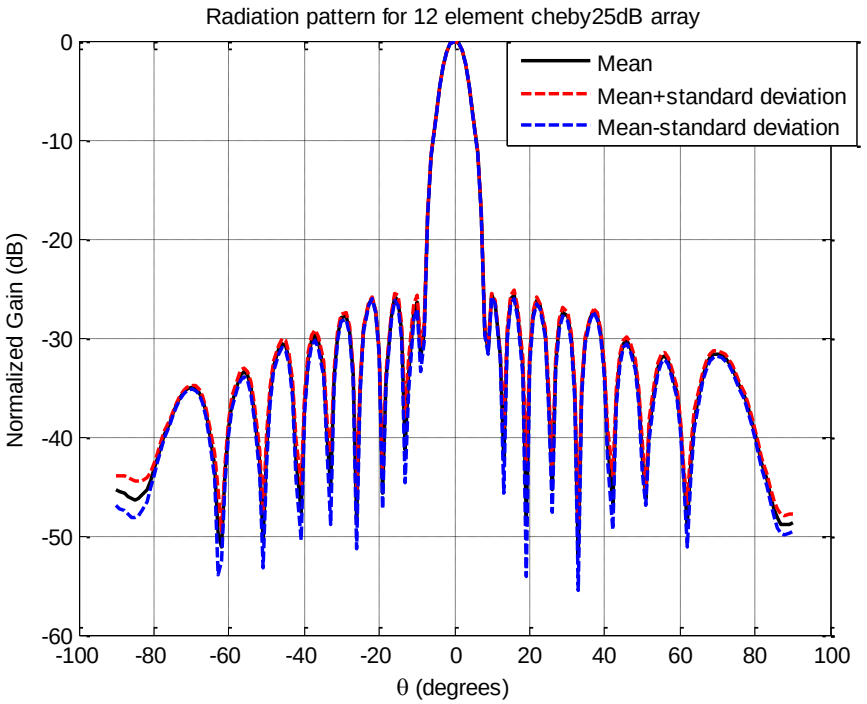

Figure 5-38 Statistical normalized radiation pattern with one standard deviation margin for Chebyshev 25 dB excitation with 10% permittivity variation.

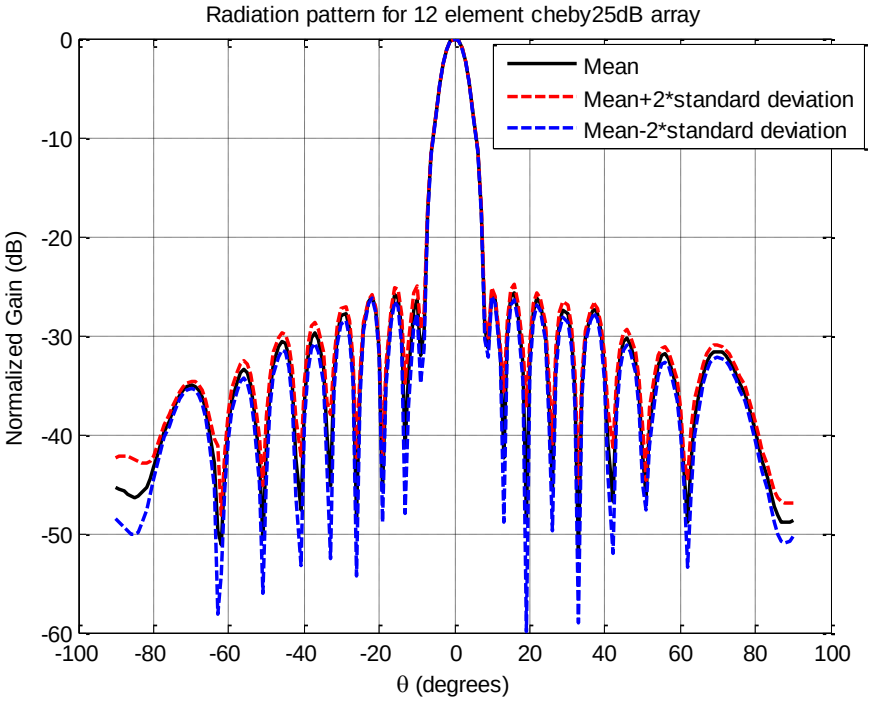

Figure 5-39 Statistical normalized radiation pattern with two standard deviation margin for Chebyshev 25 dB excitation with 10% permittivity variation.

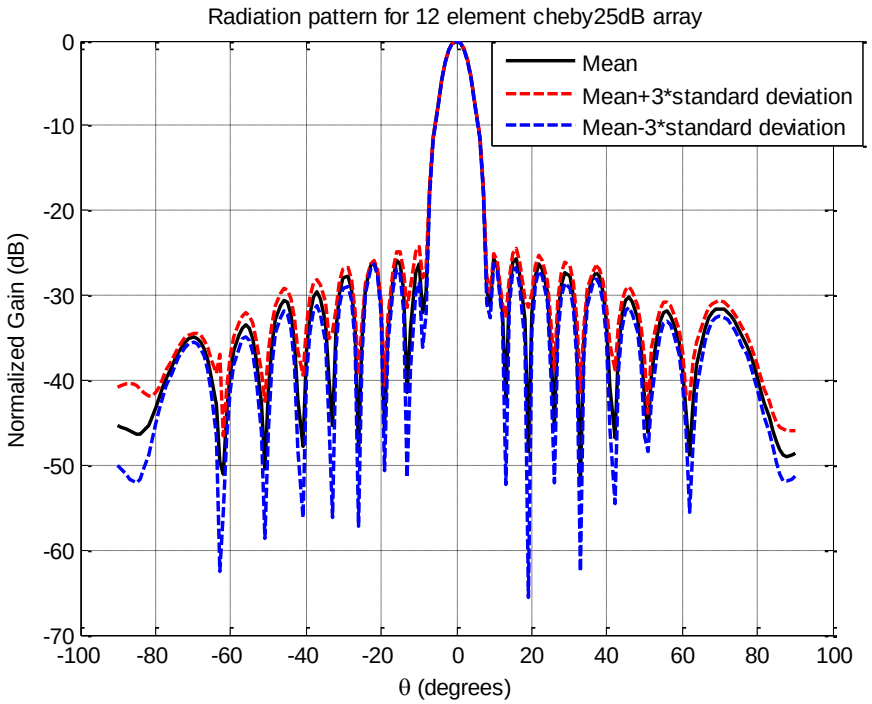

Figure 5-40 Statistical normalized radiation pattern with three standard deviation margin for Chebyshev 25 dB excitation with 10% permittivity variation.

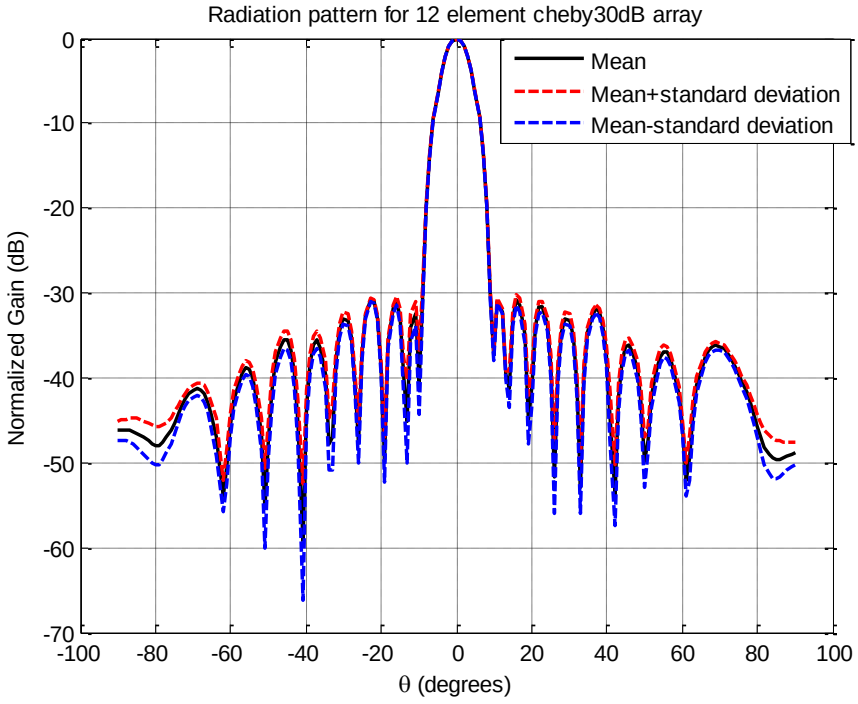

Figure 5-41 Statistical normalized radiation pattern with one standard deviation margin for Chebyshev 30 dB excitation with 10% permittivity variation.

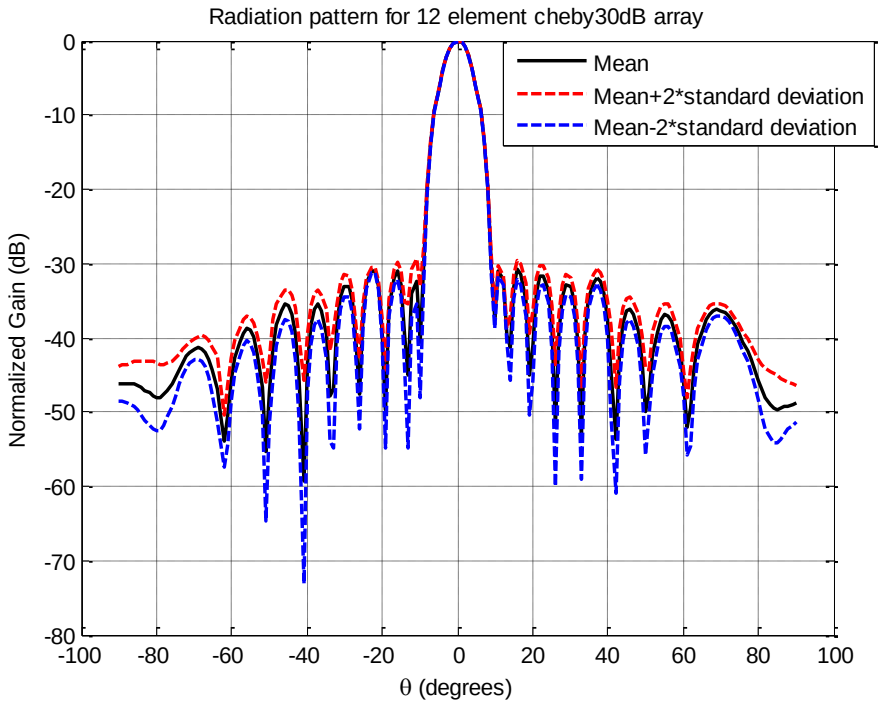

Figure 5-42 Statistical normalized radiation pattern with two standard deviation margin for Chebyshev 30 dB excitation with 10% permittivity variation.

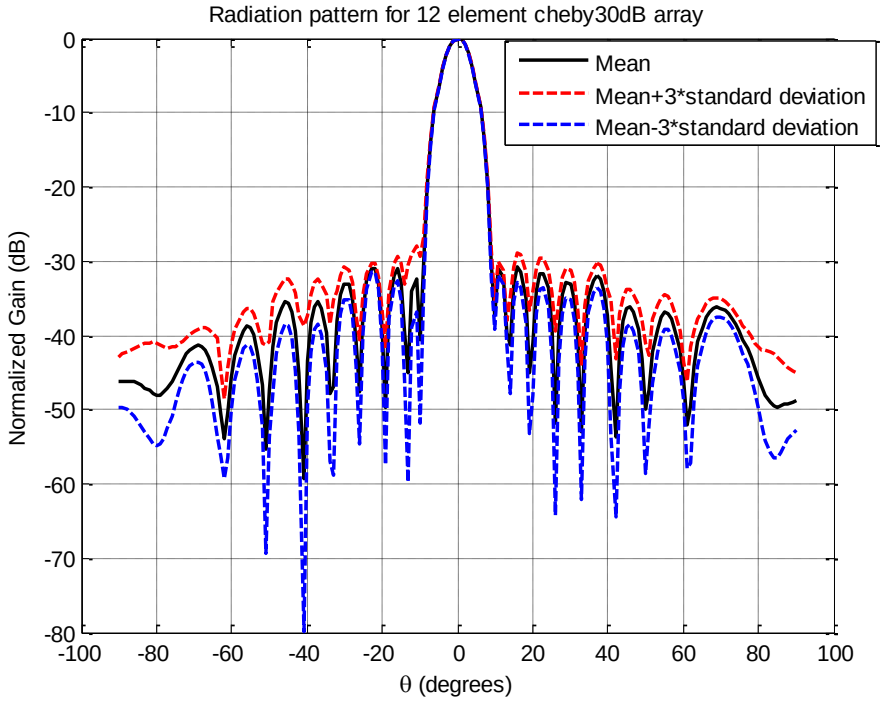

Figure 5-43 Statistical normalized radiation pattern with three standard deviation margin for Chebyshev 30 dB excitation with 10% permittivity variation.

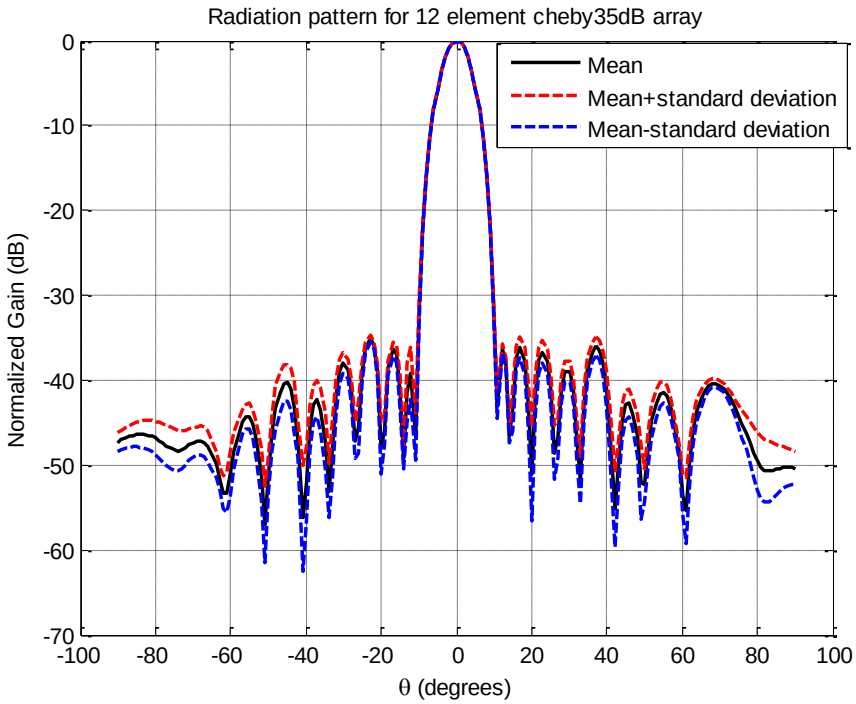

Figure 5-44 Statistical normalized radiation pattern with one standard deviation margin for Chebyshev 35 dB excitation with 10% permittivity variation.

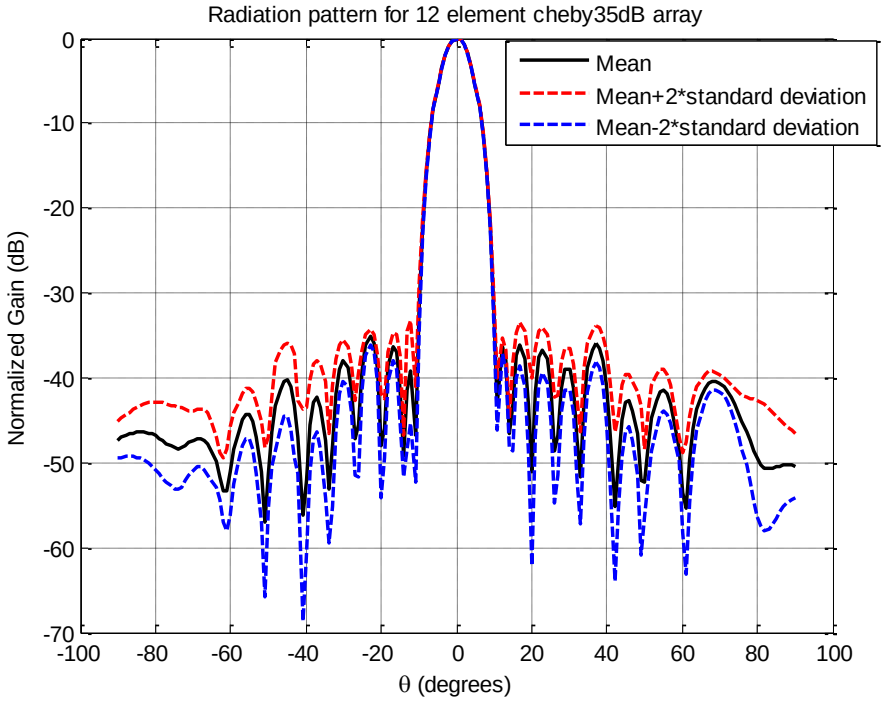

Figure 5-45 Statistical normalized radiation pattern with two standard deviation margin for Chebyshev 35 dB excitation with 10% permittivity variation.

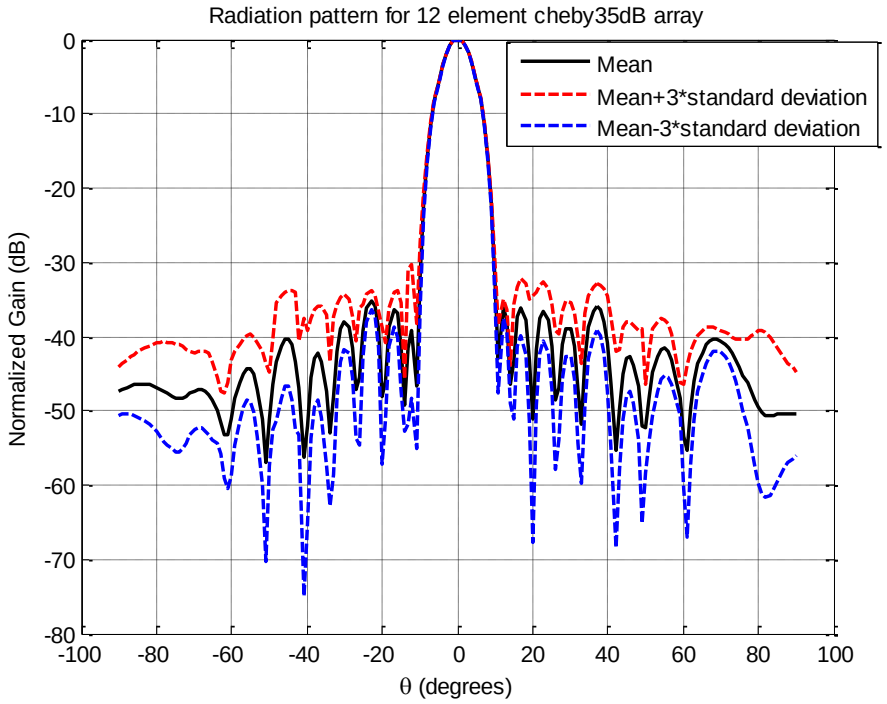

Figure 5-46 Statistical normalized radiation pattern with three standard deviation margin for Chebyshev 35 dB excitation with 10% permittivity variation.

Table 5-6 to Table 5-17 list the data for the side lobe ratio for the all the 12 cases. μ denotes the mean value, and σ is the standard deviation. From the tables, we can determine that the mean values are slightly better than the designed side lobe ratios. The variation for the 3-D sparse grid case is larger than each individual case.

Table 5-6 Permittivity impact on side lobe ratio with 5% variation (Unit: dB)

Excitation	Design	μ	+ σ	- σ	+ 2σ	- 2σ	+ 3σ	- 3σ
Triangle	-28.0	-27.7	-26.8	-28.5	-25.9	-29.3	-24.9	-29.5
Chebyshev 25dB	-24.9	-25.1	-24.9	-25.3	-24.4	-25.5	-23.8	-25.7
Chebyshev 30dB	-29.6	-29.9	-29.5	-30.4	-28.4	-30.7	-27.3	-31.0
Chebyshev 35dB	-34.1	-34.6	-33.7	-35.4	-31.9	-36.2	-26.2	-37.1

Table 5-7 Permittivity impact on side lobe ratio with 10% variation (Unit: dB)

Excitation	Design	μ	+ σ	- σ	+ 2σ	- 2σ	+ 3σ	- 3σ
Triangle	-28.0	-27.8	-26.9	-28.2	-26.2	-28.6	-25.6	-29.1
Chebyshev 25dB	-24.9	-25.7	-25.2	-25.9	-24.9	-26.1	-24.2	-26.5
Chebyshev 30dB	-29.6	-30.9	-30.2	-31.1	-29.4	-31.3	-28.1	-31.5
Chebyshev 35dB	-34.1	-35.2	-34.7	-35.6	-33.2	-36.0	-30.3	-36.6

Table 5-8 Permittivity impact on side lobe ratio with 20% variation (Unit: dB)

Excitation	Design	μ	+ σ	- σ	+ 2σ	- 2σ	+ 3σ	- 3σ
Triangle	-28.0	-27.3	-27.0	-27.6	-26.6	-27.9	-26.1	-28.2
Chebyshev 25dB	-24.9	-25.2	-24.6	-25.7	-24.2	-25.8	-23.6	-26.0
Chebyshev 30dB	-29.6	-30.1	-29.1	-30.7	-28.2	-31.1	-27.2	-31.4
Chebyshev 35dB	-34.1	-34.5	-33.2	-35.3	-31.5	-36.0	-26.0	-36.7

Table 5-9 Substrate height impact on side lobe ratio with 5% variation (Unit: dB)

Excitation	Design	μ	+ σ	- σ	+ 2σ	- 2σ	+ 3σ	- 3σ
Triangle	-28.0	-27.7	-27.1	-28.3	-26.5	-28.9	-25.9	-29.6
Chebyshev 25dB	-24.9	-25.2	-25.0	-25.5	-24.7	-25.8	-24.5	-26.0
Chebyshev 30dB	-29.6	-30.2	-29.7	-30.7	-29.2	-31.2	-28.3	-31.7
Chebyshev 35dB	-34.1	-34.9	-34.01	-35.9	-32.8	-36.7	-31.1	-37.7

Table 5-10 Substrate height impact on side lobe ratio with 10% variation (Unit: dB)

Excitation	Design	μ	+ σ	- σ	+ 2σ	- 2σ	+ 3σ	- 3σ
Triangle	-28.0	-27.4	-26.6	-28.1	-25.9	-28.5	-25.2	-28.9
Chebyshev 25dB	-24.9	-25.4	-24.8	-26.0	-24.2	-26.6	-23.6	-27.0
Chebyshev 30dB	-29.6	-30.5	-29.4	-31.6	-28.1	-32.0	-26.9	-32.4
Chebyshev 35dB	-34.1	-35.6	-33.5	-36.6	-31.3	-37.4	-28.4	-38.1

Table 5-11 Substrate height impact on side lobe ratio with 20% variation (Unit: dB)

Excitation	Design	μ	+ σ	- σ	+ 2σ	- 2σ	+ 3σ	- 3σ
Triangle	-28.0	-27.7	-27.1	-28.2	-26.5	-28.7	-26.0	-29.1
Chebyshev 25dB	-24.9	-25.7	-25.3	-25.9	-24.9	-26.2	-24.5	-26.4
Chebyshev 30dB	-29.6	-30.9	-30.2	-31.3	-29.5	-31.7	-28.7	-32.1
Chebyshev 35dB	-34.1	-35.7	-34.5	-36.7	-33.1	-37.3	-31.5	-37.8

Table 5-12 Patch width impact on side lobe ratio with 5% variation (Unit: dB)

Excitation	Design	μ	+ σ	- σ	+ 2σ	- 2σ	+ 3σ	- 3σ
Triangle	-28.0	-27.3	-27.1	-27.5	-26.2	-27.7	-25.4	-27.9
Chebyshev 25dB	-24.9	-25.4	-25.2	-25.6	-24.8	-25.4	-24.1	-25.9
Chebyshev 30dB	-29.6	-30.5	-30.2	-30.8	-29.0	-31.1	-27.5	-31.4
Chebyshev 35dB	-34.1	-35.3	-34.4	-35.7	-31.8	-36.1	-26.4	-36.5

Table 5-13 Patch width impact on side lobe ratio with 10% variation (Unit: dB)

Excitation	Design	μ	+ σ	- σ	+ 2σ	- 2σ	+ 3σ	- 3σ
Triangle	-28.0	-27.9	-26.9	-28.5	-25.8	-29.0	-24.7	-29.5
Chebyshev 25dB	-24.9	-25.8	-24.8	-26.5	-24.1	-26.9	-23.1	-27.0
Chebyshev 30dB	-29.6	-30.7	-29.1	-31.2	-27.0	-32.2	-24.4	-32.9
Chebyshev 35dB	-34.1	-34.4	-32.6	-36.1	-30.4	-37.3	-23.9	-37.7

Table 5-14 Patch width impact on side lobe ratio with 20% variation (Unit: dB)

Excitation	Design	μ	+ σ	- σ	+ 2σ	- 2σ	+ 3σ	- 3σ
Triangle	-28.0	-26.7	-26.3	-27.1	-25.5	-27.6	-24.5	-28.0
Chebyshev 25dB	-24.9	-25.2	-25.0	-25.5	-24.3	-25.8	-23.3	-26.0
Chebyshev 30dB	-29.6	-30.7	-29.4	-30.6	-28.2	-31.0	-26.9	-31.5
Chebyshev 35dB	-34.1	-34.7	-33.7	-35.6	-31.7	-36.5	-29.7	-37.3

Table 5-15 3-D sparse grid impact on side lobe ratio with 5% variation (Unit: dB)

Excitation	Design	μ	+ σ	- σ	+ 2σ	- 2σ	+ 3σ	- 3σ
Triangle	-28.0	-27.2	-26.3	-28.2	-25.4	-29.0	-24.5	-29.6
Chebyshev 25dB	-24.9	-25.6	-24.9	-26.1	-24.1	-26.5	-23.4	-26.9
Chebyshev 30dB	-29.6	-30.4	-29.1	-31.6	-27.9	-32.2	-26.7	-32.8
Chebyshev 35dB	-34.1	-34.6	-32.6	-36.7	-30.5	-38.3	-27.3	-39.2

Table 5-16 3-D sparse grid impact on side lobe ratio with 10% variation (Unit: dB)

Excitation	Design	μ	+ σ	- σ	+ 2σ	- 2σ	+ 3σ	- 3σ
Triangle	-28.0	-27.9	-26.9	-28.5	-25.8	-29.1	-24.7	-29.7
Chebyshev 25dB	-24.9	-25.3	-24.9	-25.6	-24.3	-26.9	-23.3	-27.3
Chebyshev 30dB	-29.6	-30.1	-29.6	-30.7	-27.8	-31.1	-25.2	-31.6
Chebyshev 35dB	-34.1	-34.7	-33.3	-36.1	-29.1	-36.7	-23.9	-37.4

Table 5-17 3-D sparse grid impact on side lobe ratio with 10% variation (Unit: dB)

Excitation	Design	μ	+ σ	- σ	+ 2σ	- 2σ	+ 3σ	- 3σ
Triangle	-28.0	-26.9	-26.1	-27.8	-25.3	-28.5	-23.2	-29.2
Chebyshev 25dB	-24.9	-25.0	-24.2	-25.6	-23.9	-26.1	-23.3	-26.4
Chebyshev 30dB	-29.6	-29.9	-29.3	-30.6	-28.3	-31.3	-27.2	-32.0
Chebyshev 35dB	-34.1	-34.5	-31.9	-35.8	-23.1	-36.4	-15.6	-37.1

What we are more interested in is the worst case scenarios for the side lobe ratio. For example, when considering the variation of the side lobe ratio due to uncertainties, the $+\sigma, +2\sigma, +3\sigma$ cases would have a worse side lobe ratio than we desired. That means if we want to maintain the side lobe ratio we want, there should be some compensation for suppressing the side lobe ratio due to uncertainties. As mentioned before, according to the 3σ rule, "three standard deviation" for a Gaussian random variable will cover 99.9% of all possible cases. While the techniques for doing this is beyond the scope of this dissertation, we plotted the compensation values in dB for these four different excitation cases, as shown in Figure 5-47 to Figure 5-50.

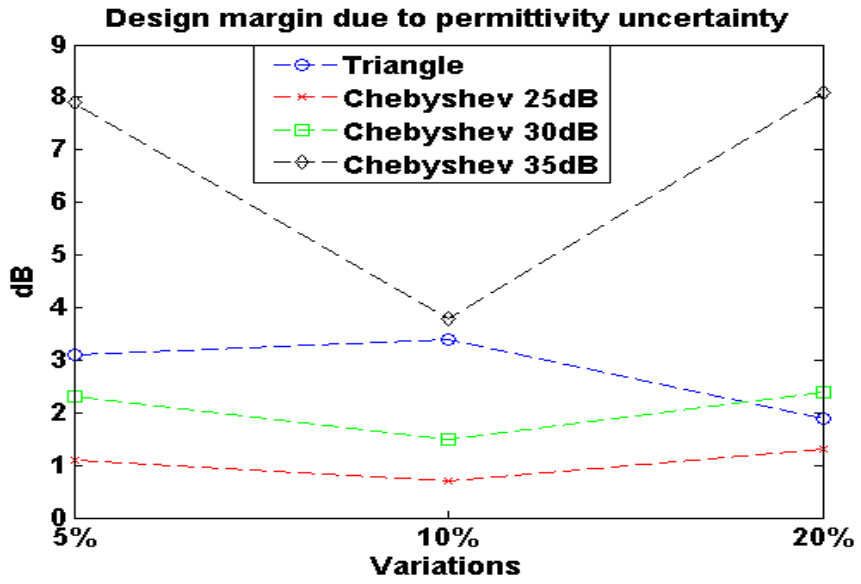

Figure 5-47 Compensation needed for desired side lobe ratio due to the uncertainty of substrate permittivity

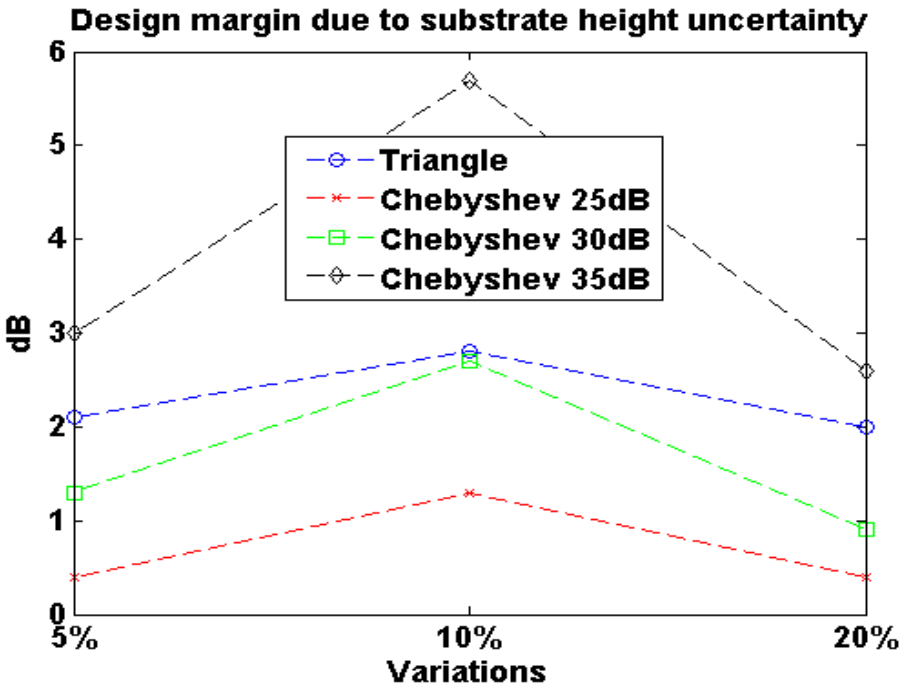

Figure 5-48 Compensation needed for desired side lobe ratio due to the uncertainty of substrate height

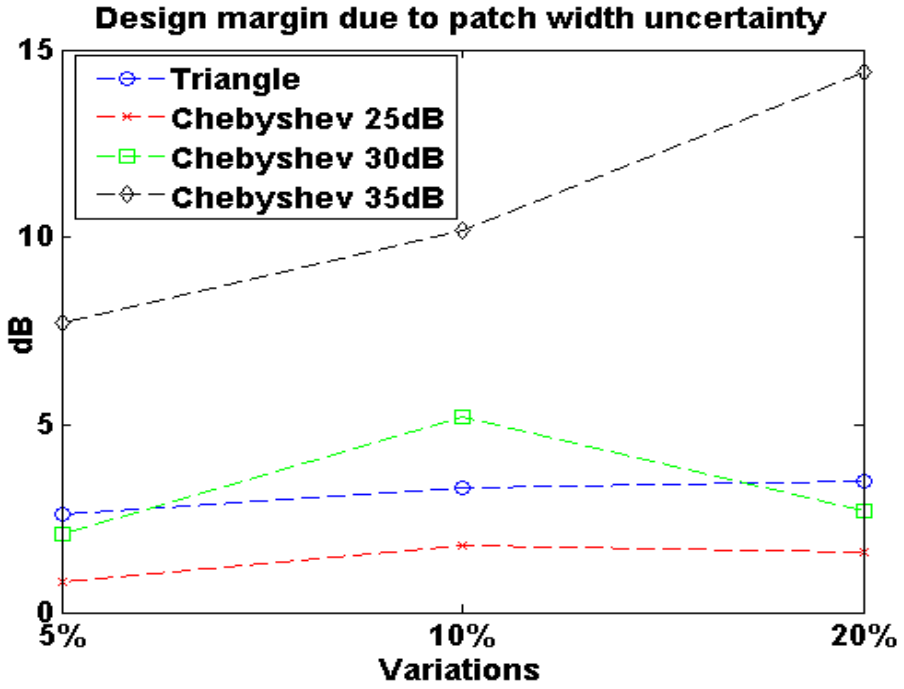

Figure 5-49 Compensation needed for desired side lobe ratio due to the uncertainty of patch width

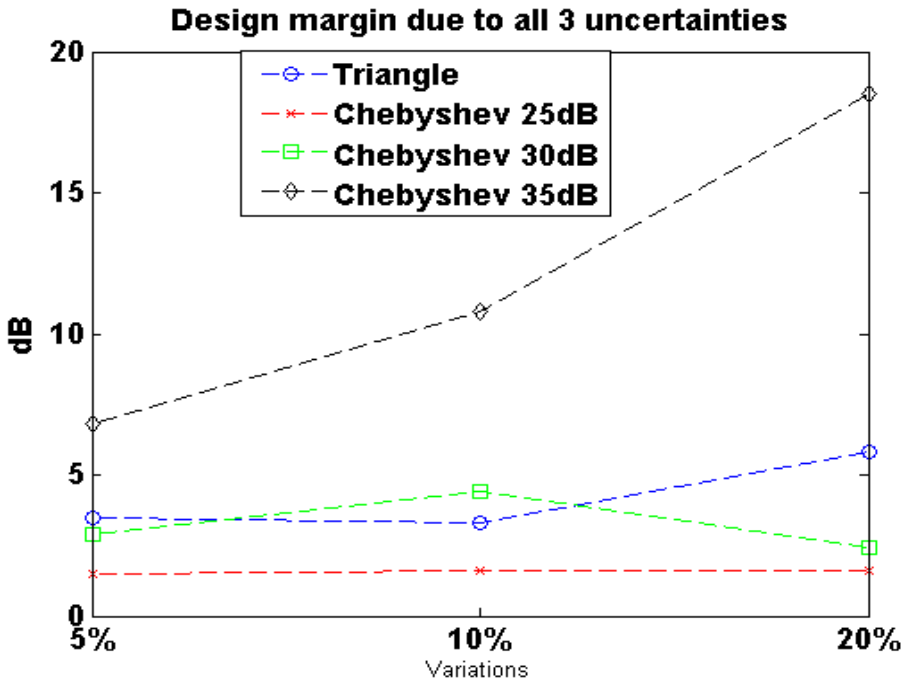

Figure 5-50 Compensation needed for desired side lobe ratio due to the uncertainty of all three parameters

From the figures, we can see that:

1) The lower value the side lobe ratio is for the original design; the bigger compensation value is needed to maintain the same side lobe ratio level. This is true for all four cases. The Chebyshev 35 dB design has the largest design margin.
2) Although we expect a larger variation for the output statistics with a larger variation of the random inputs, the side lobe ratio is not proportional to this assumption. For example, sometimes the design margin for a 5% variation from the inputs is larger than that of the 10% or 20% case.
3) The worst case for side lobe ratio happens when the 3 parameters are varying at the same time. That's because when the design parameters are varying at the same time, there is a good chance the antenna will be detuned from its original designed value at 7.52 GHz. For the single variable cases, we can see that the side lobe ratio is affected

by the patch width most, then the substrate permittivity and at last, the substrate height. If we look at the resonant frequency of the antenna as shown in (5.14), we can see that the variation in the resonant frequency will vary inversely proportional to the path width but square root of permittivity. This explains why patch width has a greater impact over permittivity. Also, the substrate height can cause the variation in the feed line's impedance, which could further affect the feeding and radiating efficiency of the antenna. However, its impact is the smallest,

$$f = \frac{c}{2\sqrt{\varepsilon_r}}\left(\frac{1}{W}\right), \tag{5.14}$$

where c is the speed of light in the free space.

Table 5-18 Permittivity impact on maximum gain (Unit: dB)

Excitation	Design	μ (5%)	σ (5%)	μ (10%)	σ (10%)	μ (20%)	σ (20%)
Triangle	18.01	17.94	0.03	17.92	0.07	17.88	0.16
Chebyshev 25dB	18.52	18.45	0.03	18.44	0.07	18.40	0.17
Chebyshev 30dB	18.23	18.16	0.03	18.15	0.07	18.11	0.17
Chebyshev 35dB	17.96	17.89	0.03	17.88	0.07	17.83	0.16

Table 5-19 Substrate height impact on maximum gain (Unit: dB)

Excitation	Design	μ (5%)	σ (5%)	μ (10%)	σ (10%)	μ (20%)	σ (20%)
Triangle	18.01	17.91	0.03	17.93	0.02	17.93	0.03
Chebyshev 25dB	18.52	18.43	0.03	18.45	0.15	18.46	0.05
Chebyshev 30dB	18.23	18.14	0.03	18.16	0.15	18.17	0.05
Chebyshev 35dB	17.96	17.87	0.03	17.88	0.16	17.89	0.05

Table 5-20 Patch length impact on maximum gain (Unit: dB)

Excitation	Design	μ (5%)	σ (5%)	μ (10%)	σ (10%)	μ (20%)	σ (20%)
Triangle	18.01	17.97	0.06	17.91	0.11	17.74	0.39
Chebyshev 25dB	18.52	18.50	0.07	18.43	0.13	18.24	0.39
Chebyshev 30dB	18.23	18.21	0.07	18.14	0.12	17.97	0.39
Chebyshev 35dB	17.96	17.93	0.07	17.88	0.11	17.70	0.39

Table 5-21 3-D sparse gird impact on maximum gain (Units: dB)

Excitation	Design	μ (5%)	σ (5%)	μ (10%)	σ (10%)	μ (20%)	σ (20%)
Triangle	18.01	17.96	0.16	17.91	0.23	17.73	0.45
Chebyshev 25dB	18.52	18.28	0.19	18.25	0.24	16.99	0.63
Chebyshev 30dB	18.23	18.13	0.12	18.15	0.17	16.70	0.62
Chebyshev 35dB	17.96	17.95	0.11	17.87	0.17	17.69	0.47

Another output we want to look at is the maximum gain for the antenna array. Again the data are listed from Table 5-18 to Table 5-19. It's observed that:

1) The mean values are slightly smaller than the designed values.
2) When the parameters vary at the same time, the variation for the maximum gain will be greater. But the actual values are quite small.
3) For different types of excitation, the variations seem to be almost the same as long as the input parameters of the antenna array are the same. This suggests that the maximum gain the array can achieve may be determined by the configuration of the array and be less vulnerable to the excitation method.

5.6 Summary

In this Chapter, the stochastic collocation scheme for solving Maxwell equations is investigated. Basic ideas and concepts such as interpolation, collocation points' selection, and post processing for output statistics are presented. The stochastic collocation method is highly preferred because the implementation is straightforward and non-intrusive, just like the Monte Carlo method. Thus, there is no need to change existing EM solvers such as the FDTD method and the Finite Element Method. On the other hand, it can achieve much faster convergence by properly choosing interpolation polynomial basis and numerical quadrature rules, which are similar to the stochastic Galerkin scheme as discussed in Chapter 4.

We used the sparse grid method based on the collocation scheme for stochastic analysis of interconnecting channels in high-speed circuit applications. To ensure the proper transmission of the channel, it is important to keep the impedance as continuous as possible. However, geometry and material uncertainties could affect the impedance of the interconnecting channels in certain degrees. Thus, it is crucial to understand the impact of these uncertainties. Numerical examples including the single-layer microstrip line, a two-layer structure with a through via, and commercial connector model are considered by analyzing the eye diagrams. It is demonstrated that we can give an accurate prediction of signal behaviors after propagating through a channel with existing uncertainties. Using the concept of the statistical eye diagram, we can provide a statistical margin with different confidence intervals. This can serve as a guide for both design and measurement when given the manufacturing error of products.

Also, we perform the uncertainty analysis in the antenna array design problems. It's

noticed that for a linear antenna array, the maximum gain is insensitive to the uncertainties of random inputs. Although the variation for the gain will be larger with a larger variation of the input parameters, the actual values are quite small. When designing an antenna array with an ultra-low side lobe, the lower the side lobe is, the greater the impact it will suffer due to the input uncertainties. Since the antenna elements are aligned close to each other, mutual coupling may also play a role in making the side lobe ratio worse than we desire. This might explain why the worst case side lobe ratio will always become worse with a larger input variation. Performing those uncertainty analyses can provide us with a set of design margin which should be considered back into the original design in order to maintain the original desired side lobe ratio.

Chapter 6 Stochastic analysis of random medium with correlations

6.1 Introduction

Due to fabrication error, there are uncertainties inevitably existing in the material properties of a product. Material properties such as permittivity and conductivity could result in variations in the system output. In Chapter 3, we assume the dielectric substrate of the microstrip line is made of a homogeneous medium. In some cases, the material parameters might show some spatial correlation with themselves. For example, the permittivity of the random medium is a function of space, with the correlation characterized by the covariance matrix. In this case, the Karhunen-Loeve Expansion (KLE) can be used to decompose the covariance matrix into a series of eigenvalues and eigenvectors. Another scenario is that the material parameters might have a correlation between each other. For example, the permittivity and conductivity are joint Gaussian variables, with the correlation described by the correlation coefficient. In this case, we can do a linear mapping of the original correlated variables to obtain a pair of independent variables. Based on the "finite nose assumption" described in [26], the stochastic collocation method can be applied to analyze multi-dimensional independent random variables cases.

In this chapter, numerical examples are calculated using the finite difference time domain (FDTD) method. All stochastic methods we mentioned above are illustrated in Section 6.2. In Section 6.3, two examples are studied using KLE. We assume the

permittivity is a spatially correlated Gaussian random process. In Section 6.4, permittivity and conductivity of a lossy medium are treated as two joint Gaussian variables. Finally, the conclusion is summarized in Section 6.5.

6.2 Theory

6.2.1 Karhunen-Loeve Expansion (KLE)

A random process can be represented by a series of deterministic functions with corresponding coefficients. This spectral representation is similar to the Fourier Transform. Consider a random process denoted as $\varpi(\mathbf{X},\theta)$, which is defined on a bounded domain $D^d, d=1,2,3$ and probability space (Ω, A, P). The process has a mean value of $\overline{\varpi}(\mathbf{X},\theta)$ and finite variance of σ^2. According to [66], the random process can be expressed as

$$\varpi(\mathbf{X},\theta) = \overline{\varpi}(\mathbf{X},\theta) + \sum_{i=1}^{\infty} \sqrt{\lambda_i}\,\xi_i(\theta)\, f_i(\mathbf{X}), \tag{6.1}$$

where λ_i and $f_i(\mathbf{X})$ are the eigenvalues and eigenvectors of the covariance matrix $C(\mathbf{X_1},\mathbf{X_2})$. By definition, $C(\mathbf{X_1},\mathbf{X_2})$ is bounded, positive definite, and symmetric. Following Mercer's Theorem [63], the covariance matrix can be decomposed as

$$C(\mathbf{X_1},\mathbf{X_2}) = \sum_{i=1}^{\infty} \lambda_i\, f_i(\mathbf{X_1})\, f_i(\mathbf{X_2}). \tag{6.2}$$

The deterministic eigenvalues λ_i and eigenvectors $f_i(\mathbf{X})$ are solutions of the integral equation

$$\int_{D^d} C(\mathbf{X_1},\mathbf{X_2})\, f_i(\mathbf{X_1}) d\mathbf{X_1} = \lambda_i\, f_i(\mathbf{X_2}) \ . \tag{6.3}$$

Due to the positive definite and symmetric property of the covariance matrix, its

eigenvectors form a complete orthogonal set which satisfies

$$\int_{D^d} f_i(\mathbf{X}) f_j(\mathbf{X}) d\mathbf{X} = \delta_{ij}, \tag{6.4}$$

where δ_{ij} is the Kronecker delta function.

The parameter $\{\xi_i(\theta)\}_{i=1}^{\infty}$ is a set of uncorrelated random variables which can be expressed by

$$\xi_i(\theta) = \frac{1}{\sqrt{\lambda_i}} \int_{D^d} [\varpi(\mathbf{X}, \theta) - \overline{\varpi}(\mathbf{X}, \theta)] f_i(\mathbf{X}) d\mathbf{X}. \tag{6.5}$$

Their mean value and covariance are given by

$$E[\xi_i(\theta)] = 0 \ , \tag{6.6}$$

$$E[\xi_i(\theta)\xi_j(\theta)] = \delta_{ij} \ . \tag{6.6}$$

Equation (6.6) indicates the variables are at zero mean and (6.7) indicates they are uncorrelated with a unit variance.

The spectral expansion in (6.1) is known as the Karhuen-Loeve expansion (KLE) [65][68][71]. It provides a characterization of a second-order random process in terms of uncorrelated random variables and deterministic orthogonal function. In practical implementation, the expansion is approximate by a finite number of terms, say *N*,

$$\varpi(\mathbf{X}, \theta) \approx \varpi_N(\mathbf{X}, \theta) = \sum_{i=1}^{N} \sqrt{\lambda_i} \xi_i(\theta) f_i(\mathbf{X}). \tag{6.8}$$

The corresponding covariance matrix is approximated as

$$C(\mathbf{X_1}, \mathbf{X_2}) \approx C_N(\mathbf{X_1}, \mathbf{X_2}) = \sum_{i=1}^{N} \lambda_i f_i(\mathbf{X_1}) f_i(\mathbf{X_2}). \tag{6.9}$$

It has been proved in [37] [67] that this truncation is optimal to minimize the mean square error. In this dissertation, we use another way to quantify the truncation error of

the KL expansion, from an energy spectrum point of view.

Before truncation, the expected energy of the process is

$$E[\int_{D^d}[\varpi(\mathbf{X},\theta)-\overline{\varpi}(\mathbf{X},\theta)]^2 d\mathbf{X}]=\sum_{i=1}^{\infty}\lambda_i\ . \tag{6.10}$$

After truncation at an order of *N*, the expected energy in the approximated process becomes

$$E[\int_{D^d}[\varpi_N(\mathbf{X},\theta)-\overline{\varpi}(\mathbf{X},\theta)]^2 d\mathbf{X}]=\sum_{i=1}^{N}\lambda_i\ . \tag{6.11}$$

Define the accumulated energy ratio (ANR) as

$$\text{ANR}=\frac{\sum_{i=1}^{N}\lambda_i}{\sum_{i=1}^{\infty}\lambda_i} \tag{6.12}$$

and it provides us an intuitive way to quantify the truncation error in terms of how much energy the *N* terms account for the total energy.

In the KL expansion, the key step is to find the eigenvalues λ_i and eigenfunctions $f_i(\mathbf{X})$ of the covariance function $C(\mathbf{X_1},\mathbf{X_2})$. This involves the solution of the homogeneous Fredholm integral equation [69], which can be obtained analytically or numerically.

For some cases, the covariance function is twice differentiable with respect to $\mathbf{X}$, then it can solved analytically with the given boundary values. For example, (6.13) shows the covariance function of a first-order stationary Markov process [70], defined within $[-a,a]$

$$C(x_1,x_2)=\sigma^2 e^{-|x_1-x_2|/b}, \tag{6.13}$$

where σ^2 is the variance associated with the random process and b is the correlation length. The analytical solution of the eigenvalues are given in (6.13) and (6.14).

$$\lambda_i = \frac{2\sigma^2 b}{b^2\omega_i^2 + 1}, i = 1,3,5,\cdots, \tag{6.14}$$

$$\lambda_i = \frac{2\sigma^2 b}{b^2\omega_i^{*2} + 1}, i = 2,4,6,\cdots, \tag{6.15}$$

where ω_i and ω_i^* are defined as

$$\omega^2 = \frac{-\lambda + 2\sigma^2 b}{\lambda b^2}, \tag{6.16}$$

and are solutions for the transcendental equations in (6.17) and (6.18)

$$1 - b\omega\tan(\omega a) = 0, \tag{6.17}$$

$$b\omega^* + \tan(\omega^* a) = 0. \tag{6.18}$$

Eigenfunctions are given in (6.19) and (6.20).

$$f_i(x) = \frac{\cos(\omega_i x)}{\sqrt{a + \frac{\sin(2\omega_i a)}{2\omega_i}}}, i = 1,3,5,\cdots, \tag{6.19}$$

$$f_i(x) = \frac{\sin(\omega_i^* x)}{\sqrt{a - \frac{\sin(2\omega_i^* a)}{2\omega_i^*}}}, i = 2,4,6,\cdots. \tag{6.20}$$

More generally, when the eigenvalues and eigenfunctions cannot be found analytically, numerical methods can be applied. Consider a Galerkin procedure, assuming the eigenfunctions of the convariance function can be expanded as

$$f_i(\mathbf{X}) = \sum_{j=1}^{N} a_j^i \Psi_j(\mathbf{X}), \tag{6.21}$$

where $\{\Psi_j(\mathbf{X})\}_{j=1}^{\infty}$ is a complete set of basis functions defined in the Hilbert space.

Substrate (6.21) into (6.3), yields the error of the Galerkin projection as

$$\begin{aligned}\delta_N &= \int_{D^d} C(\mathbf{X_1},\mathbf{X_2})\sum_{j=1}^{N} a_j^i \Psi_j(\mathbf{X}_1)d\mathbf{X_1} - \lambda_i \sum_{j=1}^{N} a_j^i \Psi_j(\mathbf{X}_2) \\ &= \sum_{j=1}^{N} a_j^i \{\int_{D^d} C(\mathbf{X_1},\mathbf{X_2})\Psi_j(\mathbf{X}_1)d\mathbf{X_1} - \lambda_i \Psi_j(\mathbf{X}_2)\}\end{aligned} . \tag{6.22}$$

The requirement for the error is its orthognality to the Hilbert space, which means the inner product of the error term with the basis function vanishes,

$$< \delta_N, \Psi_k(\mathbf{X}) >= 0, k = 1, 2, \cdots, N , \tag{6.23}$$

or explicitly,

$$\begin{aligned}&\sum_{j=1}^{N} a_j^i \{\int_{D^d} [\int_{D^d} C(\mathbf{X_1},\mathbf{X_2})\Psi_j(\mathbf{X}_1)d\mathbf{X_1}]\Psi_k(\mathbf{X}_2)d\mathbf{X}_2 \\ &-\lambda_i \int_{D^d} \Psi_j(\mathbf{X}_1)\Psi_k(\mathbf{X}_2)d\mathbf{X}_2 \Psi_k(\mathbf{X}_2)\} = 0\end{aligned} . \tag{6.24}$$

Denote

$$\begin{aligned}A_{jk} &= \int_{D^d} [\int_{D^d} C(\mathbf{X_1},\mathbf{X_2})\Psi_j(\mathbf{X}_1)d\mathbf{X_1}]\Psi_k(\mathbf{X}_2)d\mathbf{X}_2 \\ &= \int_{D^d}\int_{D^d} C(\mathbf{X_1},\mathbf{X_2})\Psi_j(\mathbf{X}_1)\Psi_k(\mathbf{X}_2)d\mathbf{X_1}d\mathbf{X}_2\end{aligned} , \tag{6.25}$$

$$B_{jk} = \int_{D^d} \Psi_j(\mathbf{X}_2)\Psi_k(\mathbf{X}_2)d\mathbf{X}_2 , \tag{6.26}$$

then (6.24) can be written as a matrix form as

$$A_{jk} \cdot a_j^i = \delta_{jk}\lambda_i B_{jk} \cdot a_j^i . \tag{6.27}$$

Then eigenvalues λ_i and expansion coefficients a_j^i can be obtained by solving (6.27). And eigenfunctions can be constructed accordingly using (6.21).

If $\varpi(\mathbf{X},\theta)$ is a Gaussian process, which is a widely accepted assumption for most random processes in engineering problems, then the appropriated choice of $\{\xi_i(\theta)\}_{i=1}^{N}$ is a vector zero-mean and unit-variance uncorrelated (independent) Gaussian random variable.

The Gaussian process has been well studied, and for the non-Gaussian process, there are also some papers [72]-[74] discussing how to deal with it.

6.2.2 Bivariate Gaussian variables with joint PDF

Two correlated Gaussian random variables X and Y have a joint probability density function (PDF) described as

$$f_{X,Y} = \frac{1}{2\pi\sigma_X\sigma_Y\sqrt{1-\rho^2}} \cdot \exp\left\{\frac{-1}{2(1-\rho^2)}\left[\frac{(x-\overline{X})^2}{\sigma_X^2} - \frac{2\rho(x-\overline{X})(y-\overline{Y})}{\sigma_X\sigma_Y} + \frac{(y-\overline{Y})^2}{\sigma_Y^2}\right]\right\}, \quad (6.28)$$

in which $\overline{X}$ and σ_X^2 are mean and variance of X, $\overline{Y}$ and σ_Y^2 are mean and variance of Y, and ρ is the correlation coefficient. The covariance between X and Y is defined as

$$C_{X,Y} = \rho\sigma_X\sigma_Y \qquad \rho \in (-1,1) \ . \quad (6.29)$$

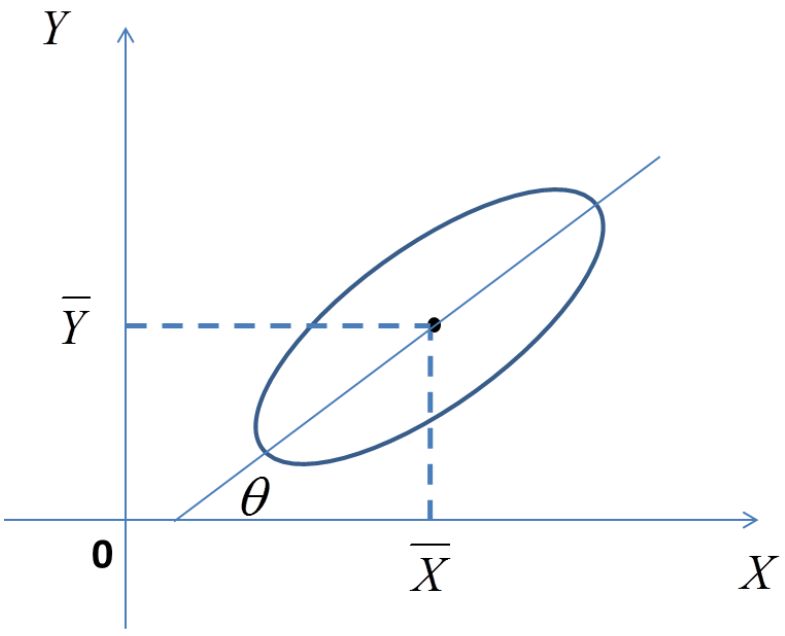

Figure 6-1 Joint probability density function of two correlated Gaussian random variables.

The projection of the joint PDF is shown in Figure 6-1. As we can see, there is an

angle between the principle axis and the X axis θ. Do a linear mapping on X and Y to get a pair of new random variables,

$$\begin{cases} X_1 = X\cos\theta + Y\sin\theta \\ Y_1 = -X\sin\theta + Y\cos\theta \end{cases}. \tag{6.30}$$

Since X_1 and Y_1 are a linear combination of two Gaussian variables, they are still Gaussian variables. Their mean values are given by

$$\begin{cases} \overline{X_1} = \overline{X}\cos\theta + \overline{Y}\sin\theta \\ \overline{Y_1} = -\overline{X}\sin\theta + \overline{Y}\cos\theta \end{cases}, \tag{6.31}$$

and variance is given by

$$\begin{cases} \sigma_{X_1}^2 = \cos^2\theta\cdot\sigma_X^2 + \sin^2\theta\cdot\sigma_Y^2 + \sin(2\theta)\cdot\rho\sigma_X\sigma_Y \\ \sigma_{Y_1}^2 = \sin^2\theta\cdot\sigma_X^2 + \cos^2\theta\cdot\sigma_Y^2 - \sin(2\theta)\cdot\rho\sigma_X\sigma_Y \end{cases}. \tag{6.32}$$

The covariance between X_1 and Y_1 becomes

$$C_{X_1,Y_1} = \frac{1}{2}\sin(2\theta)\cdot(\sigma_Y^2 - \sigma_X^2) + \cos(2\theta)\cdot\rho\sigma_X\sigma_Y. \tag{6.33}$$

Let $C_{X_1,Y_1} = 0$, then we have

$$\theta = \frac{1}{2}\tan^{-1}\left(\frac{2\rho\sigma_X\sigma_Y}{\sigma_X^2 - \sigma_Y^2}\right). \tag{6.34}$$

It means, if we rotate an angle of θ whose value is given above to get a new pair of Gaussian variables, then the two variables are uncorrelated (independent). A more detailed discussion can be found in [16].

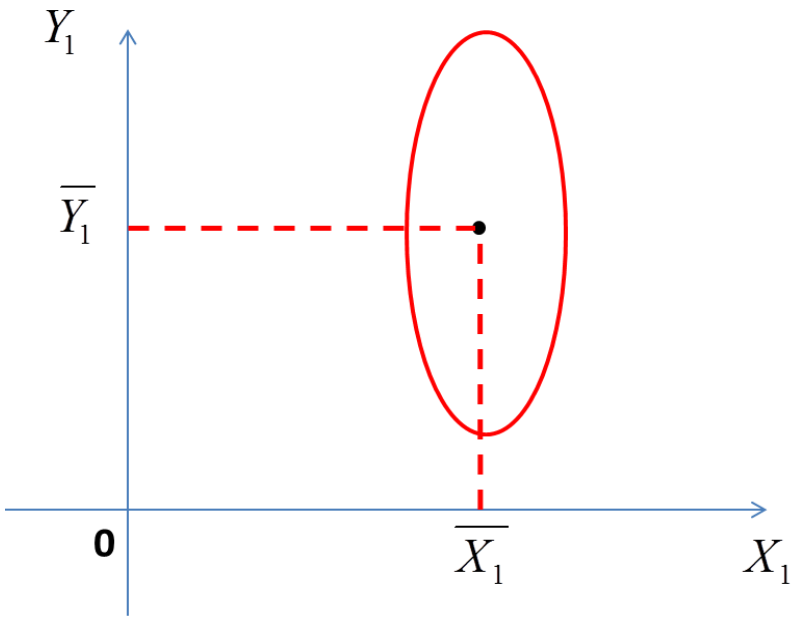

Figure 6-2 Joint probability density function of two uncorrelated Gaussian random variables.

The PDF for X_1 and Y_1 is

$$f_{X_1,Y_1} = \frac{1}{\sqrt{2\pi}\sigma_{X_1}} \exp\left\{-\frac{(x_1-\overline{X_1})^2}{2\sigma_{X_1}^2}\right\} \cdot \frac{1}{\sqrt{2\pi}\sigma_{Y_1}} \exp\left\{-\frac{(y_1-\overline{Y_1})^2}{\sigma_{Y_1}^2}\right\}. \tag{6.35}$$

The projection of the PDF is shown in Figure 6-2. As we can see, the two variables are orthogonal to each other.

6.3 Random Medium with Spatial Correlation

6.3.1 Example I: Differential Microstrip Lines

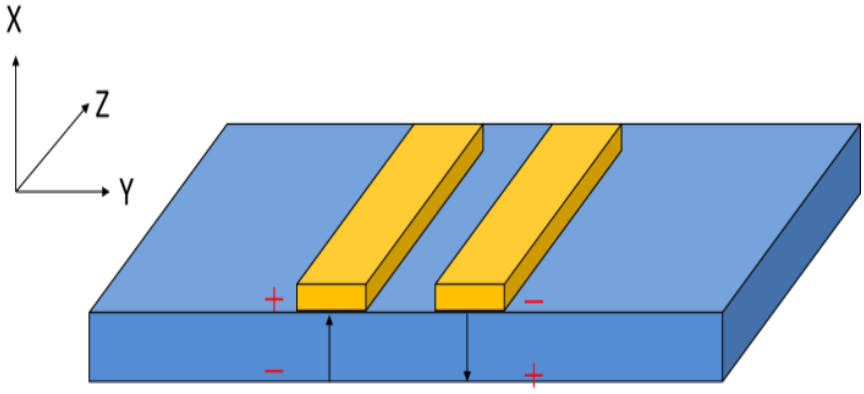

Figure 6-3 Differential microstrip line pair.

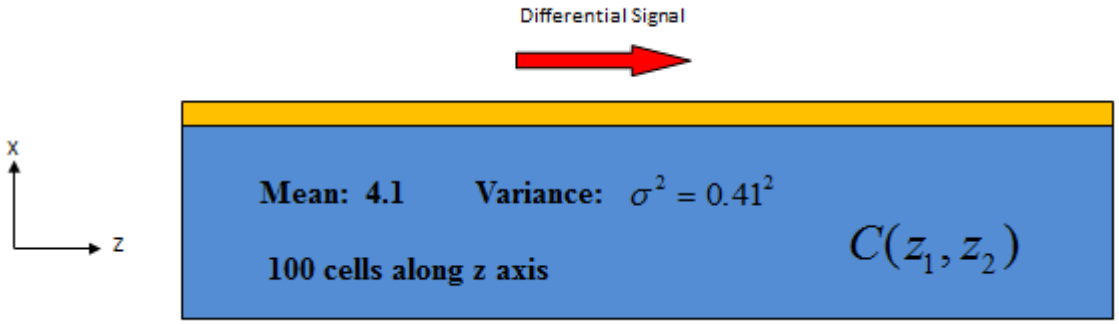

Figure 6-4 Side view of the differential transmission line.

Figure 6-3 shows a differential microstrip line structure. The substrate is made of an inhomogeneous medium with random permittivity, which is considered to be a Gaussian random process with a mean value of 4.1 and a standard deviation of 0.41. The height of the substrate is 0.8 mm. The two traces are both 1.6 mm wide and have a spacing of 1 mm. When the permittivity is set to be 4.1, the differential impedance of the microstrip pair is $100\,\Omega$. The two traces are fed with zero-phase, unit-amplitude but opposite polarized voltage sources along with a $50\,\Omega$ source resistance. The differential signal is propagating in the +z direction. In this problem, we assume the permittivity of the substrate material has a correlation along the z direction.

The covariance matrix (correlation function) is defined as

$$C(z_1, z_2) = \sigma^2 \cdot e^{-|z_1 - z_2|/L}, \tag{6.36}$$

where σ is the standard deviation of permittivity, L is the correlation length, which we assume is 1 m in this problem. There are 100 cells between the voltage source and the point we sampled. The covariance matrix is shown in Figure 6-5. After decomposition, the first six eigenvalues and eigenvectors are plotted in Figure 5 and Figure 6, respectively.

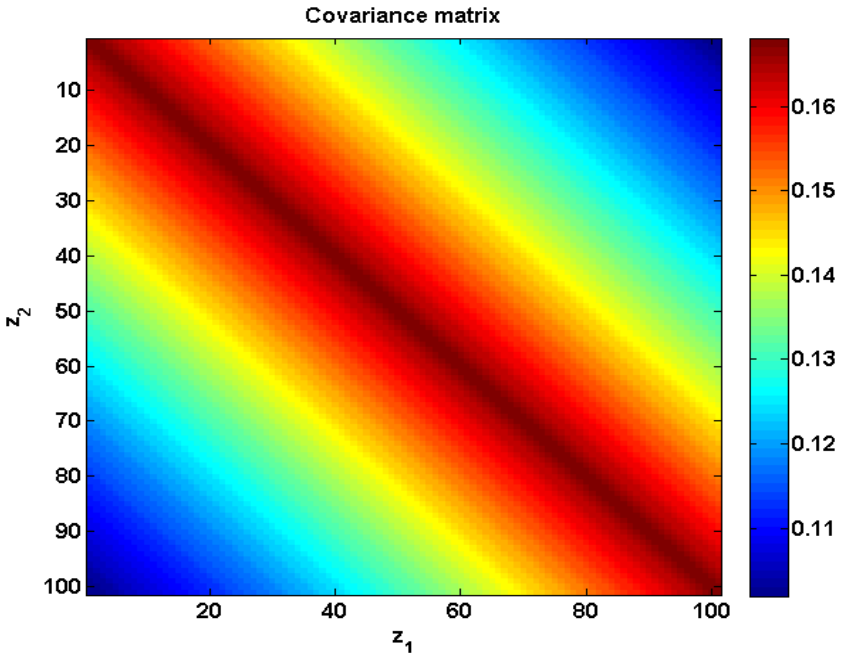

Figure 6-5 1-D covariance matrix.

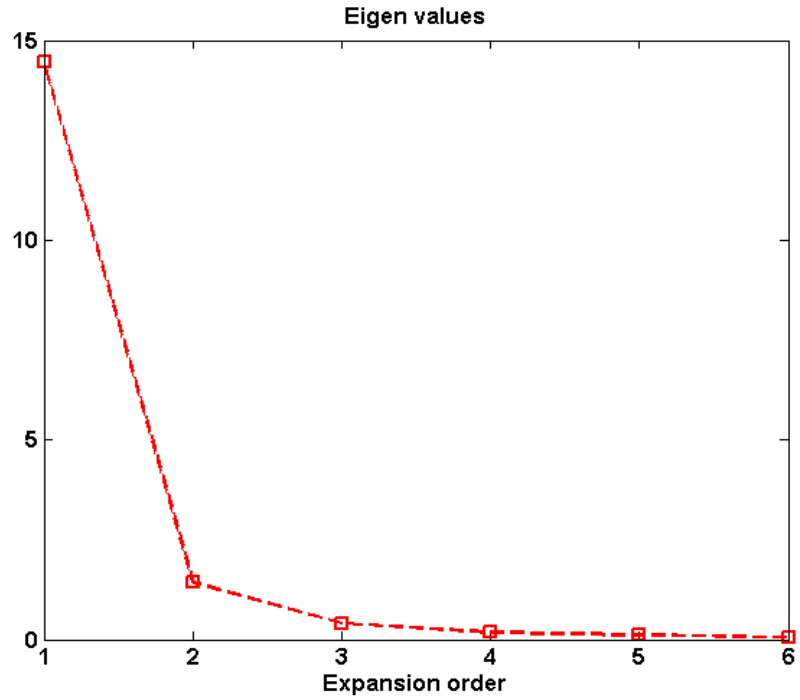

Figure 6-6 First six eigenvalues of the covariance matrix.

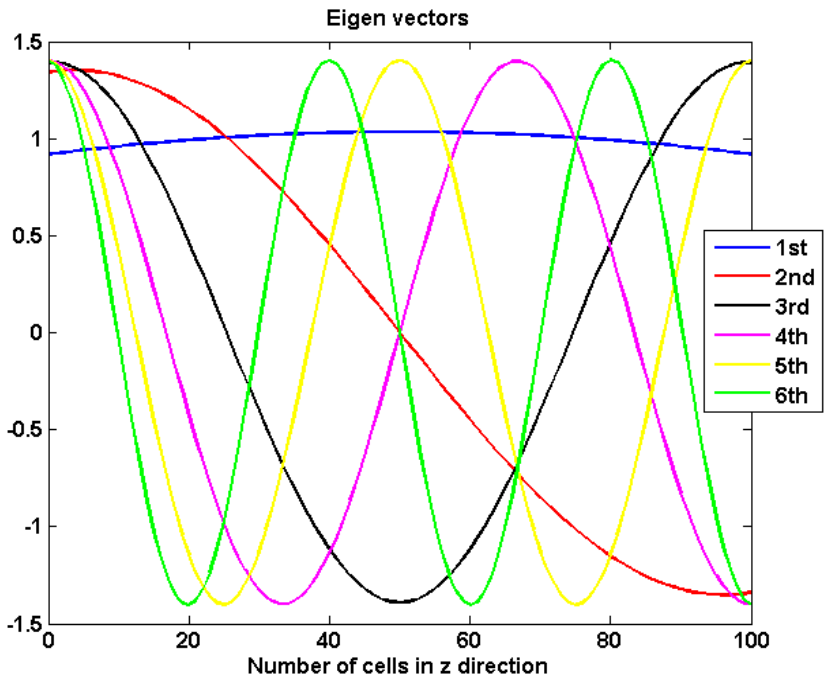

Figure 6-7 First six eigenvectors of the covariance matrix.

As defined in (6.12), the first six order of expansion accounts for about 98.15% of the total energy. The six-order KLE for the permittivity is given by

$$\begin{aligned} \varepsilon_r(z) &= \overline{\varepsilon_r}(z) + \sum_{i=1}^{6} \sqrt{\lambda_i}\,\xi_i(\theta) f_i(z) \\ &= 4.1 + \sum_{i=1}^{6} \sqrt{\lambda_i}\,\xi_i(\theta) f_i(z) \end{aligned} \quad . \tag{6.37}$$

Here, $\{\xi_i(\theta)\}_{i=1}^{6}$ are six independent, zero-mean, unit-variance Gaussian random variables. They don't have any physical meaning. However, they contribute to the variation of the stochastic process. Using the sparse grid, there will be 119 sets of random inputs. We randomly select six permittivity profiles as plotted in Figure 6-8.

The voltage wave form we are using is the same as in Chapter 5--a random trapezoid wave. After 109 times simulation and post processing, the mean value and standard deviation of the differential output voltage are shown in Figure 6-8 and Figure 6-10.

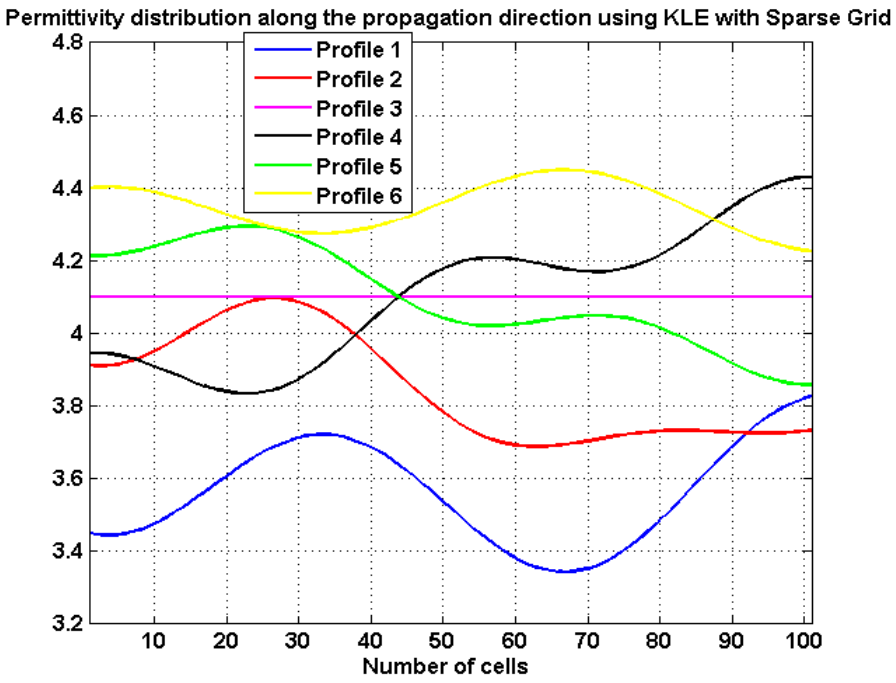

Figure 6-8 Possible permittivity distribution along the z direction using sparse grid method.

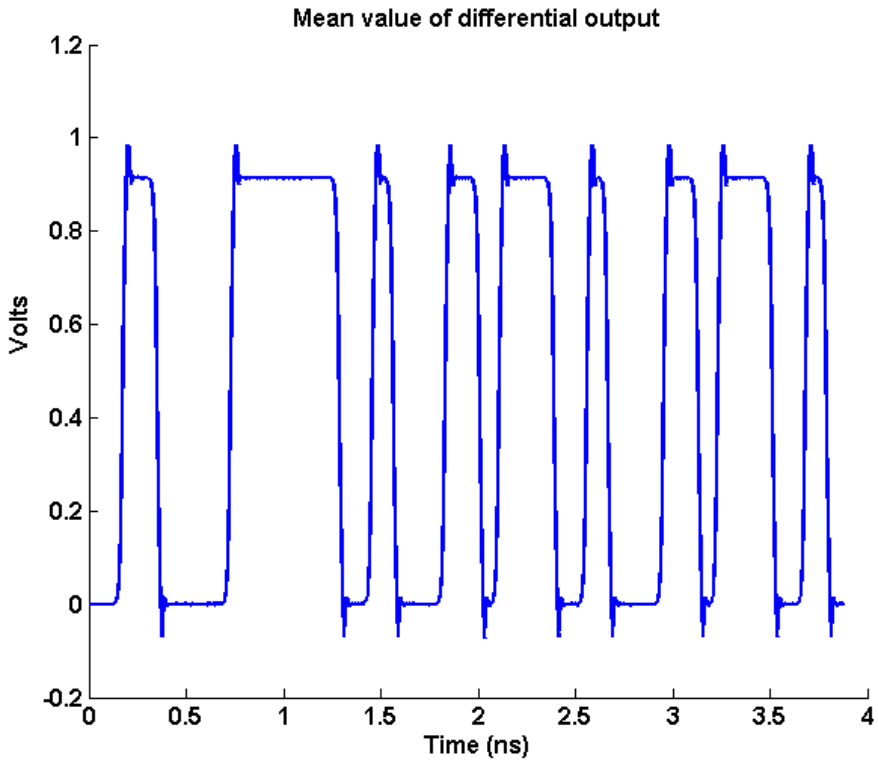

Figure 6-9 Mean value of the differential output voltage computed by sparse grid method.

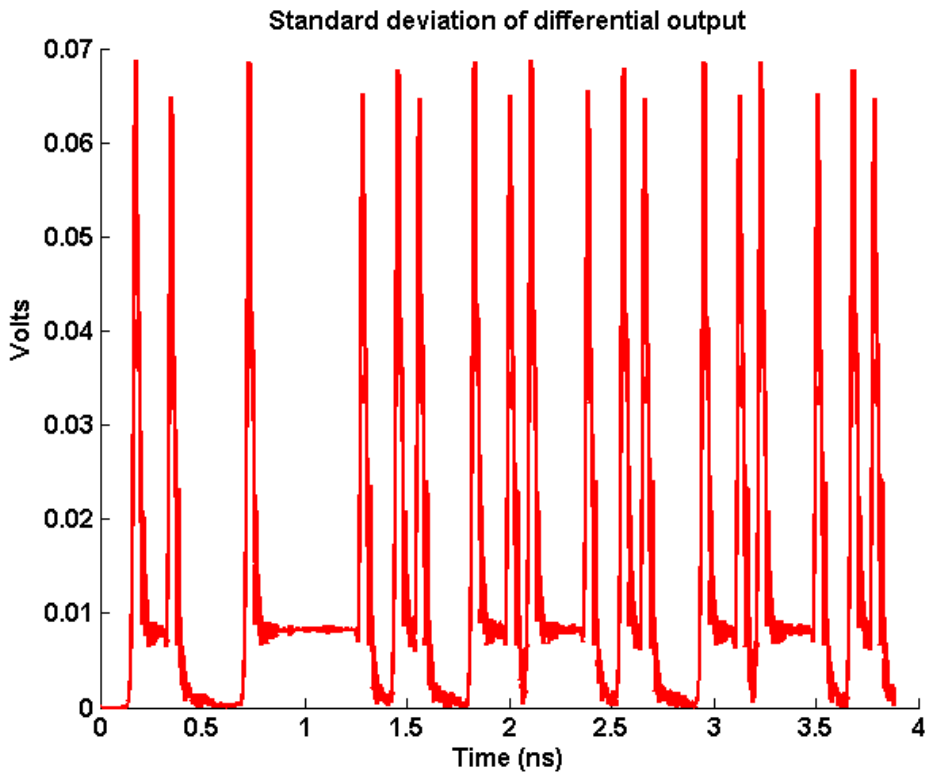

Figure 6-10 Standard deviation of the differential output voltage by sparse grid method.

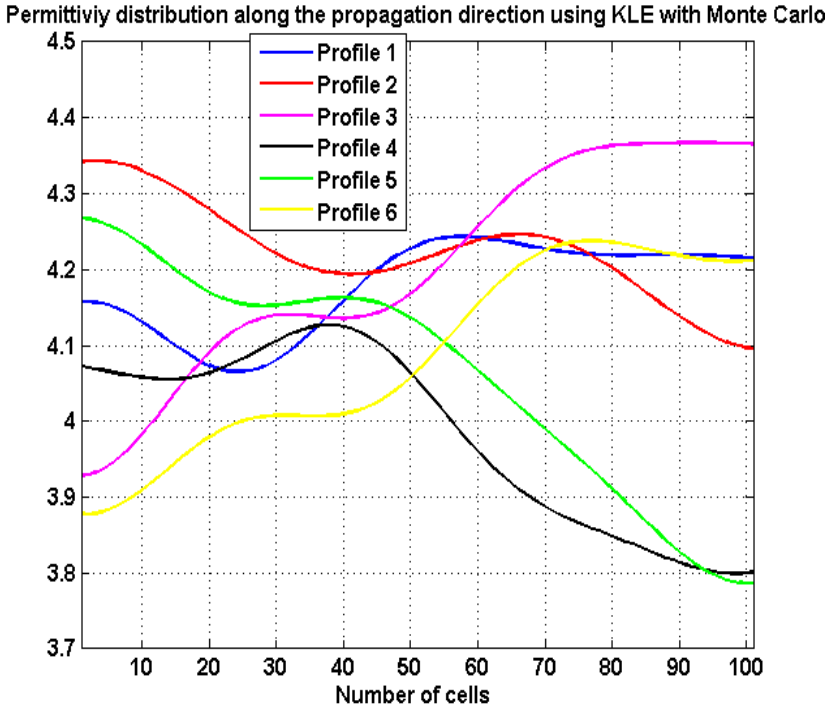

Figure 6-11 Possible permittivity distribution along the z direction using Monte Carlo method.

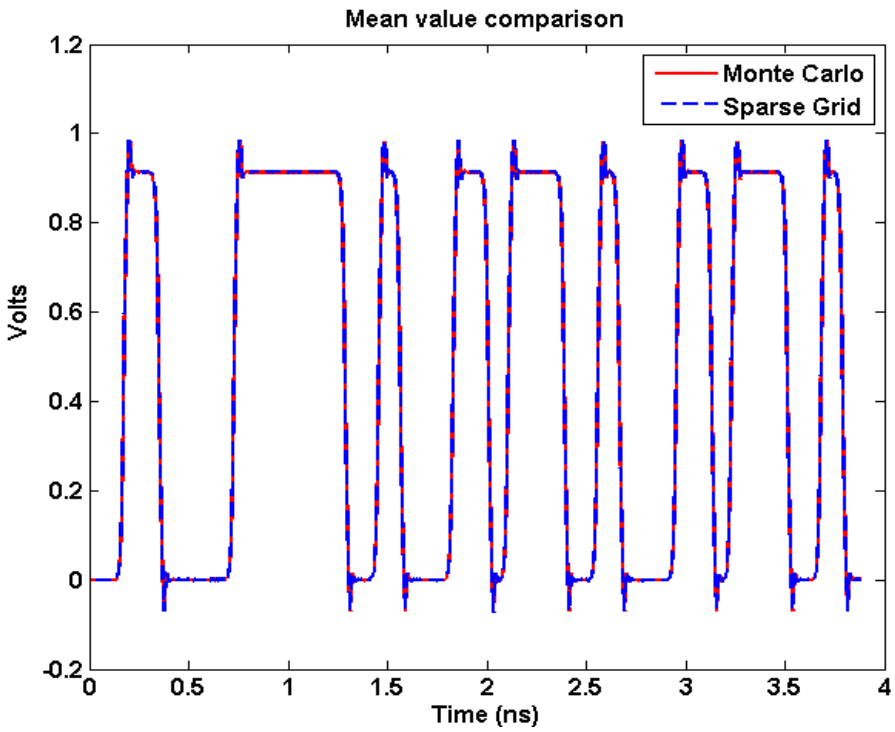

Figure 6-12 Mean value comparison of the differential output voltage by sparse grid method and Monte Carlo method.

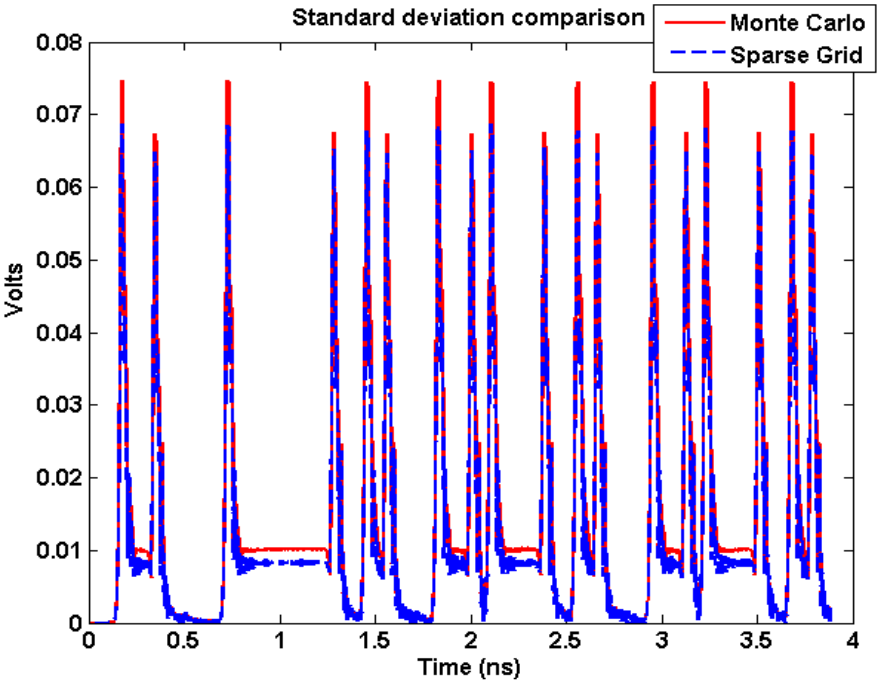

Figure 6-13 Standard deviation comparison of the differential output voltage by sparse grid method and Monte Carlo method.

To validate the statistics calculated by the SG method, we also perform 1000 times Monte Carlo (MC) simulations. The permittivity generated by the MC method is shown in Figure 6-11. And the mean and standard deviation comparison are shown in Figures 6-12 and 6-13. As we can see, they have good agreement with each other.

Next, we compare the results with the homogenous case. That is, we assume the substrate permittivity is a Gaussian random variable with same mean value 4.1 and standard deviation of 0.41. The comparison is shown in Figures 6-14 and 6-15.

It is observed that the mean values are almost the same for both correlated and uncorrelated cases. However, the standard deviation of the correlated case is much smaller than that of the uncorrelated case. If we take a look at Figure 6-5, the covariance achieves its maximum on its main diagonal, which is equal to the finite variance of the stochastic process. It means the overall variance of the output would be lower due to the correlation.

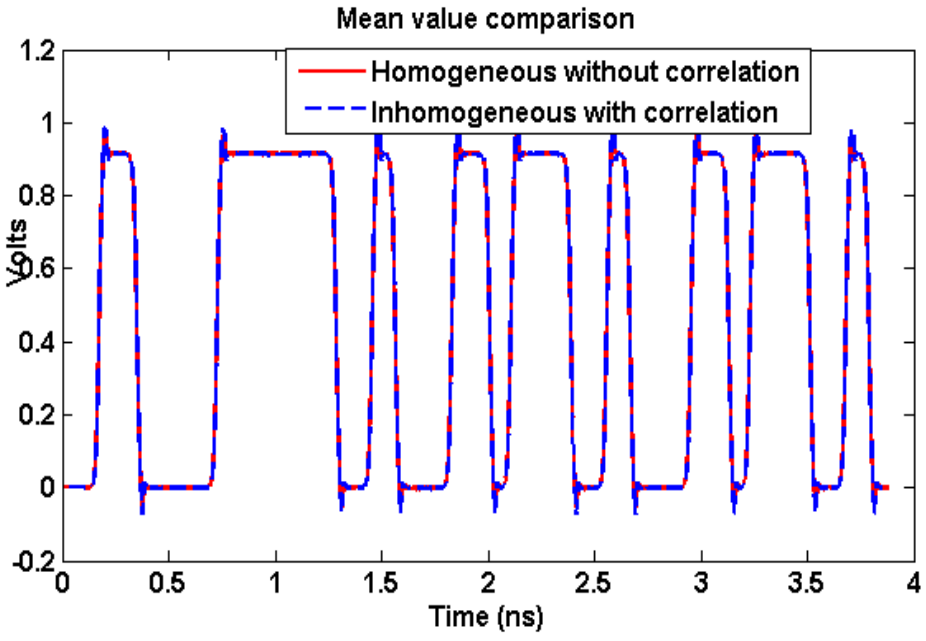

Figure 6-14 Mean value comparison of the differential output voltage between correlated and uncorrelated case.

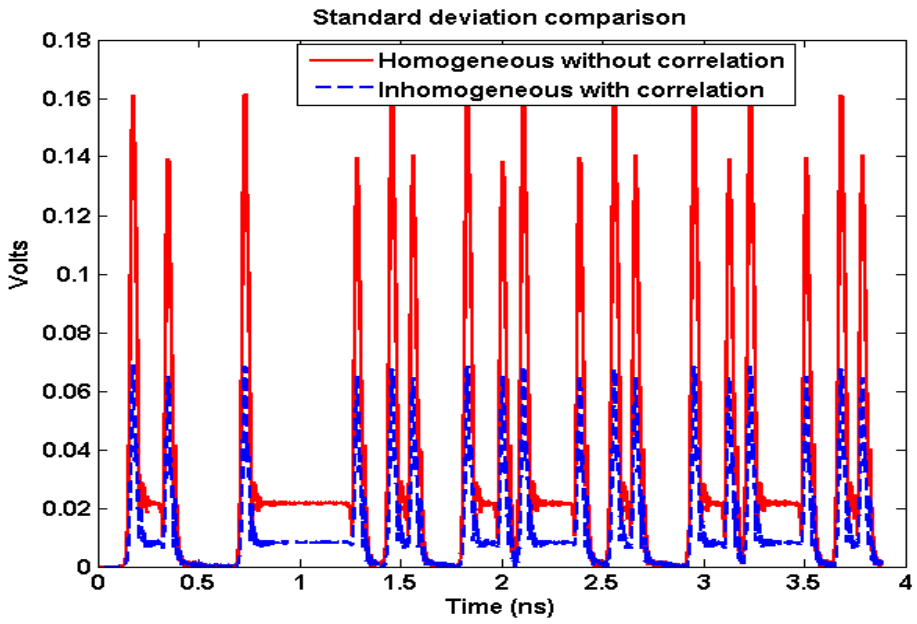

Figure 6-15 Standard deviation comparison of the differential output voltage between correlated and uncorrelated case.

6.3.2 Example II: 2D Rectangular Cavity

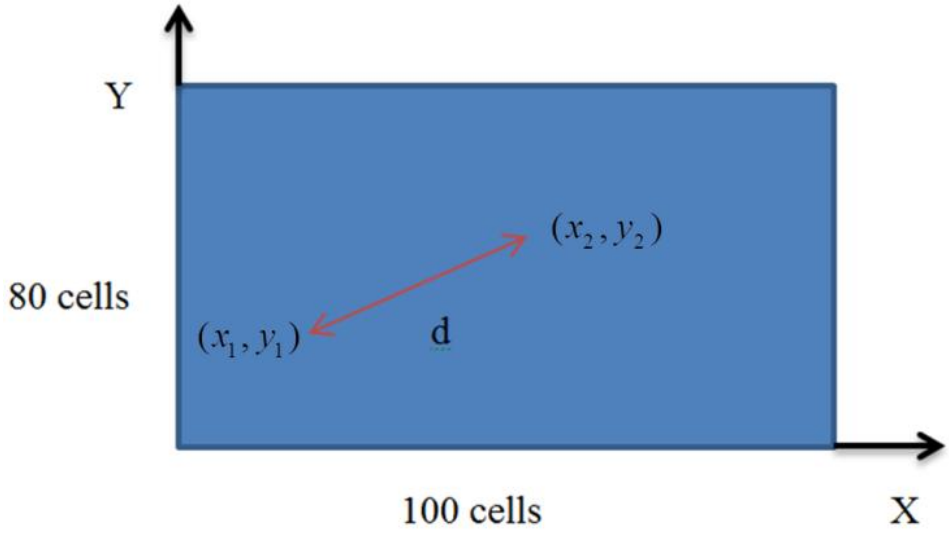

Figure 6-16 Top view of 2D Rectangular cavity filled with random medium.

Figure 6-16 shows the top view of a 2D rectangular cavity. The cavity is 10 cm long in the x direction and 8 cm wide in the y direction. It is uniformly meshed in both

the x and y direction with a size of 1 mm. So there are 100 cells in the x direction and 80 cells in the y direction, with a total of 8000 discrete points inside the cavity. PEC boundaries are applied for the four walls. The cavity is filled with random medium with spatial correlation. The medium is considered as a Gaussian random process with a mean of 2.2 and a standard deviation of 0.22. The covariance matrix is given by

$$C(x_1, y_1; x_2, y_2) = \sigma^2 e^{-d}, d = \sqrt{(x_1 - x_2)^2 + (y_1 - y_2)^2}, \tag{6.38}$$

and is plotted in Figure 6-17.

Figure 6-18 shows the first six eigenvalues of the covariance matrix in a semi-log scale. The ANR for the first six expansion orders is around 98.71%. And the first six eigenvectors of the covariance matrix are shown in Figure 6-19 to Figure 6-24.

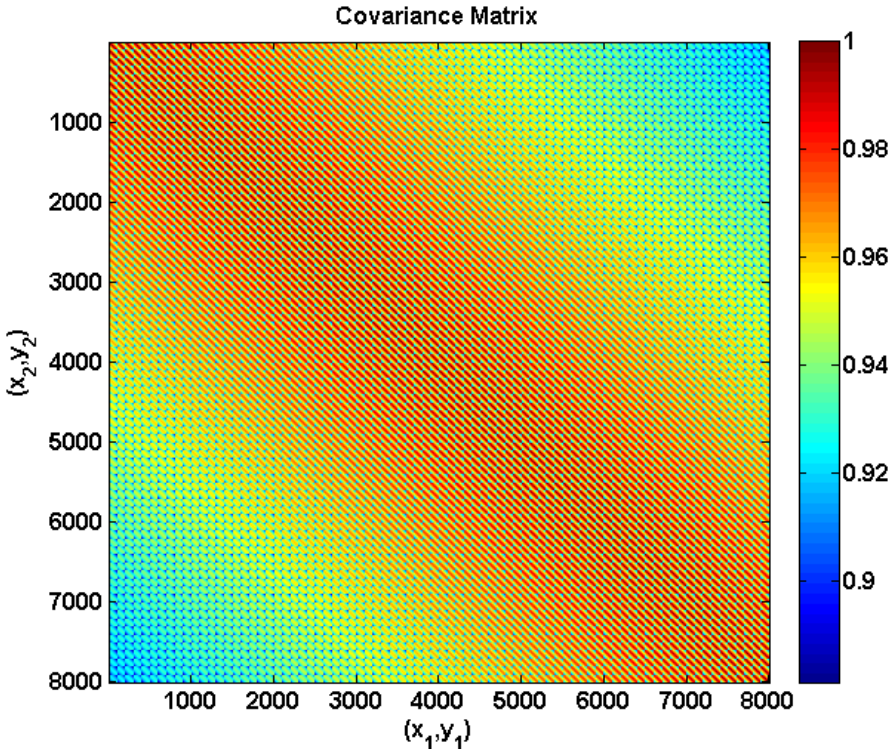

Figure 6-17 2-D covariance matrix.

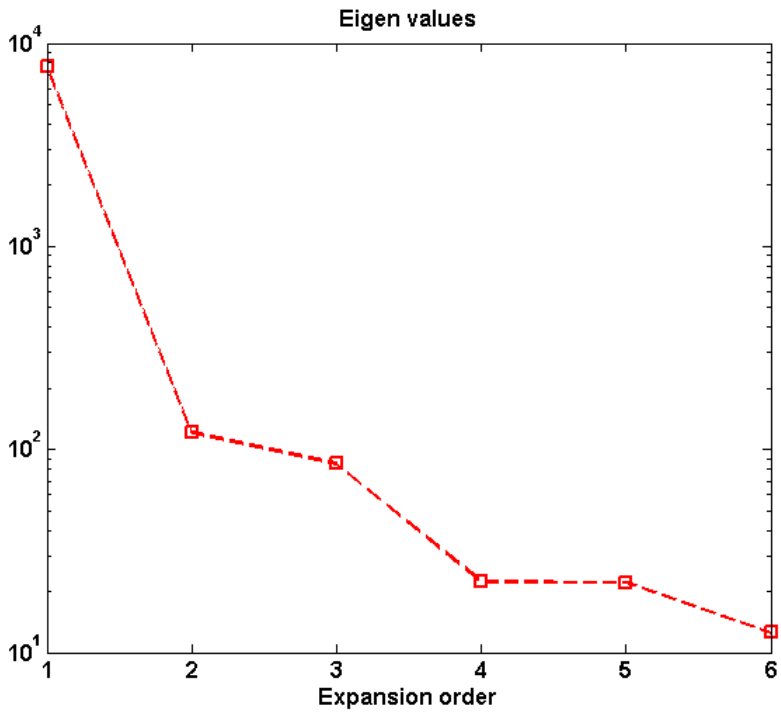

Figure 6-18 First six eigenvalues of the covariance matrix.

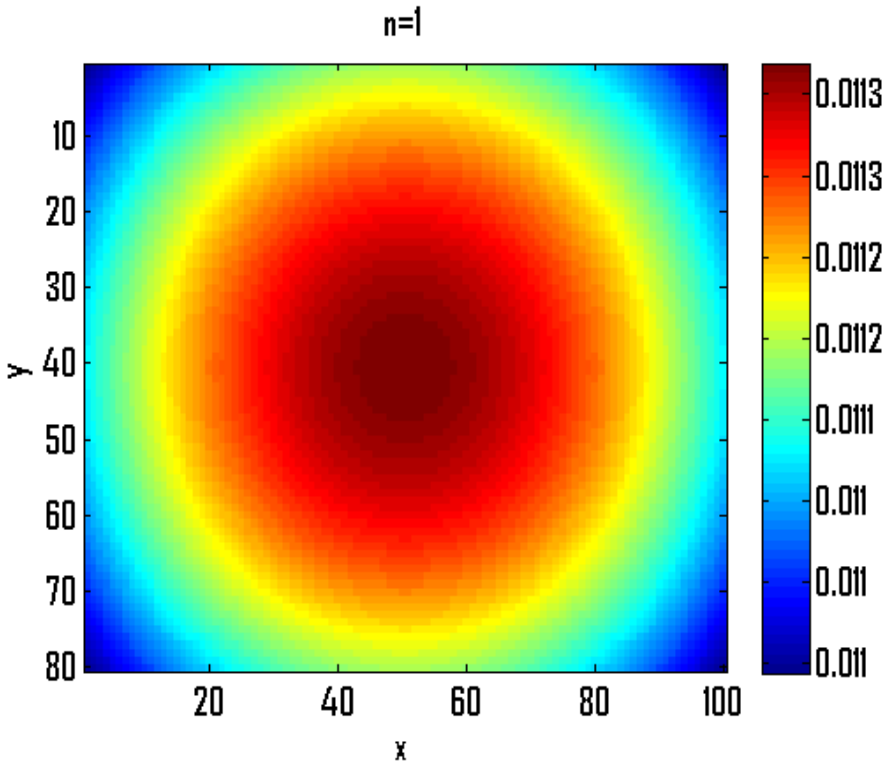

Figure 6-19 First order eigenvector of the covariance matrix.

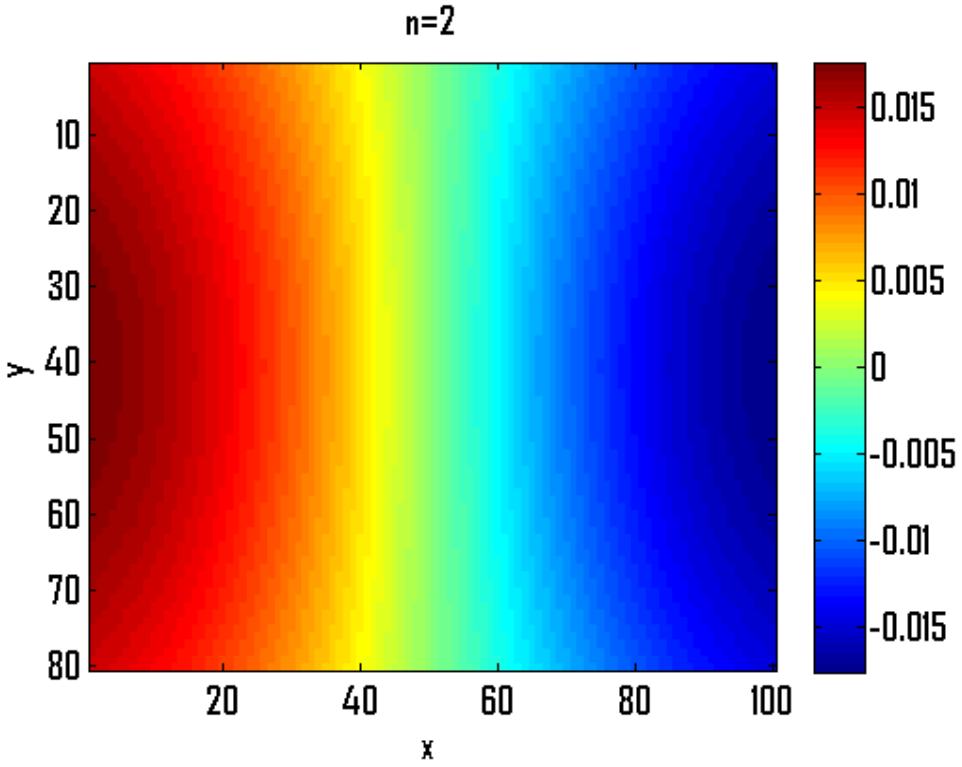

Figure 6-20 Second order eigenvector of the covariance matrix.

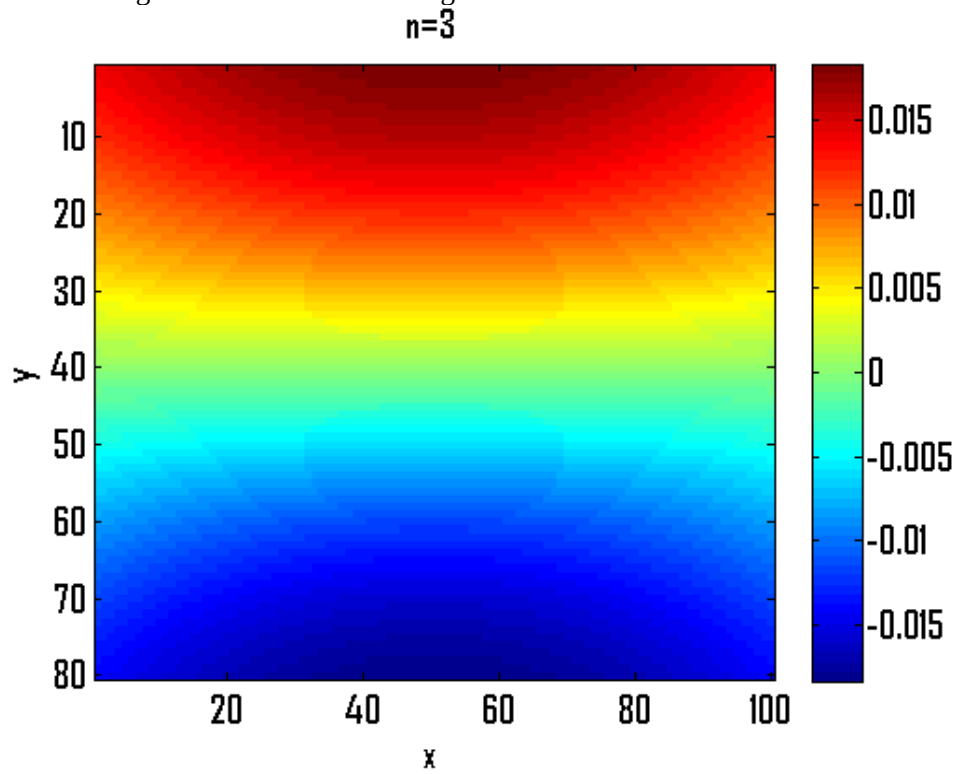

Figure 6-21 Third order eigenvector of the covariance matrix.

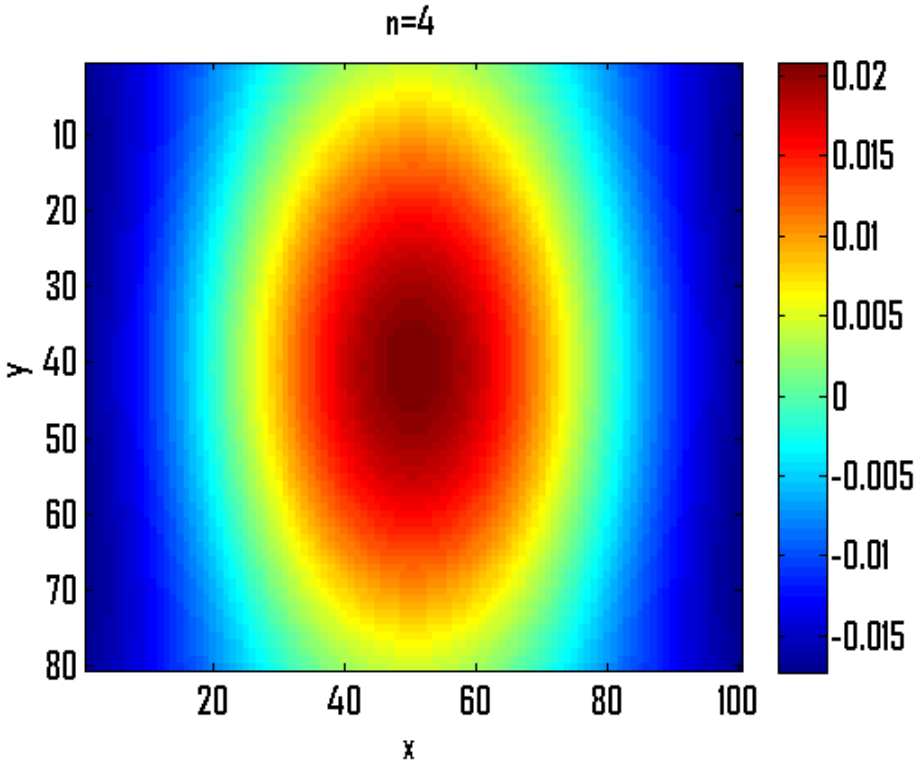

Figure 6-22 Fourth order eigenvector of the covariance matrix.

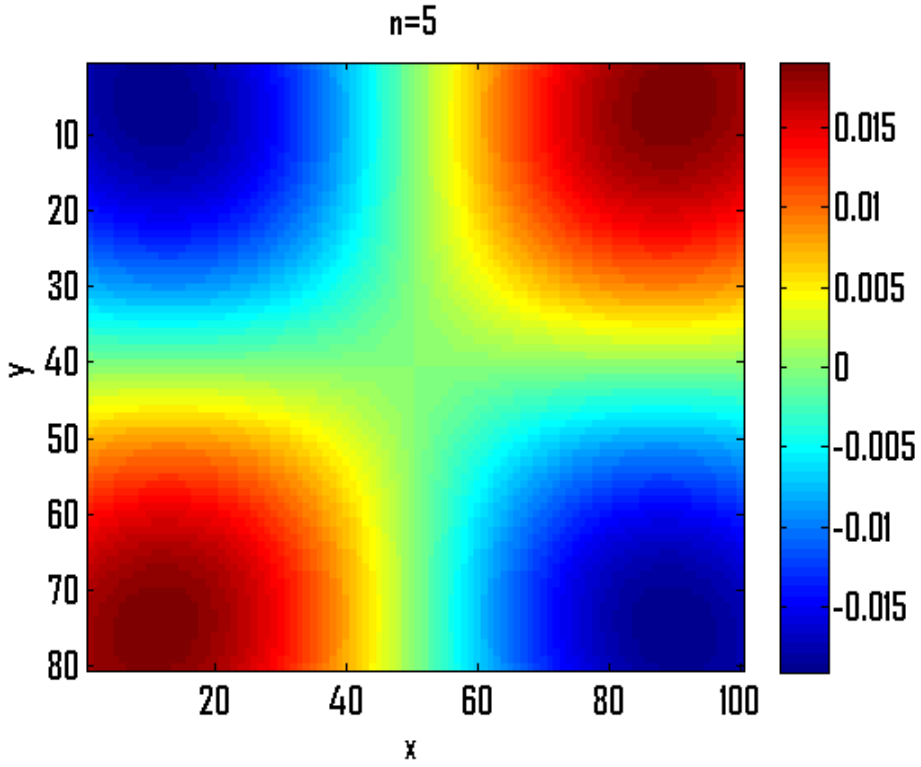

Figure 6-23 Fifth order eigenvector of the covariance matrix.

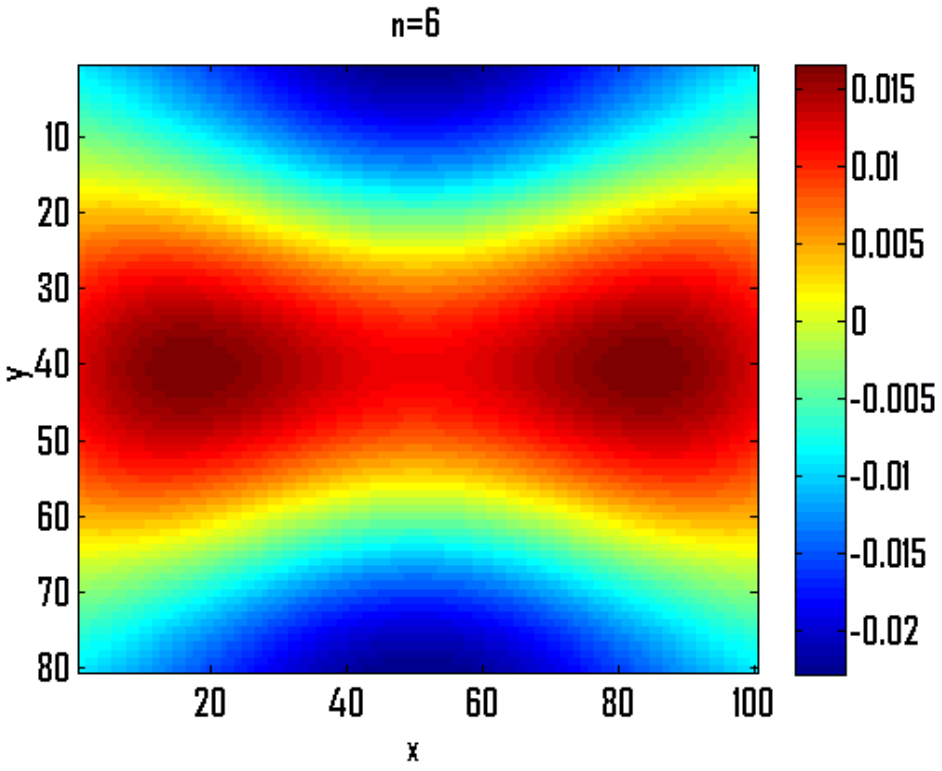

Figure 6-24 Sixth order eigenvector of the covariance matrix.

The permittivity of the material filled inside the cavity can be expressed as

$$\begin{aligned}\varepsilon_r(x,y) &= \overline{\varepsilon_r}(x,y) + \sum_{i=1}^{6} \sqrt{\lambda_i}\,\xi_i(\theta) f_i(x,y) \\ &= 2.2 + \sum_{i=1}^{6} \sqrt{\lambda_i}\,\xi_i(\theta) f_i(x,y)\end{aligned} \quad . \tag{6.39}$$

We used both the SG method (109 times) and the MC method (1000 times) to generate the permittivity profiles, as shown in Figure 6-24 and Figure 6-25, respectively. Since the PEC boundary conditions are applied, there will only be TE modes. A Gaussian pulse is placed inside the cavity. After certain time steps of FDTD simulation, a response can be captured. Using the Fourier transform, the frequency components of the resonant modes can be obtained. As a demonstration, only the resonant frequencies of the first three lowest modes are computed.

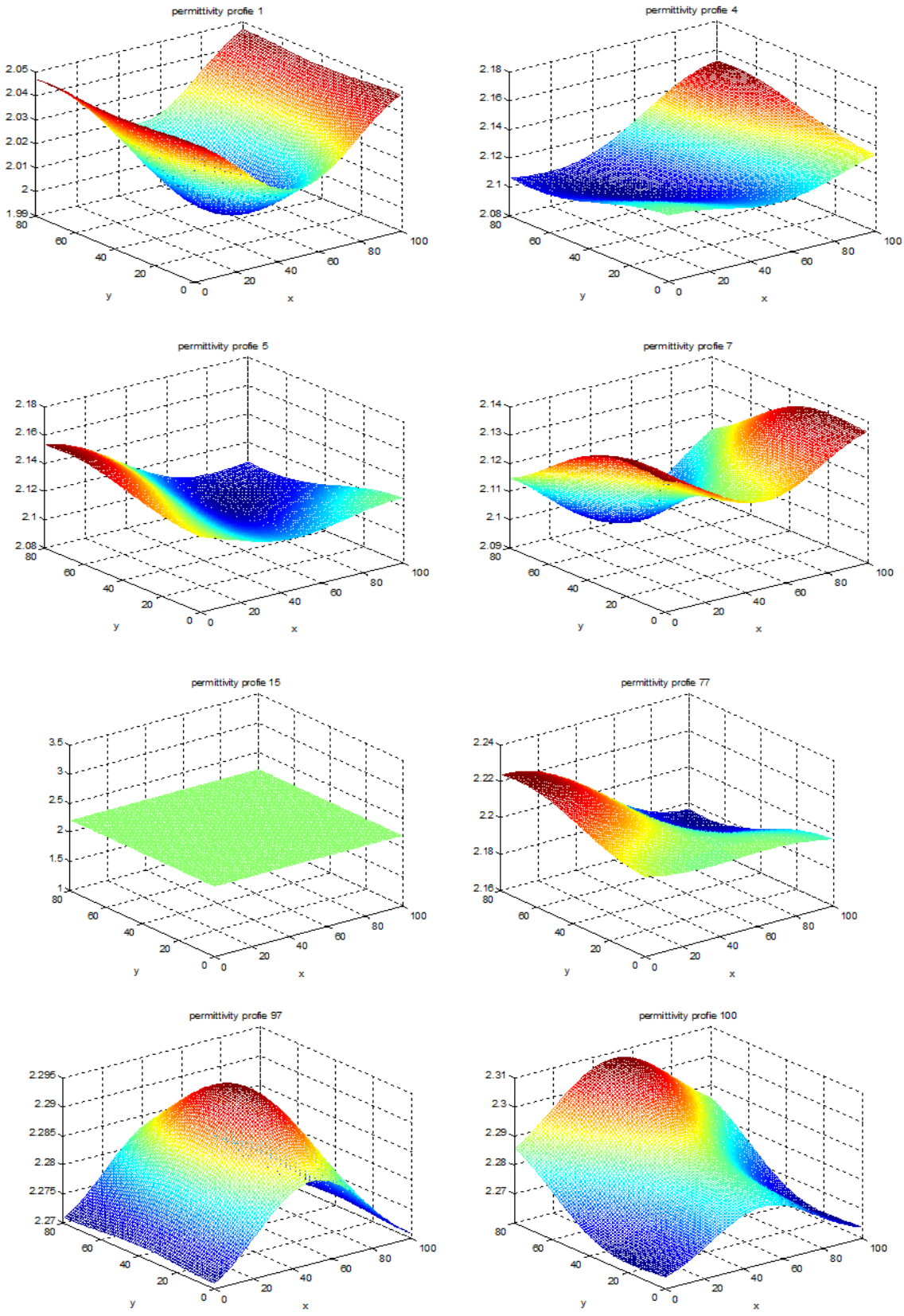

Figure 6-25 Permittivity profiles generated by sparse grid method.

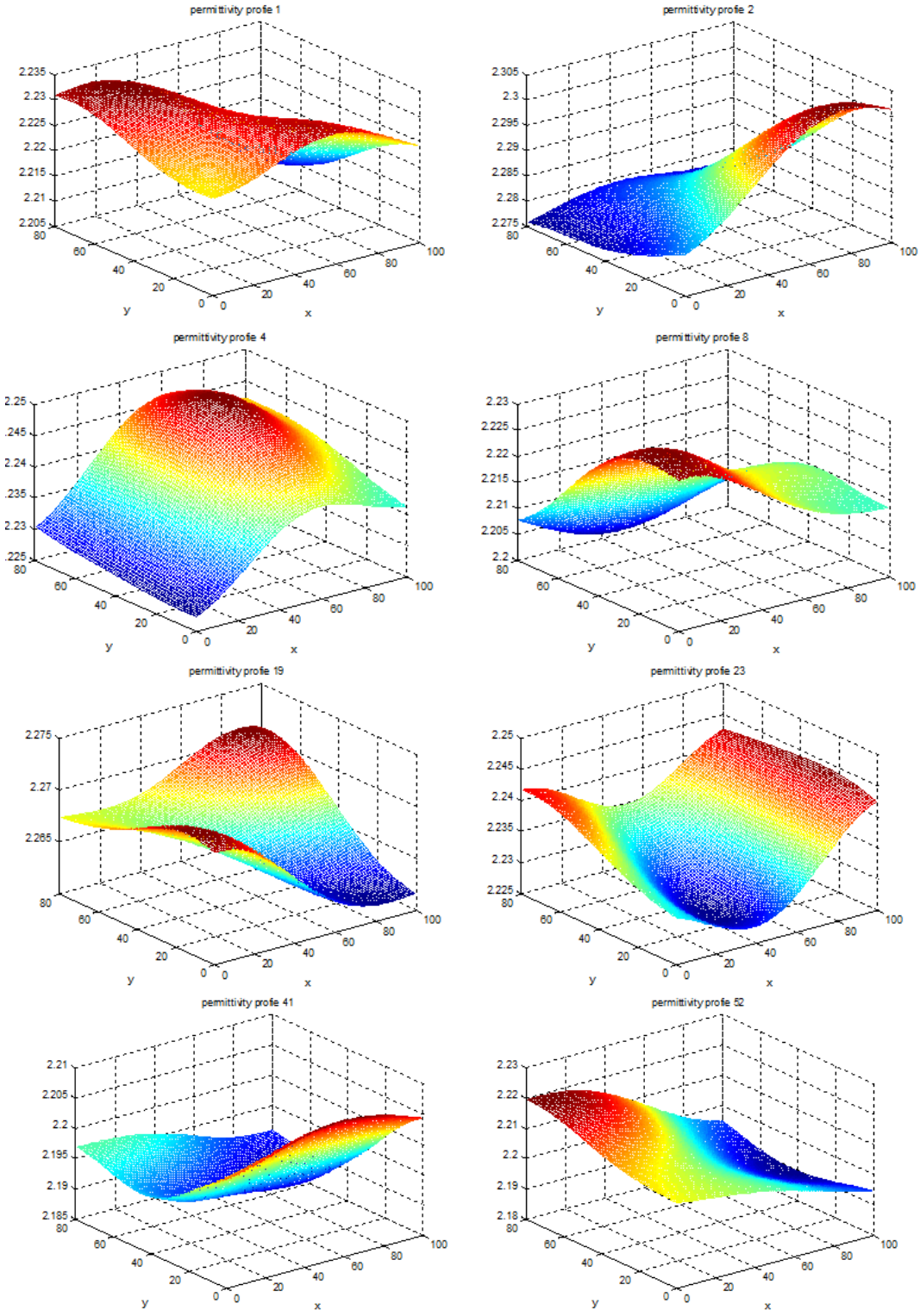

Figure 6-26 Permittivity profiles generated by Monte Carlo method.

Table 6-1 Statistics of resonant frequencies for first three modes

Case	TE_{10} mode	TE_{01} mode	TE_{11} mode
SG mean	1.0091 GHz	1.2619 GHz	1.6159 GHz
SG standard deviation	12.1519 MHz	16.6839 MHz	19.9657 MHz
MC mean	1.0095 GHz	1.2622 GHz	1.6172 GHz
MC standard deviation	11.8447 MHz	16.4816 MHz	19.6226 MHz
Homogeneous mean	1.0131 GHz	1.2667 GHz	1.6222 GHz
Homogeneous standard deviation	51.6834 MHz	64.3741 MHz	83.1035 MHz
Analytical with mean input	1.0106 GHz	1.2633 GHz	1.6177 GHz
MC mean	1.0095 GHz	1.2622 GHz	1.6172 GHz

Table 6-2 Comparison between SG and MC method

Modes	Mean	Standard deviation
TE_{10} mode	0.0396%	2.59%
TE_{01} mode	0.0238%	1.22%
TE_{11} mode	0.0804%	1.75%

Table 6-3 Mean comparison

Case	TE10 mode	TE01 mode	TE11 mode
Correlated	0.145%	0.111%	0.111%
Uncorrelated	0.109%	0.0871%	0.2782%

Also, the comparison is made between the correlated case and the uncorrelated case. The analytical values are calculated for these two resonant frequencies when the permittivity is set at 2.2. Comparison data are listed in Tables 6-1, 6-2, and 6-3. From the tables listed above, we can see that:

1) The mean value and standard deviation of the resonant frequencies predicted by the SG method and the MC method are very close to each other. As shown in Table 6-2,

if we use the value of the MC method as a reference, the percentage error of the SG method is relatively low. This proves the efficiency of the SG method compared to the MC method.

2) The mean values for the correlated case and uncorrelated case are almost the same. If we set the analytical solution as a reference, both cases show very little percentage error with respect to the reference value. That is because Maxwell equations are linear equations, and one should expect a linear relationship between the input mean and the output mean.

3) The standard deviation of resonant frequencies is sensitive to the variance of the material's permittivity. When there is no correlation, more variations are observed near the mean value, since the correlation lowers the variance of the permittivity.

6.4 Random Medium with Correlation in Probability Space

In this section, we revisited the differential microstrip line example as shown in Figure 6-3. While we keep the geometry the same, we assume the material of the substrate is homogeneous and lossy with random permittivity and conductivity. The permittivity and conductivity are considered as joint Gaussian random variables. The term to describe the loss of the transmission line is called loss tangent δ, which is defined in (6.40)

$$\delta = \frac{\sigma}{\varepsilon_0 \varepsilon_r \omega} = \frac{\sigma}{\varepsilon_0 \varepsilon_r (2\pi f)}, \tag{6.40}$$

where σ is the conductivity of the substrate material, and f is the measured frequency. The mean and standard deviation are 4.1 and 0.41 for the permittivity and 0.03 S/m and 0.003 S/m for the conductivity. 0.03 S/m will give a loss tangent of 0.015 at 9.4 GHz.

Following the mapping procedure as defined in (6.30), we can obtain two independent "permittivities" and "conductivities." Figure 6-27 to Figure 6-30 show how the mean and standard deviation are affected by the mapping with the different correlation coefficient ρ.

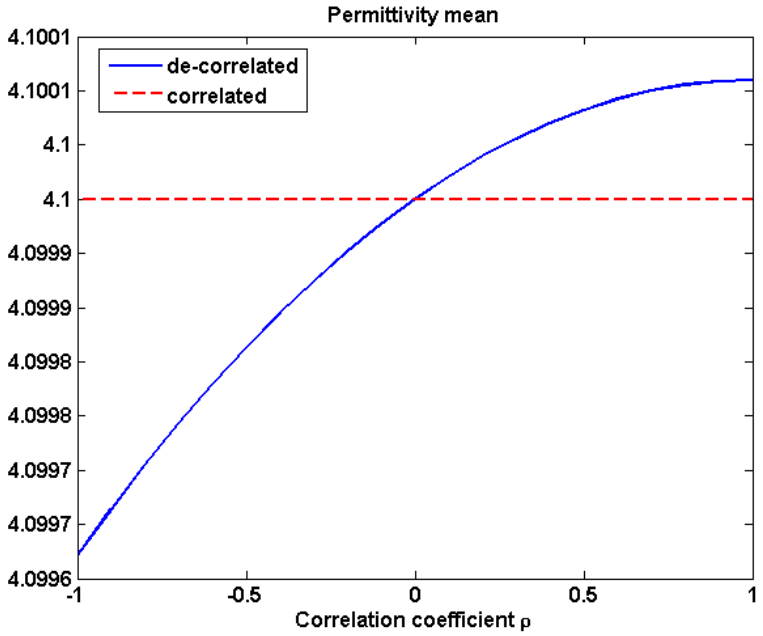

Figure 6-27 Permittivity mean varying with different correlation coefficient.

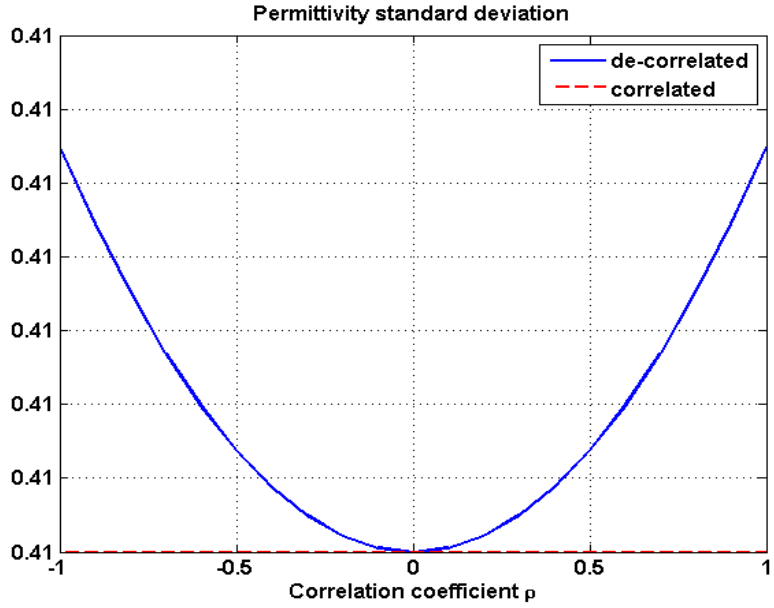

Figure 6-28 Permittivity deviation varying with different correlation coefficient.

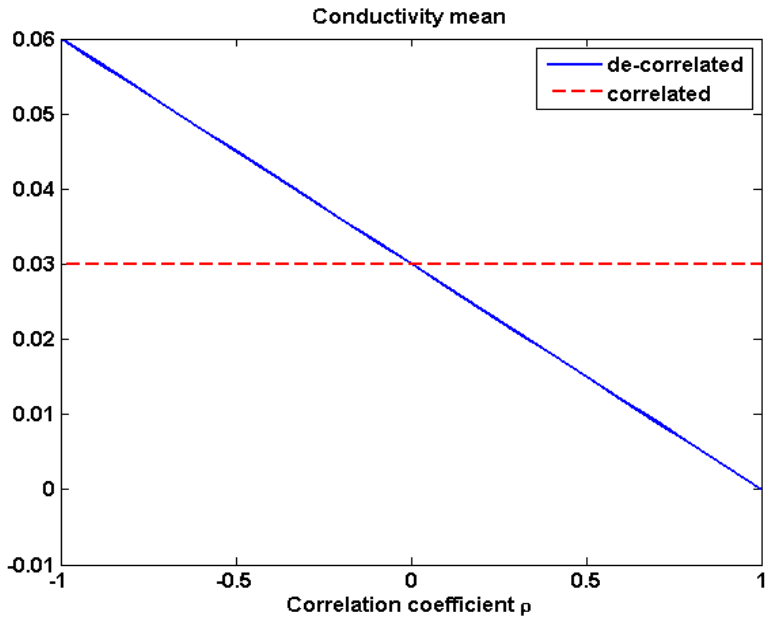

Figure 6-29 Conductivity mean varying with differernt correlation coefficient.

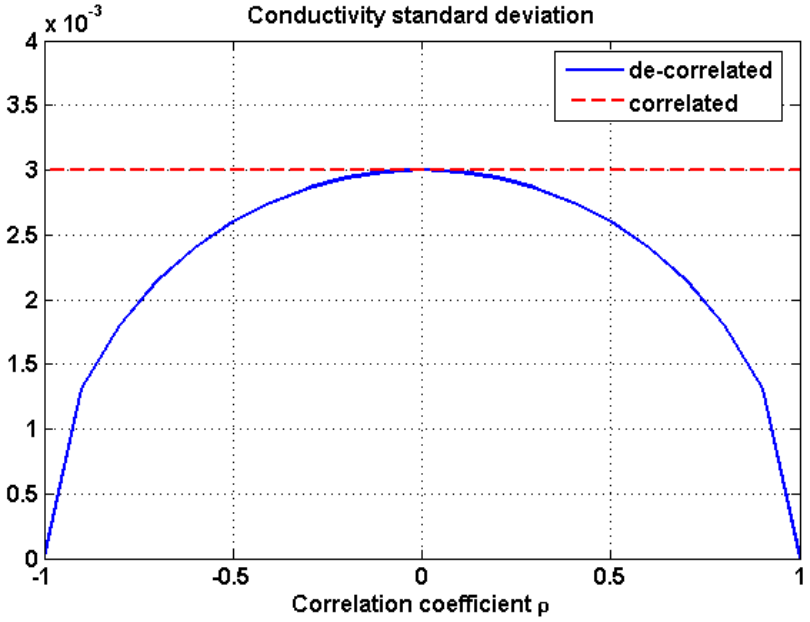

Figure 6-30 Conductivity deviation varying with different correlation coefficient.

For the new mapped mean value, permittivity will increase with a positive correlation coefficient and decrease with a negative correlation coefficient, while conductivity will increase with a negative correlation coefficient and decrease with a

positive correlation coefficient. For the new mapped standard deviation, permittivity will always increase more than the previous value and achieve its minimum when there is no correlation present; the smaller random variable will always decrease and achieve its maximum when there is no correlation present. It is symmetric to the point $\rho = 0$. For both mean and standard deviation, permittivity has changed very little while the conductivity has changed a lot. Back to (6.15) and (6.16), the new variables' mean and standard deviation are basically a weighted summary for both of the two original variables. When one variable is much larger than the other one, which is the case in this problem, the rotation angle becomes very small. At two particular points $\rho = \pm 1$, the conductivity vanishes. This violates the original assumption for a lossy medium. That is because the joint PDF as shown in (6.13) will blow up for $\rho = \pm 1$.

We performed five sets of simulation with five different correlation coefficients, which are $\rho = -0.5, -0.2, 0, 0.2, 0.5$. The input value for permittivity and conductivity are listed in Table 6-4. Each case requires 22 simulations, determined by 2D sparse grid method.

Table 6-4 Permittivity and conductivity input values for different correlation coefficients

Correlation coefficient	**Permittivity mean**	**Permittivity standard deviation**	**Conductivity mean**	**Permittivity standard deviation**
-0.5	4.09986	0.410003	0.0450003	0.00259806
-0.2	4.09995	0.4100004	0.0360003	0.00293938
0	4.1	0.41	0.03	0.003
0.2	4.10004	0.4100004	0.0239997	0.00293938
0.5	4.1008	0.410003	0.0149993	0.00259806

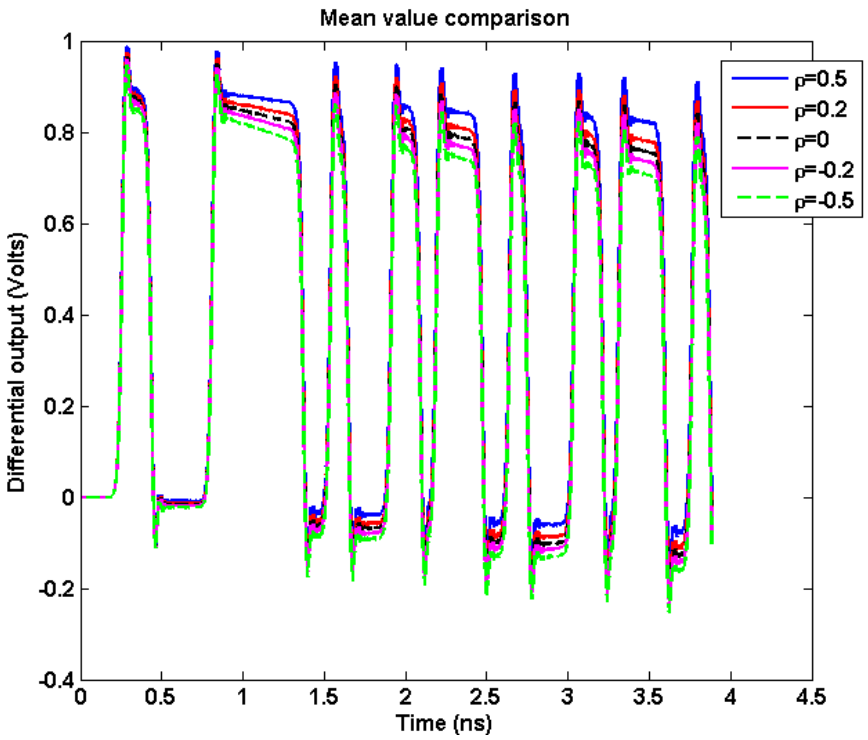

Figure 6-31 Mean value of the differential output voltage varying with different correlation coefficient.

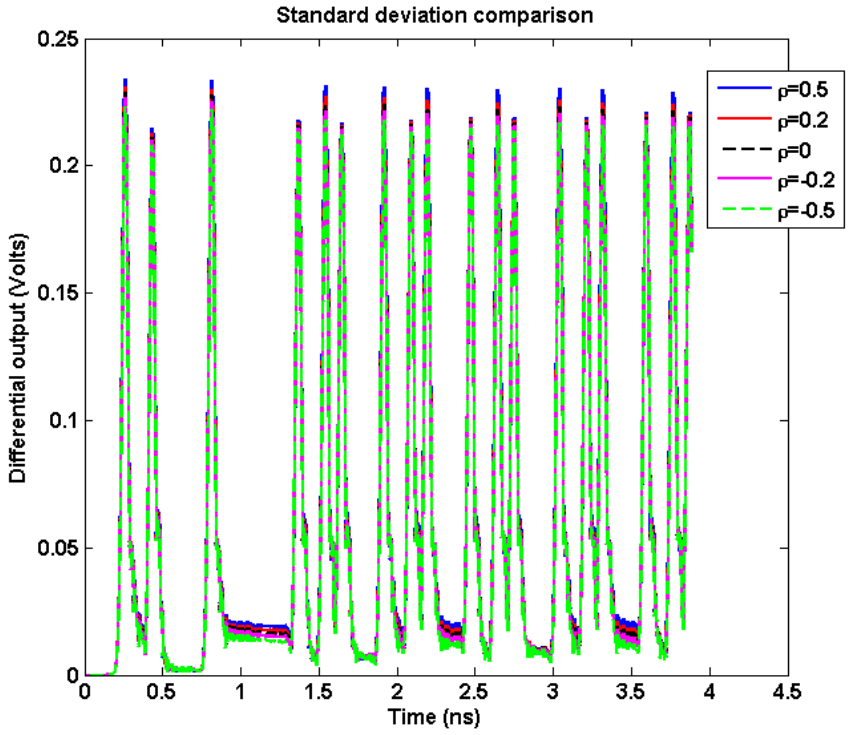

Figure 6-32 Standard deviation of the differential output voltage varying with different correlation coefficient.

According to [64], the characteristic impedance of a microstrip line is given by

$$Z_0 = \frac{120\pi}{\sqrt{\varepsilon_{eff}}[\frac{W}{d} + 1.393 + 0.667\ln(\frac{W}{d} + 1.444)]}, (\frac{W}{d} > 1), \tag{6.41}$$

where

$$\varepsilon_{eff} = \frac{\varepsilon_r + 1}{2} + \frac{\varepsilon_r - 1}{2} \cdot \frac{1}{\sqrt{1 + \frac{12d}{W}}}. \tag{6.42}$$

In the above five cases, the geometry factor remains unchanged; the mean value of permittivity changes very little, so the characteristic impedance of the transmission line changes very little. When feeding the TL with a 50 Ω resistance, from a voltage divider point of view, the actual voltage injected into the transmission line will be almost the same. This explains why the voltage amplitudes at the beginning of the mean values are almost the same. However, with the correlation coefficient decreasing, the mean value of the conductivity increases, which means the conducting loss of the substrate material increases. So with the signal propagating on the transmission line, the difference between the signals' amplitude would become larger and larger. From Figure 6-31, the standard deviations between these five cases are almost the same. And the output signal's standard deviations are also almost the same. It indicates the correlation would affect the output variations very little.

Next, for the case when $\rho = 0.5$, we validate the results with the MC method. The input data are determined by a correlated bivariate Gaussian random generator. As shown in Figures 6-30 and 6-31, both mean and standard deviation have good agreement. It tells us that for bivariate correlated Gaussian random variables, after the linear mapping technique, the current existing method used to deal with independent random variables

such as the SG method can still be applied without losing accuracy.

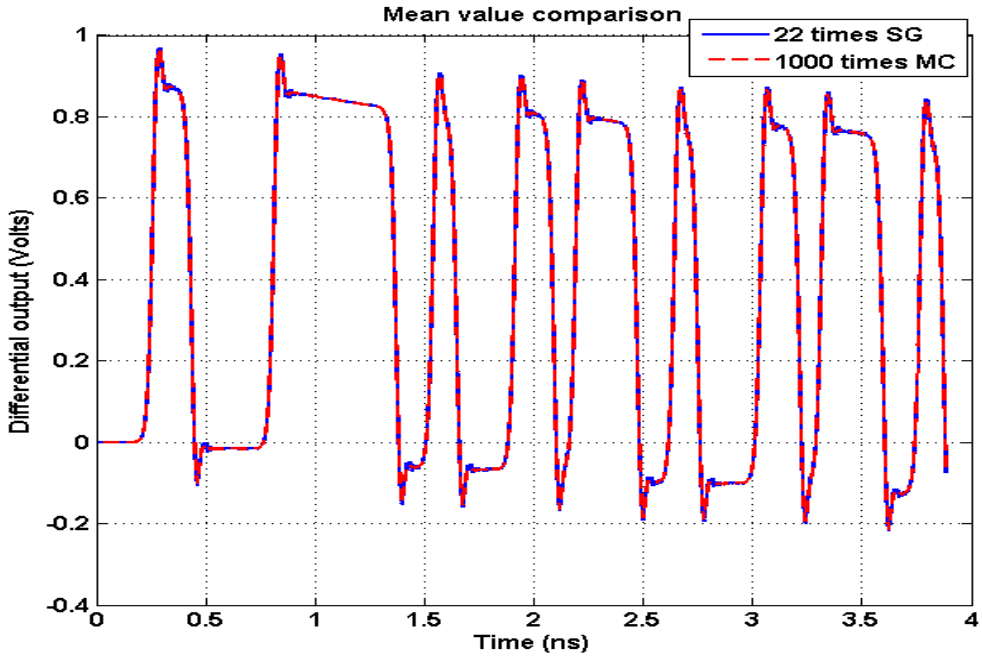

Figure 6-33 Mean value comparison of the differential output voltage by sparse grid method and Monte Carlo method when $\rho = 0.5$.

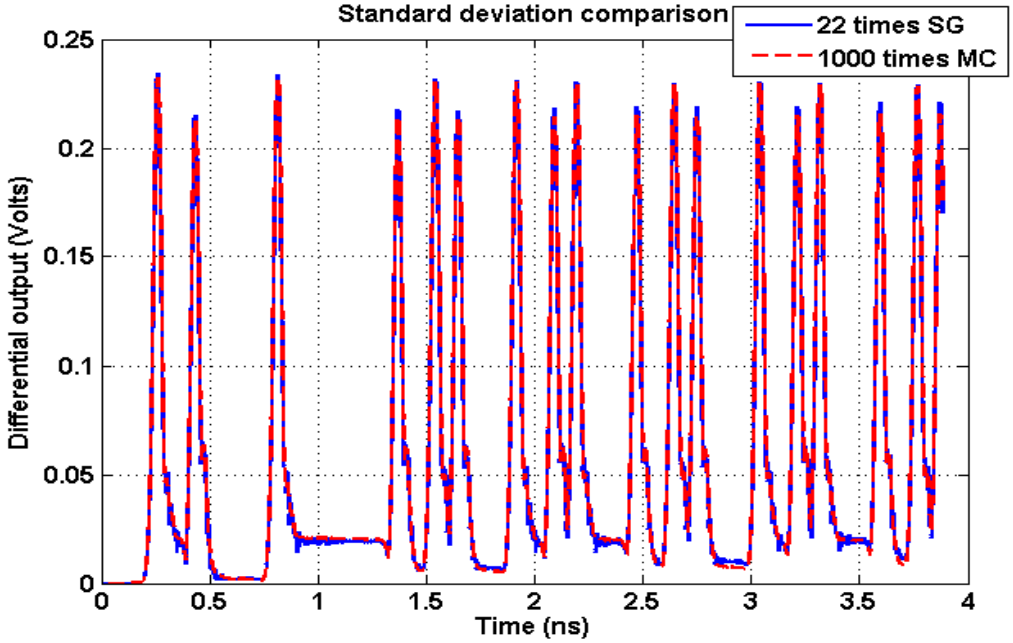

Figure 6-34 Standard deviation comparison of the differential output voltage by sparse grid method and Monte Carlo method when $\rho = 0.5$.

6.5 Summary

In this chapter, random medium with correlation in both physical space and random space are investigated. Due to the correlated nature of these two kinds of problems, a traditional uncertainty analysis method cannot be applied since it requires the probability space's ability to be characterized by a set of independent random variables. To deal with the spatial correlation, the Karhuen-loeve expansion can be used to decompose the covariance function into a set of eigenvalues and eigenfunctions. In this way, the stochastic process can be expressed by its mean value and a sum of higher order variations in terms of eigenvalues, eigenfunctions. and a set of independent random variables. For the correlation in the probability space, a linear mapping, or equivalently coordinate rotation technique, can be applied. After the linear transformation, two correlated Gaussian random variables will be uncorrelated (independent). In both of these two cases, the spare grid based stochastic collocation method can be directly borrowed from Chapter 5. And numerical examples prove them to be efficient ways to deal with this kind of correlation problems.

Chapter 7 Conclusions and Future Work

7.1 Conclusions

Stochastic analysis in the electromagnetic (EM) simulation is of great importance for a better understanding of the true physics associated with uncertainties. This dissertation introduces stochastic methods into the area of electromagnetic simulations. Due to the complex nature of EM problems, the primary goal is to find efficient ways to determine uncertainty quantifications so as to reduce the total computational cost. Compared to the traditional Monte Carlo sampling method, the proposed alternative methods such as the generalized polynomial chaos (gPC) method-based stochastic Galerkin scheme (SGS) and the sparse gird method-based stochastic collocation scheme (SCS) prove to be much more efficient.

As for computational time, SGS is favorable compared to the MC method in that it turns the original problem into solving the expansion coefficients. All the expansion coefficients can be updated the same as in the FDTD algorithm. Thus, only one simulation is required. The drawback with this feature is the demand for more memory requirements. Besides, it is relatively difficult to implement. As shown in Chapter 4, modifications are needed due to the coupling between the expansion coefficients. When large scale or complex problems are considered, tons of codes for the deterministic case might already exist. Further modification takes too much effort or is even impossible to implement.

The SCS has an obvious advantage in that it only requires repetitive realizations of existing deterministic solvers as discussed in Chapter 5, similar to the MC method. By

properly choosing interpolation polynomials, it can inherit the fast convergence as in the gPC method. And by using an efficient sampling technique such as the sparse grid method, the total number of realizations needed can be greatly reduced, especially in the multi-dimensional problems. The non-intrusive nature makes it even more powerful and useful with the help of commercial software used to analyze complex structures.

The biggest contribution of this dissertation is the stochastic analysis with the presence of correlations, both in spatial coordinates and probability space. The key step is to decompose the random process or transform the correlated random variables into a set of independent random variables. In this way, the stochastic collocation method can be applied.

7.2 Future Work

Many state-of-art stochastic computational techniques are largely based on the stochastic finite element method. Detailed reviews can be found in [75][76]. There are still many more aspects in the area of stochastic modeling that remain challenging and need further research effort. As a direction, several important areas of future work are listed below.

For the gPC-based stochastic Galerkin method, despite the computational cost concern, there are some problems observed for this kind of implementation such as long term integration and discontinuity. To handle this problem, the so called multi-element gPC method is proposed [77][78] . Furthermore, for multi-dimensional problems, the implementation of the gPC method into the existing EM solver needs more detailed investigation.

The stochastic collocation scheme is highly preferred in the statistical modeling of

EM problems, in which the selection of collocation points in critical. The sparse grid method proves an efficient way to deal with this. There are some other methods such as Stroud's rule of degree-2 and degree-3 [79]-[81], which is a better way when the problem dimension is much greater than one. Also, the adaptive sparse grid method [82] is proposed to further reduce the computational cost. Many numerical examples in the area of high-speed circuits are studies in this dissertation using the collocation method. There are a lot more applications that we can look into such as antenna array design [83][84], computational study of the human body's exposure to RF field generated by MRI coil [87][88] , etc.

The Karhuen-Loeve expansion provides a good way to characterize a random process, where the covariance function plays an important role. Throughout the analysis in Chapter 6, we are assuming the covariance decays with distance. While it is a reasonable assumption from intuitive thinking, whether it can be applied in a particular problem remains an open question. Material's spatial correlation is an interesting topic as shown in [89]. The weave of FR4 material can be modeled as a two-dimensional correlation random process. The remaining task is to extract a covariance kernel that is capable of describing the material's electrical property using the measurement date. For the correlation in the probity space, different types of random variables' correlation and their de-correlation techniques require further study.

REFERENCES

[1] D. B. Davidson, *Computational Electromagnetics for RF and Microwave Engineering*, 2nd Edition, Cambridge University Press, Cambridge, 2010.

[2] A. Talflove and S. C. Hagness, *Computational Electrodynamics: The Finite-Difference Time-Domain Method*, 3rd Edition, Artech House, MA, 2005.

[3] R. Holland and R. H. S. John, *Statistical Electromagnetics*. Taylor & Francis, Philadelphia, PA, 1999.

[4] S. A. Pignari, "Statistics and EMC," *Radio Science Bulletin*, No. 316, pp. 13–26, April, 2006.

[5] C. Chauviere, J. S. Hesthaven and L. Lurati, "Computational modeling of uncertainty in time-domain electromagnetics," *SIAM J. Sci. Statist. Comput*., Vol. 28, pp. 751-775, 2006.

[6] D. Xiu and J. S. Hesthaven, "High-order collocation methods for differential equations with random inputs," *SIAM J. Sci. Comput.*, Vol. 27, No. 3, pp. 1118-1139, 2005.

[7] B. V. Asokan and N. Zabaras, "A stochastic variational multiscale method for diffusion in heterogeneous random media," *J. Comput. Phys*., Vol. 218, No. 2, pp. 654-676, November, 2006.

[8] R. N. Allan, R. Billinton, A. M. Breipohl, and C. H. Grigg, "Bibliography on the application of probability methods in power system reliability evaluation 1992-1996," *IEEE Trans. Power Syst.*, Vol. 14, pp. 51-57, February, 1999.

[9] Karatzas and S.E. Shreve, *Brown Motion and Stochastic Calculus*,Springer-Verlag,

New York, 1988.

[10] P. E. Kloeden and E. Platen, *Numerical Solution of Stochastic Differential Equations*, Springer-Verlog, Berlin, 1999.

[11] G. S. Fishman, *Monte Carlo: Concepts, Algorithms, and Applications*, Springer-Verlag, Berlin, Germany, 1995.

[12] M. Stein, "Large sample properties of simulations using Latin hypercube sampling," *Technometrics*, Vol. 29, No. 2, pp. 143-151, 1987.

[13] B. L. Fox, *Strategies for Quasi-Monte Carlo*, Kluwe Academic, Norwell, MA, 1999.

[14] E. J. Hinch, *Perturbation Methods*, Cambridge University Press, Cambridge, 1991.

[15] V. Skorokhod, F. C. Hoppensteadt and H. Salehi, *Random Perturbation Methods with Applications in Science and Engineering*. Springer-Verlag, New York, 2001.

[16] P. Z. Peebles, *Probability, Random Variables and Random Signal Principles*, 2nd Edition, McGraw-Hill, New York, 1987.

[17] Papoulis, Probability, *Random Variables and Stochastic Processes*, 4th Edition, McGraw-Hill, Boston, 2002.

[18] T. S. Chihara, *An Introduction to Orthogonal Polynomials*, Gordon and Breach, Science Publishers, New York, 1978.

[19] D. Xiu, Numerical Methods for Stochastic Computation, A Spectral Method Approach, Princeton Unversity Press, Princeton, New Jersy, 2010.

[20] R. W. Hamming, *Numerical Methods for Scientists and Engineers*, 2nd Edition, Dover Publications, Mineola, NY, 1987.

[21] Elsherbeni and V. Demir, *The Finite Difference Time Domain Method for Electromagnetics: With Matlab Simulations*, SciTech Publishing, Herdon, VA, 2009.

[22] U. S. Inan and R. A. Marshall, *Numerical Eletromagnetics: The FDTD Method*, Cambridge University Press, Cambridge, 2011.

[23] J. Jin, *The Finite Element Method in Electromagnetics*, 2nd Edition, Wiley-IEEE Press, 2002.

[24] P. Monk, *Finite Element Method for Maxwell Equations*, Oxford University Express, New York, 2003.

[25] W. C. Gibson, *The Method of Moments in Electromagnetics*, CRC Press, Harvest, AL, 2007.

[26] Babuska, R. Tempone and G. E. Zouraris, "Galerkin finite element approximations of stochastic elliptic partial differential equations," *SIAM J. Numer. Anal.*, Vol 42, No. 2, pp. 800–825, 2004.

[27] P. Billingslev, Probability and Measure, Wiley, New York, 2012.

[28] W. H. Press, S. A. Teukolsky, W. T. Vetterling, and B. P. Flannery, *Numerical Recipes*, 3rd Edition, Cambridge University Press, Cambridge, 2007.

[29] K. S. Yee, "Numerical solution of initial boundary value problems involving Maxwell's equations in isotropic media," *IEEE Trans. Antennas Propagat.*, Vol. 14, pp. 302-307, Nov. 1966.

[30] C. Canuto, Y. Y. Hussaini, A. Quasteroni, and T. A. Zang, *Spectral Methods in Fluid Dynamic*, Springer-Verlag, 1988.

[31] O. M. Knio and O. P. Le Maitre, "Uncertainty propagation in CFD using polynomial chaos decomposition," *Fluid Dynam. Res.*, Vol 38, No. 9, pp. 616-640, 2006.

[32] O. Le Maitre, M. Reagan, H. Najm, R. Ghanem, and O. Knio, "A stochastic projection method for fluid flow: Random process," *J. Comput. Phys.*, Vol 181, pp. 9-44, 2002.

[33] D. Xiu and G. E. Karniadakis, "Modeling uncertainty in flow simulations via generalized polynomials chaos," *J. Comput. Phys.*, Vol. 187, pp. 137-167, 2003.

[34] D. B. Xiu and G. E. Karniadakis, "The Wiener-Askey polynomial chaos for stochastic differential equations," *SIAM J. Sci. Comput*, Vol. 24, No.2, pp. 619-644, 2002.

[35] P. Frauenfelder, C. Schwab and R. A. Todor, "Finite elements for elliptic problems with stochastic coefficients," *Computer Methods in Applied Mechanics and Engineering*, Vol. 194, pp. 205-228.

[36] J. Shen, "*Efficient Numerical Techniques for Uncertainty Analysis in Electromagnetic Simulations*," Ph.D. dissertation, University of Houston, Houston, December, 2010.

[37] R. G. Ghanem and P. Spanos, *Stochastic Finite Elements: a Spectral Approach*, Springer-Verlag, New York, 1991.

[38] R. S. Edwards, A. C. Marvin and S. J. Porter, "Uncertainty Analyzes in the Finite-Difference Time-Domain Method," *IEEE Transactions on Electromagnetic Compatibility.*, Vol. 52, No. 1, pp. 155-163, 2010.

[39] J. P. Berenger, "A perfect matched layer for the absorption of electromagnetic waves," *J. Comput. Phys.*, Vol. 114, No.1, pp. 185-200, 1994.

[40] S. D. Gedney, "An anisotropic perfectly matched layer absorbing media for the truncation of FDTD lattices," *IEEE Transactions on Antenna and Propagation*, Vol. 44, Issue 12, pp. 1630-1639, 1996.

[41] W. C. Chew and W. H. Weedon, "A 3d perfect matched medium from modified Maxwell's equations with stretched coordinates," *Microwave and Optical Tech. Letters*, Vol. 7, No. 13, pp. 599-604, 1994.

[42] I. Babuska, F. Nobile and R. Tempone, "A stochastic collocation method for elliptic partial differential equations with random input data," *SIAM J. Numer. Anal.*, Vol. 45, No. 3, pp. 1005-1034, 2007.

[43] L. Mathelin and M. Hussaini, "A stochastic collocation algorithm for uncertainty analysis," *Tech. Report NASA/CR-2003-212153*, NASA Langley Research Center, 2003.

[44] D. Xiu, "Efficient collocational approach for parametric uncertainty analysis," *Communications In Computational Physics*., Vol. 2, No. 2, pp. 293–309, 2007.

[45] J. Foo, X. Wan, and G. E. Karniadakis, "The multi-element probabilistic collocation method (ME-PCM): Error analysis and applications," *J. Comput. Phys.*, Vol. 227, pp. 9572–9595, 2008.

[46] Y. Marzouk and D. Xiu, "A stochastic collocation approach to Bayesian inference in inverse problems," *Commun. Comput. Phys*., Vol. 6, No. 4, pp. 826-847, 2009.

[47] J. Shen, H. Yang and J. Chen, "Analysis of electrical property variations for composite medium using a stochastic collocation method," *IEEE Transactions on Electromagnetic Compatibility*, Vol. 54, No. 2, pp. 272-279, 2012.

[48] B. Ganapathysubramanian and N. Zabaras, "Sparse grid collocation schemes for stochastic natural convection problems," *Journal of Computer Phys*ics, Vol. 225, No. 1, pp. 652-685, 2007.

[49] S. Smolyak, "Quadrature and interpolation formulas for tensor products of certain classes of functions," *Soviet Math. Dokl.*, Vol. 4, pp. 240-243, 1963.

[50] G. Wasilkowski and H. Wozniakowski, "Explicit cost bounds of algorithms for multivariate tensor product problems," *J. Complexity*, Vol. 11, pp. 1-56, 1995.

[51] G. M. Phillips, *Interpolation and Approximation by Polynomials*, Springer, New York, 2011.

[52] W. K. Liu, T. Belytschko, and A. Mani, "Probabilistic finite elements for nonlinear structural dynamics," *Comput. Methods Appl. Mech. Engrg.*, Vol. 56, pp. 61-81, 1986.

[53] H. Engels, *Numerical Quadrature and Cubature*, Academic Press, London, 1980.

[54] V. Barthelmann, E. Novak and K. Ritter, "High dimensional polynomial interpolation on sparse grid," *Adv. Comput. Math.*, Vol. 12, pp. 273-288,1999.

[55] E. Novak and K. Ritter, "High dimensional integration of smooth functions over cubes," *Numer. Math.*, Vol. 75, pp. 79-97, 1996.

[56] A. Klimke, "Uncertainty modeling using fuzzy arithmetic and sparse grids," Ph.D. Dissertation, University of Stuttgart, Shaker Verlag, Aachen, 2006.

[57] D. M. Pozar, *Microwave Engineering*, 2nd Edition, New York: Wiley, 1998.

[58] Gary Breed, "Analyzing signals using eye diagram," *High Frequency Electronics*, pp. 50-52, 2005.

[59] E. Bogatin, *Signal Integrity-Simplified*, Prentice Hall, New Jersy, 2004.

[60] C. R. Paul, *Introduction to Electromagnetic Compatibility*, 2nd Edition, John Wiley & Sons, New Jersy, 2006.

[61] M. I. Montrose, *Printed Circuit Board Design Techniques For EMC Compliance*, 2nd Edition, *IEEE Press*, New York, 2000.

[62] W. R. Eisenstadt, B. Stengel, and B. M. Thompson, *Microwave Differential Circuit Design Using Mixed-Mode S-Parameters*, Artech House, Boston, 2006.

[63] H. L. Van Trees, *Detection, Estimation and Modulation Theory*, Part I, Wiley, New York, 2001.

[64] B. C. Wadell, *Transmission Line Design Handbook*, Artech, Boston, 1991.

[65] C. Schwad and R. A. Todor, "Karhunen-Loeve approximation of random fields by generalized fast multiple methods," *J. Comput. Phys.*, Vol. 4, No. 4, pp. 501-519, 2006.

[66] M. Loeve, *Probability Theory I & II*, 4th Edition, Springer, New York, 1977.

[67] S. P. Huang, S. T. Quek, and K. K. Phoon, "Convergence study of the truncated Karhuen-Loeve expansion for simulation of random process," *Int. J. Numer. Meth. Engng.*, Vol. 52, pp. 1029-1043, 2001.

[68] G. Stefanou and M. Papadrakakis, "Assessment of spectral representation and Karhuen-Loeve expansion methods for the simulation of Gaussian stochastic fields," *Comput. Methods Appl. Mech. Engrg.*, pp. 2465-2477, 2007.

[69] L. M. Delves and J. L. Mohamed, *Computational Methods For Integral Equations*, Cambridge University Press, Cambridge, 1985.

[70] E. Parzen, *Stochastic Processes*, Holden-Day, San Francisco, 1964.

[71] K. K. Phoon, S. P. Huang, and S. T. Quek, "Simulation of second-order processes using Karhuen-Loeve expansion," *Computer and Structures*, Vol. 80, pp. 1049-1060, 2002.

[72] G. Q. Cai and Y. K. Lin, "Generation of non-Gaussian stationary stochastic processes," *Phy. Rev. E.*, Vol. 54, pp. 299-303, 1996.

[73] Y. Chen and G. Deodatis, "Simulation of highly skewed non-Gaussian vector processes," *Proceedings of the Ninth ASCE Speciality Conference on Probabilistic Mechanics & Structural Reliability*, Albuquerque, New Mexico, July 26-28, 2004.

[74] F. J. Ferrante, S. R. Arwade, and L. L. Graham-Brady, "A translation model for non-stationary non-Gaussian random processes," *Probabilist. Engrg. Mech.*, Vol. 20, pp. 215-228, 2005.

[75] G. Stefanou, "The stochastic finite element method: Past, present and future," *Comput. Methods. Appl. Mech. Engrg.*, Vol. 198, pp. 1031-1051, 2009.

[76] D. Xiu, "Fast numerical methods for stochastic computations: A review," *Commun. Comput. Phys.*, Vol. 5, No. 2-4, pp. 242-272, 2009.

[77] X. Wan and G. E. Karniadakis, "An adaptive multi-element generalized polynomial chaos method for stochastic differential equations," *J. Comput. Phys.*, Vol. 209, pp. 617-642, 2005.

[78] X. Wan and G. E. Karniadakis, "Multi-element generalized polynomial chaos for arbitrary measure," *SIAM J. Sci. Comput.*, Vol. 28, No. 3, pp. 901-928, 2006.

[79] D. Xiu, "Numerical integration formulas of degree two," *Appl. Numer. Math.*, Vol. 59, pp. 1515-1520, 2008.

[80] A. Stroud, "Remarks on the disposition of points in numerical integration formulas," *Math. Comput.*, Vol. 11, pp. 257-261, 1957.

[81] A. Stroud, *Approximate Calculation of Multiple Integrals*, Prentice-Hall, Inc., Englewood Cliffs, NJ, 1971.

[82] M. Liu, Z. Gao and J. S. Hesthaven, "Adaptive sparse grid algorithm with applications to electromagnetic scattering under uncertainty," *Applied Numerical Mathematics*., Vol. 61, pp. 24-37, 2011.

[83] C. A. Balanis, *Antenna Theory: Analysis and Design*, 2nd Edition, John Wiley and Sons, New York, 1997.

[84] R. C. Hansen, *Phased Array Antennas*, John Wiley and Sons, New York, 1998.

[85] R. S. Elliott, *Antenna Theory and Design*, Revised Edition, John Wiley and Sons, New York, 2003.

[86] R. Ross, B. Goodpaster, D. Kelly, and F. Boada, "Magnetic resonant imaging in human body composition, from quantitative to qualitative tissue measurement," *Ann. N. Y. Acad. Sci.*, Vol. 904, pp. 12-17, 2000.

[87] J. Silly-Carette, D. Lautru, M.-F. Wong, A. Gati, J. Wiart, and V. Fouad Hanna, "Variability on the propagation of a plane wave using stochastic collocation methods in a bio-electromagnetic application," *IEEE Microwave and Wireless Components Letters*., Vol. 19, No. 4, pp. 185-187, 2009.

[88] A. Christ, W. Kainz, E. G. Hahn, K. Honegger, M. Zefferer, E. Neufeld, W. Rascher, R. Janka, W. Bautz, J. Chen, B. Kiefer, P. Schmitt, H-P. Hollenback, J. Shen, M.

Oberle, D. Szczerba, A. Kam, J. W. Guag, and N. Kuster, “The virtual family – development of surface-based anatomical models of two adults and two children for dosimetric simulations,” *Phys. Med. Biol.*, Vol, 55, pp. N23-N38, 2010.

[89] S. Mcmorrow, “The impact of PCB laminate weave on the electrical performance of differential signaling at multi-gigabit data rates,” *DesignCon*, Santa Clara, California, January, 2005.